Research Center Borstel

Leibniz Lung Centre

Priority Area Infection

Research Group Cellular Microbiology

Head: Prof Dr U. E. Schaible

Comparative Analysis of Host Response in Tuberculosis Across Species

Doctoral dissertation submitted by

dissertation vorgelegt von

Hawanot Olaitan Tijani

657592

to the University of Luebeck

in partial fulfilment of the requirements of Doctoral Degree

from the Department of Natural Sciences

zur Erlangung der Doktorwürde

der Universität zu Lübeck

aus der Sektion Naturwissenschaften

Lübeck, 2024

STATEMENT OF AUTHORSHIP

I hereby declare that this doctoral dissertation has been composed by me and describes my own work, and the works of the collaborators involved in different parts of the project. Work done as collaboration with scientists at the Central Institute of Tuberculosis Moscow Russia was prior to Russia's war in Ukraine. Where I have consulted the work of others this is always clearly stated. All statements taken literally from other writings or referred to by analogy are marked and appropriately cited. This work has not yet been submitted to another examination office.

EIDESSTATTLICHE ERKLÄRUNG

Hiermit erkläre ich, dass diese Dissertation von mir verfasst wurde und meine eigene Arbeit sowie die Arbeiten der an verschiedenen Teilen des Projekts beteiligten Kollaboration Mitarbeiter beschreibt. Die Arbeiten wurden in Zusammenarbeit mit Wissenschaftlern des Zentralinstituts für Tuberkulose in Moskau, Russland, vor dem Krieg in der Ukraine durchgeführt. Wo ich die Arbeit anderer konsultiert habe, wird dies immer klar angegeben. Alle Aussagen, die wörtlich aus anderen Schriften stammen oder analog erwähnt werden, sind gekennzeichnet und zitiert. Diese Arbeit wurde nicht bei einem anderen Prüfungsbehörde vorgelegt.

_____

Hawanot Olaitan Tijani, Borstel, 2024

Supervisor and First Examiner: Prof Dr Ulrich E. Schaible
Research Center Borstel
Cellular Microbiology

Co-supervisor: Dr Christian Utpatel
Research Center Borstel
Cellular Microbiology

Examination Chairperson: Prof Dr Norbert Tautz
Universität zu Lübeck

Second Examiner: PD Dr Katrin Kalies
Universität zu Lübeck

Mentor: Dr Tobias Dallenga
Research Center Borstel
Cellular Microbiology

Date of Examination: 01. April, 2025

Date approved for printing: 02. April, 2025

Date submitted: 04. April, 2025

Finally beloved, whatsoever things are true, whatsoever things are honest, whatsoever things are just, whatsoever things are pure, whatsoever things are lovely, whatsoever things are of good report, if there be any virtue, and if there be any praise, think on these things.

Phillipians 4:8 *(New King James Version & Luther Bibel)*

Weiter, ihr lieben: Was wahrhaftig ist, was ehrbar, was gerecht, was rein, was liebenswert, was einen guten Ruf hat, sei es eine Tugend, sei es ein Lob – darauf seid bedacht!

Dedicated to Sururat Adeoti Akintunde

Acknowledgement

Thank you ……

Prof Dr Ulrich E. Schaible, *mein Doktor Vater*, for going through the uneasy process of training me. I am grateful for the intellectual ideas, suggestions, meetings and all the steps you took to ensure that my doctoral research became successful eventually. For always working to ensure funding and reports are well co-ordinated.

Cellular Microbiology, the research group of Prof Dr U. E. Schaible, as a group with different teams, together you made the work atmosphere comfortable and healthy. I appreciate Jacqueline Eich, Kristine Hagens, Dagmar Meyer, and Nina Grohmann for their technical support. Dr Matthias Hauptmann, Dr Natalja Redinger, Dr Uwe Mamat and Dr Christian Alexander, for your ideas, questions, and support. Dr Lara Linnemann, Christoph Leschczyk, Jessica Ojong, Pit Engling, Celina Porsch and Benthe Beu, the excellent “Azubis”, colleagues and other doctoral researchers in the research institute for your help and ideas.

Specifically, I would like to appreciate the following people for each of their contributions to this work:

Prof Stephan Niemann and his team, PD Dr Norbert Reiling and his team, your invaluable resources and knowledge on sequencing technology and PCR made this work up to date.

Dr Christian Utpatel for your time and ideas during the BBRS Thesis committee meetings. Vanessa Mohr, Fenyan Boysen and Tanja Niemann for excellent technical assistance of the sequencing data.

Dr Tobias Dallenga, my mentor, for patiently training me to turn ideas into experimental protocols and result. And for helping me to understand the implication of every number and data points in a graph as a likely biological process important in the bigger picture. Also, for translating the abstract.

Dr Matthias Hauptmann and Pit Engling contributed in writing the animal experiment contract “Tierversuchvertrag” on the role of Ipr1/sst1 in experimental tuberculosis.

Dr Tobias Dallenga and Jochen Behrends contributed to the characterization of the surface markers of cells in the murine lungs. Martina Hein helped with the murine cytokine.

Dr Natalja Redinger helped throughout the animal experiment and analysis of the histology data.

Kristine Hagens showed me how to work with cells from murine bone marrow.

Jacqueline Eich trained me to work with human blood and helped throughout the animal experiment.

Dr Jessica Ojong Akko-Arrey for sharing most of the already established protocols in our lab group and for teaching me RNA extraction and qPCR.

Dr Uwe Mamat, your handling of questions and careful questioning of result has made me a better researcher.

Daniela Esser, the bioinformatician that took this project beyond my capacity, for your help with analysing our complex data.

Jutta Passarger, the best secretary any researcher can dream to have, for handling most administrative documents.

Nina Grohmann, best equal opportunity officer I have ever met, for the technical help with the sequencing.

Prof Dr Vladimir Yeremeev and his team, Prof Dr Alex Apt and his team, our collaborators, for bringing your expertise to our joint topic of interest, helping us to understand better and achieve our goals together.

Prof Dr Igor Kramnik and his team, for the great work on the *IPr1* gene and the *sst1* locus in tuberculosis which laid the foundation for part of our study and for supporting our work with the B6.C3H*sst1* congenic mice.

Dr Ilka Monath and her team of animal care facility for breeding and taking care of the mice.

The Research Center Borstel, the core facility flowcytometry, the animal caretakers and the blood donation service in Borstel, IT-Network Center, for providing the appropriate environment, technical equipment, and support to make the aim of this project achievable.

Dr Sven Müller-Loennies and his team for the LPS used in the *in vitro* experiments.

Co-ordinators of the Borstel Biomedical Research school, for organizing the courses and retreats that expanded my knowledge beyond the scope of my research.

Co-ordinators of the Center for structured doctoral studies Lübeck (CDSL) for the engaging and career defining courses.

Importantly, I would like to say a big thank you to all who have taught me from preschool to this day.

My former supervisors, intellectual minds that I can recall never to embarrass but endeavour to praise Prof Dr B.O. Opere, Prof Dr D. D. Moro and Prof Dr Keme Pondei. Remembering you builds my character and conduct as an academic researcher.

My lovely family and friends, many thanks for the emotional support, for believing in me to complete this phase of my career when hope seemed lost. Big and warm thank you to my mum, dad, siblings, and those who always do their best to have my back the Ibukun-Thomas, the Onikosis, the Ogohs, Olaoluwa Ashley, Linda Ikediashi, Ayo Ngaju, Dr Ireti Ogunsulire, Dr Temitope Kuti, Christians in like faith in church, home and away including members of the Lagos State University Christian Fellowship, and my caring uncles the Okunmoyinbos, and my godparents the Idowus.

Emotionally and responsibly, I am grateful for every opportunity and positions I have served. As a mother to my daughter; as an aunt to my niece and nephew; and as comrade and confidants to colleagues and friends.

In all and through it all. I appreciate every step, bends and twists that made this journey a successful one leading to another.

Abstract

In tuberculosis (TB) studies, the extent to which host genome as well as transcriptome contribute to susceptibility and pathology has not been clearly defined. Globally still one of the most abundant infectious disease, numbers of TB cases caused by drug resistant agents of the *Mycobacterium tuberculosis* (*M. tuberculosis*) complex are increasing especially with onset of emerging and re-emerging viral diseases and other comorbidities. Our study aims to identify host specific differences in TB disease susceptibility and pathogenesis. Previously, we and others have demonstrated the detrimental role of neutrophils in necrosis, tissue damage and bacterial spread. We hypothesized that cell death modalities during the interaction of neutrophils and other myeloid cells in the lung determines pathogen restriction or spread and ultimately, disease exacerbation. We therefore designed an integrative systems biology approach from genome to cellular, tissue and animal model to better understand TB *in vitro* and *in vivo*. Inbred female congenic mice differing in their susceptibility to M. *tuberculosis* infection were studied before, during and after infection and compared to human leukocytes and RNA samples from excised lung tissue. Murine bone marrow derived macrophages from wild-type B6 in comparison to susceptible C3HeBFeJ and B6.C3Hsst1 mice showed differential responses to M. *tuberculosis*. Upon aerosol infection with *M. tuberculosis*, immune-competent but susceptible B6.I-9.3.19.8 and B6.C3Hsst1 had bigger lung lesions and higher bacterial loads than resistant B6 mice. Immune cell phenotyping of murine lung samples characterized by flow cytometry and immunohistochemistry revealed distinct composition of immune cells between susceptible and resistant mouse strains. Importantly, human PMN and PBMCs showed infection specific transcriptional profiles *in vitro* skewed towards active phagocytosis. Comparative analyses of both murine and human transcriptome identified unique genes for each data set and shared genes across the samples. Taken together, our findings will contribute to better understand TB disease processes in order to break disease transmission, reducing bacterial burden in active TB patients, shortening treatment duration, and eventually preventing disease development in latent TB cases.

Zusammenfassung

In Studien zur Tuberkulose (TB) ist das Ausmaß, in dem das Genom des Wirts und das Transkriptom zur Anfälligkeit und Pathologie beitragen, ist nicht klar definiert Weltweit ist Tuberkulose immer noch eine der häufigsten Infektionskrankheiten. Die Zahl der Tuberkulosefälle, die durch arzneimittelresistente Erreger des *Mycobacterium tuberculosis* (M. *tuberculosis*)-Komplexes verursacht werden, nimmt zu, insbesondere mit dem Auftreten neuer und wieder auftauchender Viruserkrankungen und anderer Komorbiditäten. Unsere Studie zielt darauf ab, wirtsspezifische Unterschiede in der Suszeptibilität und Pathogenese von TB-Erkrankungen zu identifizieren. In der Vergangenheit haben wir und andere die nachteilige Rolle der Neutrophilen bei der nekrose, der Gewebeschädigung und der Ausbreitung von Bakterien nachgewiesen. Wir stellten die Hypothese auf, dass die Modalitäten des Zelltods während der Interaktion zwischen Neutrophilen und anderen myeloiden Zellen in der Lunge für die Eindämmung oder Ausbreitung von Krankheitserregern und letztlich für die Verschlimmerung der Krankheit verantwortlich sind. Wir haben daher einen integrativen systembiologischen Ansatz entwickelt, der vom Genom bis zum Zell-, Gewebe- und Tiermodell reicht, um TB in vitro und in vivo besser zu verstehen. Ingezüchtete weibliche kongene Mäuse, die sich in ihrer Suszeptibilität gegenüber M. *tuberculosis* unterscheiden, wurden vor, während und nach der Infektion untersucht und mit menschlichen Leukozyten und RNA-Proben aus entnommenem Lungengewebe verglichen. Makrophagen aus dem Knochenmark von Wildtyp-B6-Mäusen im Vergleich zu suszeptiblen C3HeBFeJ- und B6.C3Hsst1-Mäusen zeigten unterschiedliche Reaktionen auf M. *tuberculosis*. Nach einer Aerosol-Infektion mit M. *tuberculosis* zeigten immunkompetente, aber suszeptible B6.I-9.3.19.8 und B6.C3Hsst1 größere Lungenläsionen und eine höhere Bakterienlast als resistente B6-Mäuse. Im Gegensatz dazu zeigte der durchflusszytometrisch und immunhistochemisch charakterisierte Immunzellphänotyp der Mäuselungen unterschiedliche Lungenläsionen zwischen suszeptiblen und resistenten Mäusestämmen. Insbesondere zeigen menschliche PMN und PBMCs *in vitro* infektionsspezifische Transkriptionsprofile, die auf eine aktive Phagozytose ausgerichtet sind. Vergleichende Analysen des Transkriptoms von Mäusen und Menschen ergaben für jeden Datensatz einzigartige Gene und

gemeinsame Gene in den Proben. Zusammengenommen werden unsere Ergebnisse dazu beitragen, die TB-Krankheitsprozesse besser zu verstehen, um die Krankheitsübertragung zu unterbrechen, die bakterielle Last bei aktiven TB-Patienten zu verringern, die Behandlungsdauer zu verkürzen und schließlich die Krankheitsentwicklung bei latenten TB-Fällen zu verhindern.

Abbreviation

Acronym	Meaning
BMDM	Bone marrow derived macrophages
CFU	Colony forming unit
DNA	Deoxyribonucleic acid
HIV	Human immuno-deficiency virus
HDT	Host directed therapy
IFN-	Interferons
IL-	Interleukins
Ipr	Intracellular pathogen resistance
I/St	I-Strong
MHC	Major histo-compatibility loci
QTL	Quantitative trait loci
LD	Linkage disequilibrium
NGS	Next Generation Sequencing
RNA	Ribo nucleic acid
sst	Super susceptibility
TB	Tuberculosis
TNF-α	Tumour necrosis factor
PCR	Polymerase chain reaction
RT-qPCR	Real time quantitative PCR
WHO	World health organization

Contents

Curriculum Vitae

1.0 Introduction

1.1 Tuberculosis: the disease, vaccine, and therapy

1.1.1 The Disease and its causative agents

From an historical perspective, today's tuberculosis (TB) was called many names including phthisis, schachepheth, tabes, the white plague, and consumption. Previous names given to TB were based on the physical appearance of the people who suffered from the disease. TB is now described both phenotypically and genotypically based on the host and pathogen characteristics. The various forms of TB in humans are either organ specific, clinical manifestation- or pathogen specific[1]. TB meningitis, miliary TB, extrapulmonary TB, and pulmonary TB refers to the organs that affected while active TB, chronic TB and latent TB describes the clinical presentation of the disease[2].

People who do not have clinical disease manifestations but confirmed to be positive for TB tests are latent carriers. Latent TB patients have the pathogen under control of the immune system and do not spread the disease[2,3]. Current estimates of latent TB are about one-fourth of the world's population. On the other hand, patients with active TB clinically show signs and symptoms of TB, they can cough or sneeze out pathogen-containing aerosol droplets from their infected lungs which may transmit the pathogen to uninfected people and probably also latent TB patients[4–6].

In terms of the pathogen virulence and response of the pathogen to drugs, TB can be drug sensitive or drug resistant. Both pulmonary and extrapulmonary TB are caused by mycobacterial pathogens belonging to the *Mycobacterium tuberculosis* complex (MTBC). The MTBC consist of genetically related mycobacteria that cause TB in humans and some animals. These include *Mycobacterium tuberculosis* (Mtb), M. *africanum*, M. *bovis*, M. *caprae*, M.

microti, M. *canetti* and M. *pinnipedii*. M. *bovis* is likely originating from Mtb. Based on virulence of clinical isolates, the most virulent strains of TB are the modern lineage and are not well adapted to the new host[7]. Less virulent well adapted strain is for example M. *africanum*. Pulmonary TB can be managed, treated, and cured. However, combination of TB and viral diseases such as HIV or other immunosuppressive situations such as anti-TNFα or corticoid therapies can further limit treatment options, hence the need for better prophylactic and therapeutic options.

Human pulmonary TB starts when a patient with active TB coughs or sneezes pathogen containing aerosols into the air (Fig 1.1 a, b). This can lead to TB in the exposed susceptible person (c) or hypothetically no reactivation or disease in a TB resistant person (d). When a susceptible individual is exposed to Mtb, the pathogen is otherwise kept in tissue structure called the granuloma which enwraps the infection focus and develops very well in immune competent individuals. Well-structured granuloma (e) can remain undetected lifelong in an immune competent individual but could break open and exacerbate leading to disease under certain circumstances such as immune compromising conditions (f, g). However, reasons for granuloma reactivation and Mtb proliferation in immune competent individuals is a controversial topic[8–12]. The focus of this research work is to characterize some of the factors that mediate TB susceptibility in immune competent individuals (Fig 1 c, d, I and e). The TB granuloma (Fig 1.1 g) which continues to keep the pathogen life-long under control in an immune competent person (i) may become disorganized and permissive for Mtb growth (f) thereby leading to reactivation and active TB (h). The life-time risk of TB reactivation is less than 10%. The possibility of TB reactivation and active TB (Fig 1.1 h, i) is widely debated. Understanding the reasons for TB development in humans is therefore important to keep the

pathogen under the control of the immune response and limit spread of the bacteria, thereby breaking TB transmission[2,13,14].

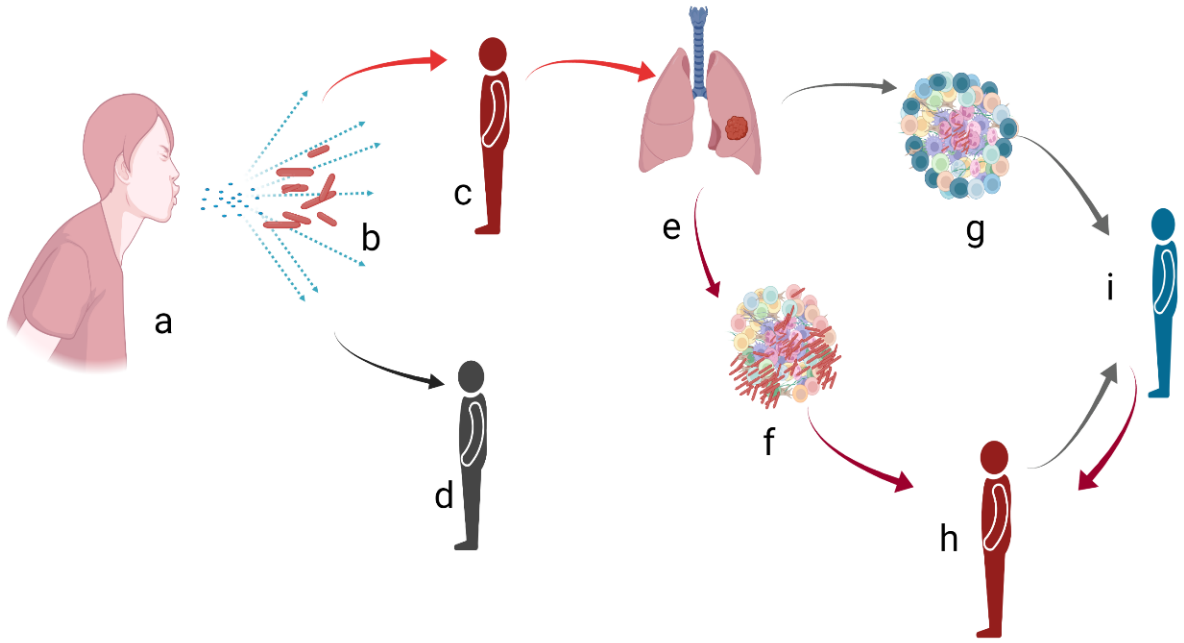

Fig. 1.1: The TB pathogenesis. Pathogen containing aerosol from active TB patient is propelled into the air by active TB patient (a) Mtb containing aerosol (b) infected person (c) exposed but uninfected person (d) TB in latent state (e) loss of granuloma integrity (f) intact granuloma with bacteria (g) active TB patient (h) probably cured TB patient (i). *Image designed using Biorender.

1.1.2 Vaccine and therapeutic intervention

There are experimental and clinical evidence supporting the hypothesis that immune response to TB is host and mycobacterial genome specific[7,15–17].

A global measure of success against an infectious disease is the existence of a helpful vaccine. M. *bovis Baccille-Calmette-Guerin* (BCG) generated by multiple passage of the cattle TB agent M. *bovis* is the vaccine approved for protection against early childhood primary TB and TB meningitis in children. It is administered intradermally at the upper side of the upper arm

once in first few weeks of life. The vaccine is, however, not sufficient to protect against adult pulmonary TB. Although the BCG vaccine remains the standard reference new anti-TB vaccines currently in development, regarding efficacy in mounting an effective protective immune response. Over the years, different vaccines have been developed and tested in clinical trials[18–20]. In phase 2b clinical trial, the M72/AS01E vaccine showed partial protection against pulmonary TB in adults[21].

Globally, the 10 million cases of pulmonary TB annually are of major concern to public health[22]. TB can be properly treated and cured but the treatment duration can range from at least six months to two years with combinations of at least two to three antibiotics depending on the susceptibility or resistance status of the pathogen. Drug susceptible TB cases are declining by the years while drug resistant cases keep increasing even despite introduction of new antibiotics. Drug susceptible TB cases can be managed, treated, and cured with the combination of Isoniazid and Rifampicin for 6 months. Resistance to Isoniazid and Rifampicin which are the first line antibiotics, is said to be, multi-drug resistance TB (MDR-TB). If the pathogen is then additionally resistant to one of the second line drugs including injectables ones such as amikacin or carbapenem, this is described as extensive drug resistant TB (XDR-TB). The available drugs for MDR-TB and XDR-TB such as Bedaquilin pretonamid require administration for a long time and these drugs have adverse side effects.

Therefore, the need for well tolerated but effective host-directed therapeutic options accompanying antibiotic therapy are urgent so that doctors, families, health insurance and major stake holders can make well informed decision for treatment options and regimen[23].

1.2 Epidemiology

Incidence of TB has been historically described along with industrialization and urbanization. Global TB cases are defined as drug susceptible, drug resistant or multi-drug resistant TB (MDR-TB). Over the last twenty years, incidence of TB cases has been on gradual decline. In contrast, MDR-TB cases keep increasing. According to WHO 2023 global TB report for year 2022, India, China, Indonesia, Philippines, Pakistan, Democratic Republic of Congo, Bangladesh, and Nigeria are the countries that account for two-thirds of the estimated 10.6 million TB cases with at least 100 000 incidences[22]. Globally, about 10.6 million people fell ill with TB in the year 2022. However, due to the COVID-19 pandemic, TB case notification diminished drastically (Fig. 1.2).

The overlapping profile of drug and pathogen toxicity makes it rather difficult to treat MDR-TB. The interaction between drugs and pathogen renders the host defenceless depending on the immunological barriers available.

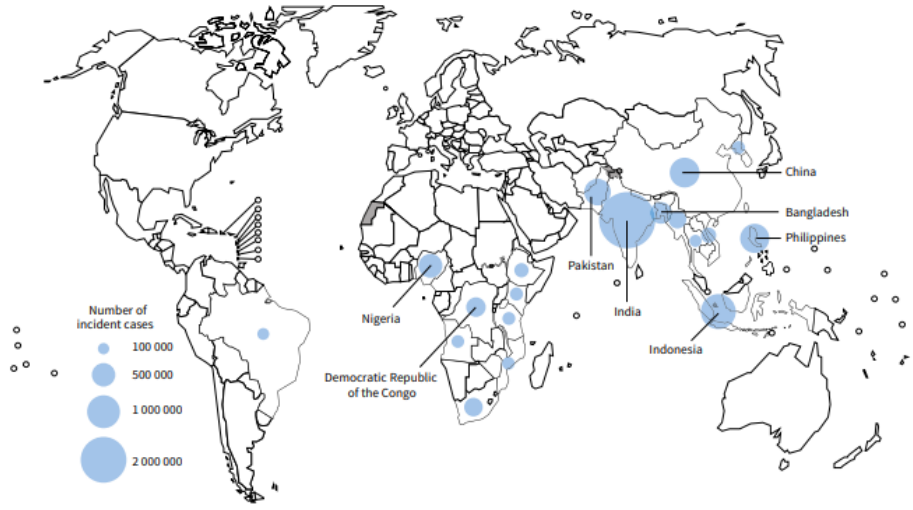

Fig. 1.2: Global estimate of TB incidence for the year 2022 for countries with at least 100 000 incident cases. The country with highest incidence rate of about 200 000 per 100 000 population is India. Countries with at least 100 000 incidence cases are China, Indonesia, Philippines, Democratic Republic of Congo, South Africa and Nigeria *WHO 2021*.

However, the concept of trained immunity, that is unspecific stimulation of the innate immune system leading to epigenetic imprinting, offers a new possibility to protect genetically susceptible hosts[20,24,25]. The potential preference of host directed therapy (HDT) against general antibiotics is hypothetically the reconstruction of immunological barriers but the long-term effect of HDTs have not been clearly defined.

1.3 Immune Response Against TB

The immune response against *Mycobacterium tuberculosis* (Mtb) begins and end with the host and pathogen characteristics. Granuloma formation and maintenance is critical for both host and pathogen survival. Proper knowledge of host and mycobacterial genetics is required to tilt the balance towards an appropriate host immune response.

An active TB patient is the reservoir for Mtb transmission. This host spreads Mtb by coughing or sneezing into the environment (Fig 1.1a). The airborne mycobacteria possess immune activating characteristics that can induce varied immune responses in the newly infected human host[26–29]. Inhalation of pathogen containing aerosol (Fig 1.3a) is followed by phagocytosis by lung resident alveolar macrophages and active recruitment of neutrophils (PMN) and monocyte derived macrophages to site of infection. Infected alveolar macrophages migrate and transport Mtb into the lung interstitium and become subsequently surrounded by other innate myeloid derived immune cells (b) while antigen processing and presenting cells such as dendritic cells migrate and carry Mtb antigens to draining lymph nodes. Upon appropriate antigen presentation, primed CD4 and CD8 T cells differentiate, proliferate and become activated to mount an effective antigen specific immune response, and B cells are also recruited to the lung (Fig 1.3)[30–32].

Tissue resident alveolar macrophages in the lungs are believed to be the first cells to phagocytose Mtb. However, other innate cells surveying the lungs quickly communicate and initiate pathogen associated molecular signals. Depending on the pathogen load, cellular signalling, myelopoiesis, and extravasation continues until homeostasis is restored. Mtb can exploit excess inflammation from immune competent host. Cellular necrosis and Mtb replication is a result of counter activity of host immunity and bacterial pathogenicity. Highly virulent strains of Mtb have evolved mechanisms to lyse the phagosome and replicate (c) in the next host cells including myeloid derived antigen processing cells which are recruited to the site of inflammation upon emergency myelopoiesis.

Breaking the cycle of cellular necrosis by host-directed therapies are the keys to restoring lung remodelling and structured granuloma formation (Fig 1 d, e, f).

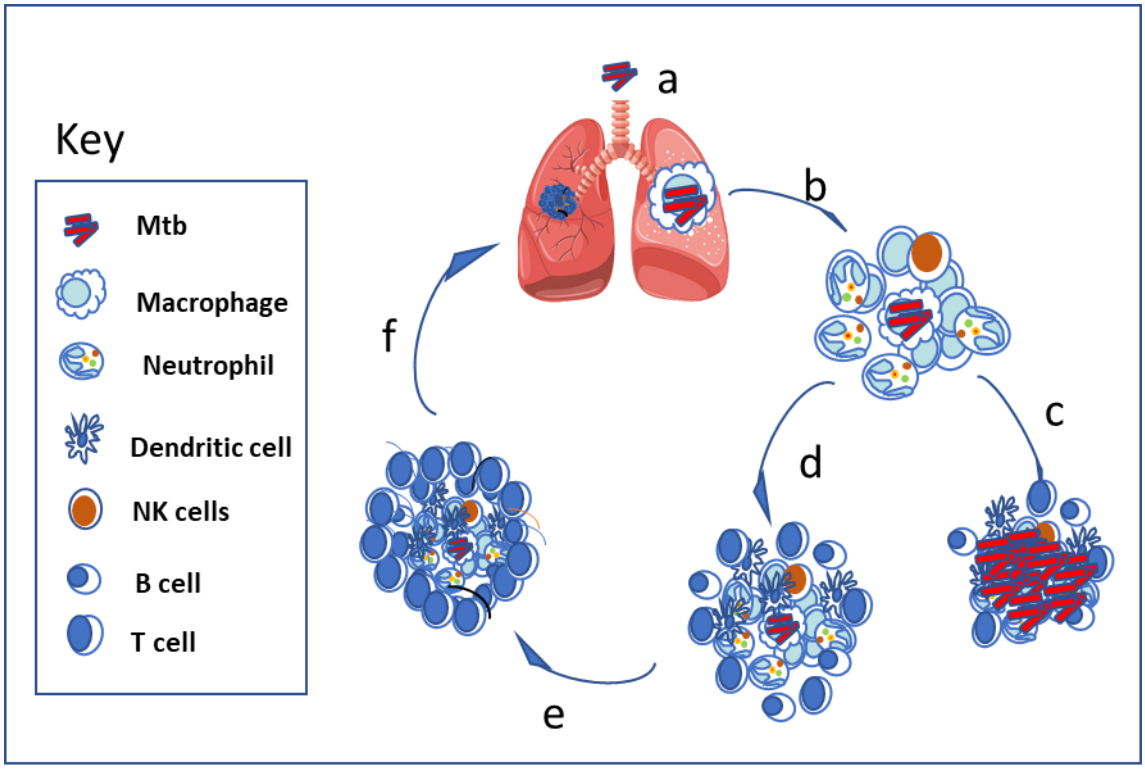

Fig. 1.3: Mtb and granuloma formation. After Mtb (a) inhalation and uptake by alveolar macrophage, innate immune cells especially neutrophils are recruited to the lungs to contain the infection (b), uncontrolled Mtb replication and repeated cycle of cell death may lead to death of the host (c),

dendritic cells, B cells and T cells may accumulate around the cellular lesions (d) leading to Mtb control and protective granuloma (e) and eventually latent TB (f)[33,34]

The entire process of mounting and maintaining immune responses against Mtb depends largely on the host genetics. Differential responses to TB across geographical populations depend on several factors. Age, gender, and co-morbidities like existing bacterial and viral infection, smoking or type 2 diabetes make treatment difficult. The role of the granuloma in controlling Mtb replication and spread is a function of the host, as well as the mycobacterial pathogenicity[35–37].

Furthermore, genes mediating susceptibility and immune response to TB are important for signal transduction, cell recruitment and tissue remodelling. Genes regulating the IFN-ɣ and IL-12 axis have been the most prominent in mediating TB susceptibility and reactivation in immune competent individuals. These genes regulate cellular migration to site of infection, innate immune cell activation and inflammatory T helper 1 cell differentiation as well as prevention of infection spread[38–40]. The role of IFN-ɣ in controlling Mtb depends on the murine model analysed while the role of IFN-ɣ in human TB is less clarified[9,41]. The phenotypic differences in lung pathology depends on the amount and duration of pro-inflammatory and anti-inflammatory cytokines secretion and their mutual counter regulation. While pro-inflammatory cytokines such as IL-1β, IL-6, IL-8, IL-12, IL-18, IL-23, IFN-ɣ, TNF-α are required to control the pathogen, anti-inflammatory cytokines IL-10 and TGF-β mediate resolution of inflammation and restore homeostasis.

Early production of IFN-ɣ by $CD4^+$ and $CD8^+$ T cells recruited to the lungs is beneficial in activating macrophages in concert with IL-15 (in humans) whereas prolonged IFN-ɣ secretion is associated with continuous PMN recruitment and disease exacerbation[42–44]. In mice, IFN-ɣ

activated macrophages secrete nitric oxide (NO) and TNF-α and thereby control Mtb replication by inducing apoptotic cell death in infected macrophages[45]. The macrophages either become apoptotic or necrotic depending on the inflammatory micro-environment[32,46]. Wild type resistant B6 mice infected with Mtb have lower PMN counts, in contrast in active TB patients, PMN are the most abundant infected leukocytes[6,42]. The proinflammatory cytokine, IL-8, mediates PMN recruitment to the site of infection and can be detrimental. Recruited PMN actively phagocytose Mtb, produce reactive oxygen species (ROS) which however does not kill Mtb. The oxidative stress in the PMN leads to necrotic PMN death and PMN extracellular trap (NET) formation. PMN-NETosis has been claimed to be a defence mechanism to restrict Mtb[41,47,48]. However, our group found that necrotic cell death of infected PMN promote mycobacterial growth in macrophages, which subsequently take up infected PMN. In contrast PMN apoptosis prepares Mtb for efficient subsequent killing by macrophages[32].

The phenotypic differences in TB pathology can be genotypically characterized based on the gene products that induce and resolve lung inflammation during Mtb infection. Drawing inferences based on experimental studies requires caution because some observations from experimental murine TB are not completely represented in human TB. In humans, the genes mediating TB susceptibility have been studied mainly in the blood or peripheral blood derived cells[39,49]. One study that focused on lung tissue from TB patients provided evidence of differential gene regulation within the granuloma but how these genes mediate lung pathology versus protection was not clearly defined[50].

Genetic differences in the host remains the underlying factor for differences in disease susceptibility to infection including tuberculosis. Spontaneous mutations leading to single

nucleotide polymorphisms has remained unnoticed over the years due to differences in penetrance. Phenotypic and epigenetic changes have been studied in relation to disease exposure[20,51]. Exposed but not active TB patients can remain undetected lifelong. The 1929 Lübeck TB vaccine disaster has to this day shown that susceptibility to any infectious diseases is both host and pathogen genome specific[52]. Most of the differences observed in any infectious disease is largely dependent on how the host responds to the disease. The host responses either leads to a proper well balanced immune response clearing or controlling the pathogen or it leads to exacerbating inflammation and pathology, which may eventually cause autoimmunity, fighting against self-defence mechanisms[20,53,54].

1.4 Aim and Objectives

The aim of this project was to study TB associated host response and identify host genes that can serve as putative targets for host directed therapy in experimental and clinical TB. To achieve this, the following objectives were formulated, and experiments were designed for these objectives:

1. Monitor infection process in resistant B6. vs susceptible (B6.I-9.3.19.8 and B6.C3H-sst1) littermates
2. Characterize host-specific innate immune cell activities *in vitro*
3. Analyse host pulmonary transcriptomes in Mtb infected lungs from patients and resistant versus susceptible mice in a comparative manner.

2.0 Materials

2.1.0 General consumables

2.1.1.1 Tubes, Plates & Pipette Tips

S/N	Consumables	Company	Unique ID/Catalog #
1	50 ml tubes	Corning	COS 430829
2	15 ml tubes	Corning	COS 430791
3	2 ml tubes	Sarstedt	72.694.006
4	1.5 mL tubes	Sarstedt	72.692.005
5	1.5 mL Microfuge Tubes Nonstick, RNAse/DNAse free	Applied Biosystem	AM-12450
6	Spin-X centrifuge tube filter	Costar	COS 8160
7	1.5 mL tubes PCR Performance Tested	Sarstedt	72.706.400
8	0.5 mL tubes PCR Performance Tested	Sarstedt	72.735.002
9	Multiply®-µStrip 0.2 mL chain	Sarstedt	72.985.002
10	8-Lid chain, flat	Sarstedt	65.989.002
11	24-well cell culture plates flat-bottomed	Sarstedt	S 833921
12	96-well cell culture plates flat-bottomed	Sarstedt	S 833924
13	96-well cell culture plates U-bottomed	Sarstedt	S 833925
14	96-well plate dark flat bottom	Greiner Bio-One	GB655077
15	96-well PCR Plate without skirt	Sarstedt	72.1978.202
16	96-well 300 µL plate	Thermo Scientific	AB-0796
17	96-well 0.8 mL plate	Thermo Scientific	AB-0859
18	Primaplate 96-well PCR plate	Steinbrenner Laborsystem	SL-PP96-2
19	Light cycler 480 Multi-well Plate 96 + qPCR Seal	VWR	732-1463
20	2 mL Pipette	Corning	COS 4486
21	5 mL Pipette	Corning	COS 4487
22	10 mL Pipette	Corning	COS 4488
23	25 mL Pipette	Corning	COS 4489
24	Pipette tips Biosphere Plus 0.6 – 20 µL	Sarstedt	70.1116.210
25	Pipette tips Biosphere Plus 2 – 200 µL	Sarstedt	70.760.211
26	Pipette tips Biosphere Plus 1000 µL	Sarstedt	70.3050.255
27	Pipette tips 1 -30 µL	Biolab	61-AN031G-MRS
28	Pipette tips ART 1000G	Thermo Scientific	2079G
29	Pipette tips ART 200G	Thermo Scientific	2069G
30	Pipette tips ART-1000 REACH Barrier	Thermo Scientific	2079-HR
31	Pipette tips ART-300 Barrier	Thermo Scientific	2070-HR
32	Pipette tips ART-200 Barrier	Thermo Scientific	2069-HR
33	Pipette tips ART 20P aerosol resistant	Thermo Scientific	2149P-HR

2.1.1.2 Other Consumables

S/N	Consumables	Company/Source	Unique ID/Catalog #
1	AMPure XP Beads	Beckman Coulter	A63881
2	RNAClean XP Beads	Beckman Coulter	A63987
3	Aqua B. Braun	B. Braun	0082479E
4	Cuvettes	Sarstedt	67.742
5	Cuvette lid	Carl Roth	X.K25.1
6	Canula 26G 3/8'' 0.45 x 10mm	Becton Dickinson	300300
7	Canula 23G 1'' 0.6 x 25mm	Becton Dickinson	300800
8	Canula 20Gx 1 1/2'' 0.9 x 40mm	Becton Dickinson	301300
9	Cell strainer 70µM	Corning	431751
10	1 ml syringe	Becton Dickinson	303172
11	10 ml syringe	Becton Dickinson	309110
12	BD Plastipack Luer-lock™ 50ml	Becton Dickinson	300865
13	Alu-Sealing Tape, pierceable	Sarstedt	95.1995
14	T25 flask closed cap	Sarstedt	83.3910
15	Alu-Sealing Tape, pierceable	Sarstedt	95.1995
16	Microseal 'A' Film	BIO-RAD	MSA5001
17	Microseal 'B' Seal	BIO-RAD	MSB1001
18	Petri-dish	Sarstedt	S 821472
19	Parafilm	Bemis	PM 996
20	Nasco Whirl Pak bags	Omnilab	B01064
21	Superfrost® Glass slide and cover slip	R. Langenbrinck	03-0060
22	Chamber slides		
23	Chamber plates	Sastedt	94.6077.307
24	Embedding cassette		

2.1.2 Agar, Broth & Media Reagents

S/N	Agar, broth, or Media	Company/Source	Unique ID/Catalog #
1	Asparagine	Becton Dickson	214410
2	7H9 Broth	Becton Dickson	271310
3	Seven H11 agar	Becton Dickson	212203
4	DPBS (10X)	Gibco	14200067
5	DPBS	Pan Biotech	P04-36500
6	Histopaque	Sigma	11191
7	Percoll	Sigma	P1644
8	DMEM	PAN Biotech	P04-03600

10	RPMI-1640	PAN Biotech	P04-17500
11	Fetal Calf serum	PAN Biotech	P30-3306
12	Bovine serum	Biowest	S0250-500
13	L-Glutamine	PAA	M11004
14	Goat serum	PAA	B15035
15	Normal Syrian Hamster serum	Jackson	007-000-0001

2.1.3 Chemicals, Enzymes, Substrate & Inhibitor

S/N	Consumable	Company/Source	Unique ID/Catalog #
1	Bovine serum albumin BSA	Serva	11926.03
2	Hydrogen peroxide solution	Sigma-Aldrich	216763-100mL
3	Nitrate Reductase from *Aspergillus niger*	Sigma-Aldrich	N7265-2UN
4	DNase I	Zymo Research	E1010
5	Citric acid	Sigma-Aldrich	C2404
6	Natriumcitrate dihydrate	VWR	1.06448.0500.8
7	Sulfanilamide	Sigma-Aldrich	S9251-100G
8	Sulphuric acid 25%	Merck	1.00716.1000
9	N-(1-Naphthyl) ethylenediamine dihydrochloride	Aldrich	N9125-10G
10	Ortho-phosphoric acid (H_3PO_4)	Merck	1.00573.1000
11	Natriumnitrite 0.1 mol/L (0.1N)	Fluka	70776 (N12)
12	Ethylene-diamine-tetra acetic acid EDTA	Roth	8043.3
13	Ethanol 410 (100%)	Walter CMP GmbH	UN1170
14	Ethanol 200 proof (absolute) 500 mL	VWR	E7023
15	Erythrocyte Lysis Buffer 10X	Biolegend	420302
16	SuperScript II Reverse Transcriptase	Invitrogen by Thermo Fisher Scientific	18064-014
17	O phenylenediamine dihydrochloride (OPD)	Sigma-Aldrich	P-1526
18	Proteinase Inhibitor	Roche	04 693 159 001
19	Liberase™ Research Grade	Roche	05 401 119 001
20	Paraformaldehyde (PFA))	Carl Roth	0335.3
21	RNase Zap	Invitrogen by Thermo Fisher Scientific	AM9780, AM9782

21	DNA-Exitus Plus	PanReac Applichem	A7089, 0500
23	Dimethyl Sulfoxide (DMSO)	Sigma-Aldrich	D2650-100ML
24	Tri-reagent	Zymo Research	R2050-1-200
25	Tween 20	Sigma-Aldrich	P9416-100ML
26	Tween 80	Sigma-Aldrich	P8074-100ML
27	Triton x-100	Carl Roth	3051.3
28	Paraffin		
29	Xylene	VWR	28.975.360

2.1.4 Cytokine, Antibodies and Kits

2.1.4.1 Murine Antibodies from Biolegend

S/N	Target	Antibody Conjugate	Clone	Specie & Isotype	Excitation laser	Catalogue No.	Dilution
1	T cell	α-CD3-APC-Cy7	17A2	Rat IgG2b, k	Red 633 nm	100222	1:200
2	T cell	α-CD4-PECy7	GK1.5	Rat IgG2b, k	Blue 488 nm, Green 532 nm, or Yellow Green 561nm	100422	1:200
3	T cell	α-CD8a-PerCp	53-6.7	Rat IgG2a, k	Blue 488 nm	100732	1:200
4	T cell, B Cell	α-CD279 (PD-1) FITC	29F.1A12	Rat IgG2a, k	Blue 488 nm	135214	1:100
5	B cell	α -CD19 brilliant violet	6D5	Rat IgG2a, k	Violet 405 nm	115546	1:200
6	Macrophage	α -CD68 Pacific Blue	FA-11	Rat IgG2a	Violet 405 nm	137028	1:400
7	Neutrophil	α-Ly-6G APC	1A8	Rat IgG2a, k	Red 633 nm	127614	1:400
8	Innate cell	α-CD274 (PD-L1) PE	10F.9G2	Rat IgG2b, k	Blue 488 nm, Green 532 nm, or Yellow Green 561nm	124308	1:200

9	Isotype Control IgG2a	IgG2a-PerCP		Rat IgG2a, k	Blue 488 nm	400530	1:200
10	Isotype Control IgG2b	IgG2a-PE		Rat IgG2a, k	Blue 488 nm	400636	1:200

2.1.4.2 Other Antibodies

S/N	Antibody	Company	Catalogue No.	Dilution
1	Primary antibody TIB 120 MHC II unlabeled	Jackson	100222	1:500
2	Secondary antibody Peroxidase Goat anti-Rat igG	Jackson	112-035-167	1:2000

2.1.4.3 Cytokine & Kits

S/N	Cytokine and Kits	Company/Source	Catalog #
1	Murine recombinant IFN-ɤ	Peprotech	315-05
2	Murine recombinant TNF-α	Peprotech	315-01A
3	Cytotocity Detection Kit (LDH)	Roche	11644793001
4	HS RNA Kit (15 nt), 500, 4C	Agilent Technologies	5191-6574
5	NGS Fragment (1 – 6000bp) 500, 4C	Agilent Technologies	5191-6576
6	Qubit 1X dsDNA High Sensitivity Assay kit	ThermoFisher Scientific	Q33230
7	Direct-zol RNA MiniPrep	Zymo Research	R2052
8	RNA Clean & Concentrator-5	Zymo Research	R1013
9	Truseq Stranded RNA CD Indexes	Illumina	20019792
10	Truseq Stranded Total RNA Library Prep Globin	Illumina	20020612
11	Nextseq 500/550 High Output Kit v2 (150 Cycles)	Illumina	FC-404-2002
12	Nextseq 500/550 High Output Kit v2.5 (150 Cycles)	Illumina	20024907
13	Maxima first strand cDNA synthesis kit with dsDNase	Thermo Scientific	K1672
14	LightCycler 480 SYBR Green 1 Master	Roche	04887352001

15	LEGENDplexTM Mouse Inflammation Panel (13-Plex)	Biolegend	740150

2.1.5 Reagents for staining

S/N	Reagents	Company/Source	Unique ID/Catalog #
1	TB staining kit	BD	212522
2	Mayer's Haematoxylin	Roth	T865.2
3	Eosin	Roth	7089.2
4	Ziehl-Neelsen carbol-fuchsin	Roth	A130.1
5	Loefflers Methylene Blue	Roth	AE64.3
6	Masson Goldner Trichrom	Morphisto	12043.00500
7	Entellan	VWR	1079610500

2.1.6 Working solutions for histology staining

S/N	Buffer	Composition
1	Ethanol	100% Ethanol 96% v/v Ethanol 70% v/v Ethanol
2	HCl-Alcohol	0.5% HCl in 70% v/v Ethanol
3	Eosin	1:10 in Aqua dest 1 drop Acetic acid
4	Ziehl-Neelsen carbol-fuchsin	1 tablets protease inhibitor, 0.5% Tween80 in 25 mL ddH_2O
5	Loefflers Methylene Blue	1:10 in Aqua dest.

2.1.7 Primers

Primers for human genes from Merck

S/N	Forward	Forward Primer Sequence	Reverse	Reverse Primer Sequence
1	SPN_F	GGCTTCTCAGCCCTGGATTT	SPN_R	CCATGTGCCCTGGGAAAGAT
2	CD19_F	TGTGTTCCCTTGTGGGCATT	CD19_R	GGTTTCCATAAGACGGGGCA
3	TNFRSF13B_F	GTCAAAGTCCGGCCAAGTCT	TNFRSF13B_R	CACTGTCTGGGATGTGTGGG
4	CR2_F	ATCTCCTCCTGTGACTCGCT	CR2_R	GCTGGCTGGGTTGTATGGAT
5	COL1A1_F	CCCAGCCACCTCAAGAGAAG	COL1A1_R	AAGCCGAATTCCTGGTCTGG
6	COL5A3_F	ATTTCTGCCCCTGTGGGATG	COL5A3_R	GGCCCAGTTCAAACCCAAAC
7	AGRN_F	ATACCTTGGCCTTTGACGGG	AGRN_R	CAGCTCTGGCTTGGTGACG
8	TCF4_F	CCGATGACGAGGGTGATGAG	TCF4_R	GTCTCCCATTCCAGGGTGTG
9	SCRIB_F	AGTCACCGGACTTTGCTGAG	SCRIB_R	GCACAGTGCCACATCTTCAG
10	SLFN11_F	TTCCTGAAGCCGAATGGTCC	SLFN11_R	AGGTGTTGTTTTGCCCTGGA
11	AHR_F	CCACTTCAGCCACCATCCAT	AHR_R	AAGCAGGCGTGCATTAGACT
12	LRRC2_F	AATAACCTGACCGACCTGCC	LRRC2_R	TGGTCCCCACTGACGACTAA
13	RAP1B_F	TGGATACTGCAGGAACGGAG	RAP1B_R	ATGACTTTTTGCGAGCCTTCC
14	PODNL1_F	AGCAAGCTGCATAGCCTTGA	PODNL1_R	CTGGGGACAGTGTGGCTAAC
15	BCAM_F	CAGCCCGGAGTATACGCTTT	BCAM_R	AAGACAGCAACGACGAGGAG
16	MPO_F	TGCTGCCCTTTGACAACCTG	MPO_R	TGCTCCCGAAGTAAGAGGGT
17	GAPDH_F	GGAGCGAGATCCCTCCAAAAT	GAPDH_R	GGCTGTTGTCATACTTCTCATGG

2.2.0 Buffer & Media Composition

2.2.1 Buffer Composition

S/N	Buffer	Composition
1	Block buffer	10% v/v Goat serum 0.01% v/v Tween 20 in DPBS
2	Cell lysis buffer	0.5% v/v Triton X-100 in DPBS
3	Dilution buffer	0.05% v/v Tween 80 in DPBS
4	0.1M Citric acid pH 5.09	4,8g Citric acid in 250 mL H_2O 14,7g Natrium citrate in 500 mL H_2O 205 mL Citric acid + 295 mL Natrium Citrate Mix gently Adjust to pH 5

5	MHC II Peroxidase Substrate buffer	1 mg O-phenylenediamine dihydrochloride per mL 0.1 M Citric acid pH 5.09 +1µL H_2O_2
6	Nitric Oxide Assay Buffer A	1% Sulphanilamide 1g Sulfanilamide in 100 mL Aqua dest.
7	Nitric Oxide Assay Buffer B	0.1% N-(1-Napthyl) ethylenediamine dihydrochloride in 5% Orthophosphoric acid (H_3PO_4) 5.82 mL H_3PO_4 + 9.2 mL distilled H_2O +0.1g N-(1-Napthyl) ethylenediamine dihydrochloride
8	Flow cytometry buffer for FC-block	1% v/v CD16/32, 1% Rat serum and 1% Syrian hamster serum in PBS
9	Flow cytometry buffer for cell staining	1% v/v FCS, 0.1 % NaN3 and 2mM EDTA in PBS
10	Lung perfusion buffer	0.2% EDTA in PBS
11	Lung & liver lysis buffer	2 tablets protease inhibitor, 0.05% Tween80 in 50 mL ddH_2O
12	Spleen lysis buffer	1 tablets protease inhibitor, 0.5% Tween80 in 25 mL ddH_2O
13	Organ digestion buffer	50 µg/mL Liberase 100 µg/mL DNase I in RPMI 1640 (without Calcium)
14	WTA buffer	1% w/v BSA, 0.05% Tween80 in ddH_2O

2.2.2 Medium Composition

S/N	Media	Composition
1	7H9 Broth	4.8g 7H9 broth 0.05% Tween80 10% OADC in 1 L H_2O
2	7H11 Agar	19g 7H11 agar 5 mL glycerol 1g Asparagine 10 % Bovine serum in 1 L H_2O

3	Murine BMDM DMEM Complete Medium	10% FCS 1% L-Glutamine 1% Herpes
4	Murine BMDM DMEM differentiation Medium	10% FCS 1% L-Glutamine 1% Herpes 10% LCSN 5% Horse Serum
5	Murine BMDM DMEM Freezing Medium	20% FCS in Murine BMDM DMEM Complete Medium 20% DMSO in Murine BMDM DMEM Complete Medium
6	Murine BMDM Medium for Infection Experiment	90% Murine BMDM DMEM Complete Medium 10% Murine BMDM DMEM differentiation Medium
7	Human PBMC & PMN Medium	10% FCS 1% L-Glutamine In RPMI medium

2.3 Thermal Cycle Programs

S/N	Thermal Cycle Programs	Cycle Description
1	RNA Denature	Preheat lid option 100 °C Cycles - 68 °C for 5 minutes - Hold at 4 °C
2	Elu-2-Frag-Prime	Preheat lid option 100 °C Cycles - 94 °C for 8 minutes - Hold at 4 °C
3	Synthesize 1st Strand	Preheat lid option 100 °C Cycles - 25 °C for 10 minutes - 42 °C for 15 minutes - 70 °C for 15 minutes - Hold at 4 °C
4	Second Strand Marking	Preheat lid option 30 °C Preheat the thermal cycler to 16 °C Incubate - 16 °C for 1 hour
5	ATAIL70	Preheat lid option 100 °C

		Cycles - 37 °C for 30 minutes - 70 °C for 5 minutes - Hold at 4 °C
6	Library PCR	Preheat lid option 100 °C 98 °C for 30 seconds 15 Cycles of - 98 °C for 10 seconds - 60 °C for 30 seconds - 72 °C for 30 seconds 70 °C for 5 minutes Hold at 4 °C
7	DNase Maxi	- 37 °C for 2 minutes
8	RT-Maxima	- 25 °C for 10 minutes - 50 °C for 10 minutes - 85 °C for 5 minutes Hold at 4 °C
9	qPCR	Pre-incubation 95 °C for 10 minutes Amplification 45 Cycles of - 95 °C for 10 seconds - 63 °C for 10 seconds - 72 °C for 10 seconds 72 °C for 1 seconds Melting curve - 95 °C for 10 seconds - 65 °C for 10 seconds - 97 °C continuous

2.4 Equipment

S/N	Devices & Equipment	Company/Source	Unique ID
1	Magnetic Stand-96	Life Technologies	AM10027
2	Film Sealing Roller for PCR Plate	BIO-RAD	MSR0001
3	Ear punch		
4	Balance	Satorius	U 5000 D
5	Balance	UniBioCAP	AP224W Shimadzu
6	Centrifuges	Thermo Scientific	Heraeus Multifuge 3SR+ Heraeus Pico 17

7	Vortexer	Scientific Industries	Vortex-Genie 2
8	Microplate shaker	Neuation Technologies	iSHAK BL UNO VT
9	NanoQuant plate and reader	Tecan	NanoQuant infinite M200 PRO
10	Plate Reader	Bio Tek	Synergy Cytation
11	Thermal Cycler	BioLab	SensoQuest Labcycler
12	Spectrophotometer	Jenway	Jenway 6320D
13	Safety workbenches	Hera Safe MSC advantage	Thermo Scientific
14	Incubators	Hera Cell	Thermo Scientific
15	Fastprep	MP Biomedicals	Fastprep-24™ 5G
16	Fluorometer	Invitrogen by Thermo Fisher Scientific	Qubit 3.0 Qubit Flex
17	Light Cycler 480 II	Roche	LightCycler 480 SN 25038
18	Microtome	Leica Biosystems	Leica RM 2155
19	Microscope	Olympia	
20	Fragment Analyzer	Advanced Analytical Technologies, Inc.	SN # 3418
21	Nextseq 500	Illumina	NB502145 NS500547

2.5 Mice

S/N	Murine strain	Genotype
1	C57Bl/6J	Wild type
2	C3HeB/FeJ	Wild type
3	B6.C3Hsst1	Congenic
4	B6.I-9.3.19.8.18	Congenic

2.6 Software

S/N	Software	Description & Version
1	Ms Word	Microsoft Office 16
2	Ms Excel	Microsoft Office 16
3	GraphPad Prism	GrapPad Prism 9.4.0
4	Biorender	
5	Fragment Analyzer control software	FA version 1.2.0.11
6	PROSize Fragment Analysis software	PROSize 3.0 3.0.1.6
7	Gen5	Gen5 v3.10
8	R R-studio	R-4.2.1 RStudio-2022.07.1

9	Magellan	Magellan 7.2
10	*i*-Control	i-control 1.12
11	Fastq illumine filter	Filter_illumina_index-1.0.4
12	FastQC	fastqc_v0.11.9
13	Cutadapt	cutadapt 2.8
14	Samtools	samtools-1.10
15	Bowtie	bowtie2-2.3.5.1
16	Tophat	tophat-2.1.1
17	Gencode	Human Gencode 41 Mouse Gencode M30
18	Prinseqlite	Prinseq-lite-0.20.4
19	KEGG	Kyoto encyclopaedia of gene and genome

2.7 Reference Genomes

S/N	Reference Genome	Description & Version
1	Murine	mm10
2	Human	hg38

3.0 Methods

The methods applied in this study are specific for each sample type and the aim of the analysis. This study was designed to cover both cellular and whole tissue transcriptome. Bacterial burden was estimated by CFU assay, MHC II expression was tested by established peroxidase ELISA; staining of murine lungs to visualize cell infiltrates and Mtb was performed. Murine lung immune cell phenotype was characterized by staining for surface markers and measured by flow cytometry. Total RNA seq after rRNA depletion was carried out for both human and murine lung samples.

3.1.1 Mtb culture

One week prior to each infection experiment, one or two 1 mL frozen stock aliquot(s) of Mtb H37Rv or *M. bovis* BCG-DsRed was/were thawed and cultured in 8-9 ml complete 7H9 broth. Additionally, 50 µg/mL Hygromycin was added to Mtb-DsRed culture. After incubation at 37 °C for 3 days, 1-2 ml of culture was passaged in 8-9 ml fresh medium, then cultured further for 3 days. Bacteria were harvested by centrifugation at 3500 *xg* 4 °C for 10 minutes. Pellet was resuspended in 1 ml DPBS and then filled up to 10ml with DPBS. After a second centrifugation wash-step (3500 *xg* 4 °C for 10 minutes), pellet was resuspended in 1 ml DPBS, followed by five times passage through a 27-gauge needle and 1ml syringe to achieve a single cell suspension. Single cell bacteria suspension was diluted 1:10 in 4% paraformaldehyde and the OD was determined at λ=580nm. For human PBMC and PMN infection, bacteria were opsonized. From the remaining bacterial suspension, 500 µL were mixed with 500 µL fresh human plasma (reserved during PBMC and PMN isolation) for opsonization, 30 minutes at RT.

3.1.2 Murine *in vitro* experiment

3.1.2.1 Preparation of murine bone marrow derived macrophages

To investigate strain specific differences in host response at the cellular level, bone marrow derived macrophages (BMDM) were prepared from 8 – 12 weeks old female C57BL/6J, C3HeB/FeJ and B6.C3Hsst1 mice. Three mice per strain were euthanized using CO_2. Mice were disinfected by dipping in 70% pure ethanol and dissected with the aid of forceps and scissors. From both hind legs, the femurs were cut above the knee and below the hip and collected in DMEM medium. After removing flesh and cartilage, bone marrow was collected

by flushing with DMEM medium with the aid of cannula. Cells were centrifuged at 485*g* 4 °C for 5 minutes. Pellet was resuspended in BMDM differentiation medium, and cells were counted. Cells were cultivated at a density of 5 x 10^6 per petri dish in 10 mL BMDM differentiation medium at 37 °C, 7% CO_2 for 5 days. Additional 5 mL medium was added to the cells and cultured further for 2days. On day 7, differentiated BMDM were harvested using cell scrapper. After harvest, the cells were centrifuged, resuspended in complete DMEM medium, and counted. Aliquots of 1 x 10^7 BMDM in 1 mL BMDM freeze medium were prepared and preserved as frozen stocks in liquid Nitrogen. For each BMDM *in-vitro* experiment, thawed cells were washed twice and counted before seeding at a density of 1 x 10^5 per well in a 96-well plate flat bottom.

3.1.2.2 BMDM MHC II expression and Nitric oxide secretion

To determine the host cell specific response to inflammatory stimuli, 1 x 10^5 BMDM from B6, C3HeB/FeJ and congenic B6.C3Hsst1 mice were untreated, treated overnight with 500 IFN-ɤ only, 20ng/mL TNF-α only, 1µg/mL LPS only, 500 IFN-ɤ and 20ng/mL TNF-α, or 500 IFN-α and 1µg/mL LPS and incubated overnight at 37 °C. The cell supernatants were transferred to 96 well plate and frozen at -20 C for Nitric oxide (NO) measurement.

For MHC II expression assay, cells were fixed with 150 µL 4% paraformaldehyde for 30 – 45 min at RT. Fixed cells were then incubated overnight in 200 µL block buffer (10% Goat serum and 0.01% Tween 20 in PBS) at 4 °C. The buffer was then exchanged with 200 µL unlabelled primary antibody (TIB 120 MHC II 1:500 in block buffer) and incubated for about 30 min -1 h at RT, then washed with PBS. After washing, 200 µL secondary antibody (Goat anti-rat peroxidase diluted 1:2000 in block buffer) was added per well and incubated for 30 min – 1h at RT, then washed with PBS. Afterwards, 100 µL of MHC II peroxidase substrate buffer was added per well, the reaction was stopped with 50 µL/ well 25% Sulphuric acid. The optical density (OD 490 nm) was determined on the Tecan reader, measurement was taken using the Magellan 7.0 software.

Nitric oxide test buffer A (1% Sulphanilamide) and buffer B (0.1% N-(1-Napthyl) ethylenediamine dihydrochloride in 5% Orthophosphoric acid) were prepared as previously described[55]. For buffer A, 1g Sulphanilamide was weighed and transferred to a 200 mL bottle with a magnetic stirrer. To dissolve solute thoroughly, first 50 mL distilled water was added

to the bottle containing 1g sulphanilamide and stirred at 500 mot, 100 °C for 1 - 2h, then filled up to 100 mL. For buffer B, 5.82mL of H3PO4 was added to 94.2 mL distilled water (5% orthophosphoric acid), then 50 mL of the diluted acid was added to 0.1g N-(naphthyl) ethylene dihydrochloride, thoroughly mixed at 500 mot, 100 °C for 1 – 2h, then filled up to 100 mL with the remaining diluted acid. Buffer B wrapped with aluminium foil and kept in dark. For each reaction, 25 µL of buffer A, 25 µL of buffer B and 50 µL of sample or standard was added per well and incubated at RT for 15 min. Serial dilutions of Sodium Nitrite ($NaNO_2$ in PBS) was done to generate standard curve. With PBS as blank for standard and cell medium as blank for cell supernatant, OD 540 nm was measured on the Tecan reader Megallan 7.0. and the amount of NO in each sample was calculated on Excel sheet using the Trend formula.

3.1.2.3 BMDM CFU and LDH assay

To determine Mtb growth rate in the cells, and Mtb induced necrotic cell death, bacterial colony forming units (CFU) and lactate dehydrogenase (LDH) enzyme activity assays were performed. Frozen stocks of BMDM from C57BL/6J mice (B6), C3HeB/FeJ (C3H) and congenic B6.C3Hsst1 mice were thawed, washed, and seeded at cell density 1 x 10^5 per well in a 96-well plate flat bottom. Cells were either untreated (IFN-$\gamma^{-/-}$); pre-treated but not maintained (IFN-$\gamma^{+/-}$); not pre-treated but maintained (IFN-$\gamma^{-/+}$); or pre-treated and maintained (IFN-$\gamma^{+/+}$) in 500 units/mL IFN-γ. Cells were infected with 1 x 10^5 Mtb (MOI=1) and incubated 37 °C 7.5 % CO_2. Culture mediums in cells for 1d, 2d and 3d time points culture medium was exchanged with fresh medium with or without 500 units/mL IFN-γ at 2h post infection. At each time point, cell supernatants were collected and stored at -80 °C for LDH assay. For CFU assay, cells were lysed, plated on agar, incubated at 37 °C for 3 weeks and bacteria colonies were counted.

The LDH is an enzyme located in the cell cytoplasm which when found in cell culture supernatant can be measured to estimate the extent of necrotic cell death. Necrosis leads to damage of cell plasma membrane, therefore contents of the intracellular milieu leaks into the extracellular environment. The LDH assay is an enzyme substrate reaction. The enzyme was provided with the substrate, lactate, and a tetrazolium salt. This leads to catalytic oxidation of lactate to pyruvate and production of nicotinamide adenine dinucleotide (NADH). The NADH converts the tetrazolium salt to a coloured product whose absorbance can be

measured. Lysing the total cell to induce release of relatively all LDH enzyme gives the 100% LDH activity, hence mathematically the percentage LDH activity in the cell can be calculated with relative to the 100% LDH activity as previously reported [56] (see % LDH activity calculation below). The LDH assay was performed with the LDH kit from Roche. In each well of a flat bottom 96-well plate, 50 µL of the LDH buffer was mixed with 50 µL of samples, 0.5% Triton X-100 lysed cells, for 100% LDH activity values, or cell medium, for 0% or blank values, then incubated at RT for 30 min. The OD 490 nm was measured on the BioTek reader with the Gen5 software.

$$\%LDH\ Activity = \left(\frac{OD\ test\ values - OD\ blank\ values}{OD\ 100\%\ values - OD\ blank\ values}\right) * 100$$

3.2 Human leukocyte *in vitro* experiment

The human blood is a fluid tissue that is composed of many cells. The white-blood cells (leukocytes) are uniquely generated from the bone marrow to meet both homeostatic and immune defence need of the human body.

PBMC and PMN perform dual role of fighting against pathogen and removing dead cells after pathogen control is complete. Therefore, these two largely defined cell populations are attractive tools for in vitro studies including diagnostics and therapeutic studies.

3.2.1 PBMC & PMN isolation

Peripheral blood mononuclear cells (PBMC) and Neutrophils also known as polymorphonuclear (PMN) cells were isolated from 60 mL heparinized human peripheral blood derived from anonymous donors. 30 mL blood was slowly overlaid on 20 mL Histopaque by pipetting and centrifuged at 800 *xg* for 20 minutes at room temperature (RT), acceleration 7, break 1. After separation, 5 mL serum was reserved for opsonization of bacteria. The first phase or ring of PBMC was pipetted into new tube and filled up to 50 mL with RPMI, followed by washing and enumeration of the cell numbers. The second phase above the erythrocyte layer was pipetted into new tube and filled up to 50 mL with RPMI medium and centrifuged at 485 *xg* at RT for 5 minutes. Supernatant was carefully discarded, and the cell pellet was resuspended in 2 mL RPMI medium. Percoll 100% was prepared by mixing 45 mL Percoll and 5 mL 10X DPBS. Percoll density gradient 85%, 80%, 75%, 70% and 65% was prepared by mixing

8.5 mL, 8 mL, 7.5 mL, 7 mL, and 6.5 mL 100% Percoll with 1.5 mL, 2 mL, 2.5 mL, 3 mL, and 3.5 mL DPBS respectively. To further purify the PMN, Percoll density gradient was prepared by slowly pipetting 2 mL 85%, 80%, 75%, 70% and 65% Percoll solutions on top of each other in a 15 mL Falcon tube. The 2 mL cell suspension was then pipetted on the 65% Percoll solution and centrifugation was done at 800 g for 20 minutes at RT, acceleration 7, break 1. PMN that settled between the 75% and 70% layer were isolated into a fresh 50 mL tube which was filled up with RPMI and washed by centrifugation (485 *xg* at RT for 5 minutes). Supernatant was discarded, and the cell pellet was resuspended in 1ml complete RPMI medium for PMN. Cell numbers were determined using 1:100 dilution in a Neubauer counting chamber.

3.2.2 PBMC & PMN infection, RNA extraction and Microscopy

For RNA extraction, 8 – 10 x 10^6 PBMC and PMN were seeded per well in a 24 well plate with or without Mtb infection, MOI = 3. Uninfected and Mtb infected cells were incubated overnight at 5% CO_2. Cells were centrifuged at 485*g* 5minutes 4 °C. After removing the supernatant, cell pellet was resuspended in 500 µL Trizol and samples were frozen at -80 °C until RNA extraction. For Microscopy, 3 x 10^6 PBMC and PMN were seeded in a culture chamber slide, also infected at MOI of 3. Uninfected and Mtb infected cells were incubated overnight at 5% CO_2. Cells were fixed with 4% PFA.

3.2.3 PBMC & PMN Acid fast and haematoxylin combined staining

This combined acid fast and haematoxylin staining helps to visualize the acid fast mycobacterial and cell nucleus.

PFA were removed by pipetting. Fixed cells were left to air dry then rinsed with water. Cells were stained for 4 min with TB Carbolfuchsin and rinsed gently under running water. After rinsing, the samples were immersed in 2 – 3 cuvettes of TB decolorizer to remove excess Carbolfuchsin dye. Samples were then rinsed shortly in water and stained with Meyer's Hematoxylin for 1 min, then rinsed again with water. Samples were dehydrated with 96% ethanol, 2 x 2min 100% ethanol and immersed in Xylol, then embedded in Entellan.

3.3 Animal experiment

First, we focused on the resistant B6 and the susceptible B6.I-9.3.19.8 to understand the role of the MHC II locus I-9.3.19.8 from susceptible I/St mice in mediating disease pathology. This was done in collaboration with our colleagues in Moscow, Russia, specifically the Laboratory for Immunogenetics as headed by Prof. Alex Apt. Inbred resistant C57BL/6JCit (B6) and relatively susceptible B6.I-9.3.19.8/Cit (9.3.19.8) were bred at the Animal Facility in Moscow, all experimental protocols were approved by the Animal care committee (IACUC protocols #2, 7, 8, 11 approved March 8, 2017). We received RNA samples and processed the samples for transcriptome analysis.

Secondly, we studied the role of the super susceptibility to tuberculosis (*sst1*) locus in B6.C3Hsst1 congenic mice in contrast to resistant B6 mice following aerosol infection. This animal experiment was approved under the license V 242-15929/2021. Inbred resistant C57BL/6J (B6) and relatively susceptible B6.C3Hsst1 were bred at the Animal Facility in FZB, all experimental protocols were approved by the Animal care committee. We analysed the bacterial load in the lung, liver, and spleen, and further characterised the lung pathology and immune cell phenotype. This animal experiment was divided into two consecutive experiments with three (3) time points (See appendix 7.2).

3.3.1 Aerosol infection

Inbred resistant C57BL/6J (B6) and relatively susceptible B6.C3Hsst1 were bred at the Animal Facility in FZB, experimental protocols were approved by the ethics committee. All precautions and preparation for aerosol infection according to internal standard of the Research Center Biosafety level 3 was adhered to. 8 – 14 weeks old female C57BL/6 and B6.C3Hsst1 were infected per aerosol with Mtb H37Rv. Bacterial stock for aerosol infection was thawed. The Microbiological safety cabinet KC-1 and Inhalation Exposure System (IES, Glascoll) with Ventri-unit were switched on. The mice were placed individually into the special designed cage system with holder and metal disc for closing. Thawed bacterial infection stock was passed 10x through 1 mL syringe 18G Cannula to achieve single bacteria cell suspension. Calculated volume for 100 CFU infection dose was diluted in 10mL water and injected into the nebulizer. The aerosol device was set to 900s preheat, 2400s nebulizing time, 2400s cloud decay time. And 900s decontamination time. At the end of the aerosol cycle, mice were transferred to the experimental cages with food and water. At day 1 post aerosol infection, 2

– 3 mice were sacrificed by $C0_2$, mice were dissected and whole lung were homogenized in 1 mL WTA buffer and plated on 7H11 agar, 10 plates per mice 100µL each. Plates were then incubated for 28 days, and bacterial colonies were counted to estimate the infection dose delivered to the lungs of the mice. At each experimental time points, 4 to 10 mice per group were sacrificed for end point read-outs which include mycobacterial load, lung histology, immune cell phenotype, cytokine, chemokine assay and lung transcriptome.

3.3.2 Scoring

Prior to aerosol infection, the mice ear marked for easy identification, then weighed. After aerosol infection, infected and uninfected mice were scored (scale of 1 – 5) once weekly according to the four criteria on Table 1 below. An average score from each criterion was calculated and mice with average score below 3 were to be sacrificed and removed from the experiment in accordance with animal protection act.

Table 1: Mice scoring

Score	Activity	Body weight	Appearance	Behaviour
1	Very active	Unaffected or increased	Shiny and smooth skin or fur	Normal
2	Active	<10% reduction	Minor skin or fur defect	Minor deviation
3	Less active	10 – 20% reduction	Dull fur, irregular body openings, and increased muscle tone	Restriction in movement, unusual behaviour
4	Minor to no activity	20 – 30 % reduction	Unkempt fur, abnormal muscle tone, shivering and/or abnormal posture	Isolated, lethargic, and aggressive
5	Not active	>30% reduction	Cramps, paralysis, cold and shivering	Auto aggression and pain during handling

3.3.3 Lung histology

Mice were sacrificed by CO_2, disinfected, and dissected. To reduce the frequency of blood cells in the lung, perfusion was done. The lung was excised and fixed in 4% PFA 4 °C overnight, then transferred into PBS and stored at 4 °C. To visualize the lung lesions and the bacteria in the lungs, paraffin embedded lung sections were processed and stained (Haematoxylin, Eosin (HE), Ziehl-Neelsen (ZN) and Masson Goldner (MG) staining procedures).

3.3.3.1 Paraffin embedding and sectioning

Fixed lungs from uninfected and infected mice were dehydrated in increasing ethanol concentrations (Autotechnikon Microm, STP 120, Thermo Fisher). Then incubated in Xylene and embedded in 65 °C heated paraffin casting station (Leica EG1140C), see table 2 below. The paraffin embedded blocks were sectioned (Leica RM 2155) and expanded in a 37 °C paraffin stretch bath (Leica 1052). Samples were picked out of the water bath carefully with slides (Superfrost® microscope slide). Two consecutive sections of the lung lobes of each mouse were mounted on each slide. The samples were dried overnight at 37 °C. Prior to each staining procedure, paraffin was removed from each sample immersion in Xylene and decreasing concentrations of ethanol and rinsed in distilled water see table 3. Processed lung samples were arranged on a staining rack. Stain reagents were prepared and filled into glass cuvettes. After each staining procedure, samples were dehydrated. Dehydrated samples were immersed in Xylene. Samples were then embedded in Entellan and covered with glass slips carefully without air bubbles on samples.

Table 2: Workflow for paraffin embedding

Step	**Time (h)**
4% PFA	1
70% Ethanol	1
80% Ethanol	1
90% Ethanol	1
96% Ethanol	1
100% Ethanol	3 x 1
Xylene	2 x 1
Paraffin 65 °C	2 x 1.5

Table 3: Workflow for paraffin removal

Step	Time
Xylene	2 x 10 min
100% Ethanol	2 x 2 min
96% Ethanol	2 x 2 min
70% Ethanol	2 min
Distilled H_2O	2 min

3.3.3.2 Haematoxylin Eosin staining

The HE staining procedure helps to identify cell types and tissue structure. Cell nucleus stain retain the blue colour of the primary dye while the cytoplasm and other tissue structures are counter stained with the pink Eosin dye.

Samples were immersed in Meyer's Haematoxylin for 10 min and rinsed under running water until ridded of excess dye, then counter stained in Eosin for 1 min and rinsed shortly in distilled water. Stained samples were then dehydrated in increasing series of ethanol (70%, 96% and 100%), 2 min each.

3.3.3.3 Ziehl Neelsen staining

This differential staining procedure helps to visualize mycobacteria which are stained red by the Carbolfuchsin dye.

Samples were immersed three times in Carbolfuchsin and warmed gently over flame, then allowed to cool for about 5 min. Samples were then immersed in water and then 1 min in Methylene blue. Samples were then rinsed by immersing in 2 times in water, then dehydrated in 96% and 2 x 100% ethanol, 2 min each.

3.3.3.4 Masson Goldner staining

The Masson Goldner staining procedure helps to visualize collagen fibres and thus provide a clear contrast for the granulomatous lung lesion.

Samples were immersed in haematoxylin (Wiegert A) for 15 min, then rinsed under running water for about 8 min. Afterwards the samples were stained with Acid fuchsin-Ponceau-Azophloxin for 4min, then 1% Acetic acid for 30 sec. The samples were then stained with Phosphomolybdic acid orange G for 30 min, and immersed again in 1% Acetic acid for 30 sec. The samples were then stained with the light green-Goldner III dye for 6 min and immersed in 1% Acetic acid for 2min then rinsed under running water for 2min. Dehydration was done once in 96% ethanol and 2x 100% ethanol and immersed in Xylene, followed by embedding in Entellan.

3.3.4 Lung immune cell phenotype

Mice were euthanized by CO_2 inhalation. Euthanized mice were dipped briefly in 70% ethanol to disinfect prior to dissection. Lung perfusion was done to reduce circulating blood cells. Perfused lungs were minced and transferred into 50mL tubes containing 2mL organ digestion buffer. Enzymatic digestion was done at 37 °C 1h 30min in water bath with shaking. Cells were pressed gently through 70 µM cell strainer and the strainer were rinsed with 20 mL cold FACS buffer. Afterwards, cells were centrifuged at 485*g*, 4 °C for 5minutes and supernatants were discarded, and the cell pellets were resuspended in 5 mL 1X erythrocyte lysis buffer and incubated for 1 min. Lysis was stopped with 20 mL FACS buffer and cell suspension was again filtered through 70 µM cell strainer. Followed by centrifugation at 485*g*, 4 °C for 5minutes. Supernatants were discarded and cell pellets were resuspended in 1 mL FACS buffer. Cells were counted on the ViCell automated cell counter, and 1 x 10^5 cell in 150µL FACS buffer were pipetted into 96-well plate U-bottom. Cells were then centrifuged at 485 *xg*, 4 °C for 5minutes, and supernatants were discarded. Cell pellets were resuspended in 100 µL Fc-block solution and incubated for 10 minutes at RT followed by centrifugation at 485*g*, 4 °C for 5 minutes.

Supernatants were discarded, and cell pellets were suspended in antibody solution. Unstained cells were resuspended in FACS buffer. Incubation was done in the dark at RT for 15minutes. Cells were then centrifuged at 485 *xg*, 4 °C for 5minutes, supernatants discarded, and cell pellet resuspended in 4% paraformaldehyde, incubated for 15 min at RT and again washed by centrifugation at 485 *xg*, 4 °C for 5 minutes. Supernatant were discarded, and cell pellet were resuspended in 180 µL PBS.

Samples were wrapped in aluminum foil and kept in dark until analysis on FACS Canto flow cytometer.

3.3.5 Cytokine Assay

Cytokine concentrations were measured using the Legendplex murine inflammation panel kit. The assay was performed according to the manufacturer's kit manual. Murine lung homogenates were transferred into spin-X tubes and centrifuged 1500g 4 °C 5min. Tissue, debris, and cell-free supernatants were stored transferred into sterile 96-well plate. 25 µL of assay buffer, pre-mixed beads (having different sizes and granularity specific for each cytokine) and either prepared standards or samples were mixed and incubated with shaking for 2 hours at RT. Beads were pelleted by centrifugation and supernatants were discarded. After washing, pellets were resuspended in 25 µL detection antibody solution and incubated with shaking for 1 hour followed by addition of 25 µL SA-PE and incubation for 30 minutes with shaking. Centrifugation and washing steps were repeated and pellets were resuspended in wash buffer. Data acquisition was done on the MACSQuant 10 flow cytometer, and the FCS files were analyzed online with the Legendplex software.

3.4 RNA extraction and library preparation

To analyse the host transcriptome by RNA-seq, RNA was extracted from host cells and lung samples (see table 4). Minced lungs in Trizol were processed with FASTprep and RNA samples were extracted using the Zymo RNA MiniPrep kit. RNA samples were quantified on TECAN reader by measuring the OD ratio at wavelength ratio 260 nm to 280 nm using the iControl software. Fragment analysis of the RNA samples was done using DNF-472 High Sensitivity RNA Analysis Kit, 15 nt. With starting concentration of 100ng/µL DNase treated (RNA clean and concentrator™ -5, Zymo Research) total RNA were prepared for sequencing using the TruSeq® Stranded Total RNA Library prep globin kit with Ribo-zero. RNA and DNA library fragments were measured using the Advanced Analytical Fragment Analyzer and analysed with the PROSize software. Quantification of the DNA library was done on the Quibit device with the Qubit 1X dsDNA High Sensitivity Assay kit. Fragment analysis of library for sequencing was done using the DNF-473 Standard Sensitivity Analysis Kit. Library was diluted to 10 nM each, normalized, denatured, and pooled for sequencing. Final concentration of pooled library was about 1.3 – 1.8pM with 8 – 12 samples per run. Sequencing was done on Illumina Nextseq® instrument with Nextseq® 500/550 High output kit v2, 150 cycles. Pre-processing and demultiplexing of the data was done on Illumina BaseSpace. See section 3.5 below for bioinformatic analysis.

Table 4: Description of RNA samples

Sample types		Number of samples/ donor
Human	FCT	20, n = 10
	NON-FCT	12, n = 6
	NON-TB	12, n = 6
	In Vitro (human PBMC and PMN)	12, n = 3
Murine	B6 versus B6.I-9.3.19.8	45
	B6 versus B6.C3Hsst1	84

3.5 Bioinformatic Analysis

After quality filtering and trimming of bad quality nucleotides as well as adapter sequences using the programs cutadapt and prinseq, reads were mapped with Tophat2 against the murine reference mm10 or human hg38 as appropriate. HTSeq with the Gencode annotation M15 was applied to compute the read counts per gene. Differentially expressed genes were determined with the R package DeSeq2 followed by gene set enrichment analyses with the online tools InnateDB for KEGG pathways and g:Profiler for gene ontology terms. All protein-protein interaction networks were based on connections annotated in the STRING database with medium confidence scores.

3.6 Quantitative Polymerase Chain Reaction (qPCR)

To validate some of the genes differentially expressed in the RNAseq data, qPCR was done. Human RNA samples were DNAse treated (Thermal cycling program DNase Maxima) and transcribed to cDNA (Thermal cycling program RT Maxima). Primers were diluted in nuclease free water to 100 µM. Serial dilution (100%, 50%, 10%, 1%, 0.5%, and 0.1%, nuclease free water control 0%) of pooled cDNA samples was prepared to generate standard curve and calculate the efficiency for each primer. Each sample were then processed with each primer for qPCR. Primer standard and samples were amplified on the LC480 Thermal cycler (Thermal cycling program qPCR). See tables 4, 5 and 6 below for reaction mix for DNase treatment, cDNA synthesis and qPCR.

Table 5: DNase reaction mix

Reagent	Volume per sample
10X DsDNase buffer	1 µL
dsDNase	1µL
Template RNA	8 µL

Total volume per well = 10 µL

Table 6: Transcribe RNA to cDNA reaction mix

Reagent	Volume per sample
5X Reaction Mix	4 µL
Maxima Enzyme Mix	2 µL
Nuclease free water	6 µL
DNase treated sample (table 4)	10 µL

Total volume per well = 20 µL

Table 7: qPCR reaction mix

Reagent	Volume per sample
Nuclease free water	3.8 µL
Roche Syber green master mix	5 µL
Primer Mix (100 µM)	0.2 µL
Standard or Sample	1 µL

Total volume per well = 10 µL

4.0 Results

4.1.0 Study Design

The purpose of this study is to understand human and murine host responses based on transcriptome changes in response to Mtb infection. The study was designed as shown in Fig 4.1 below. RNA transcripts from excised lung tissue of TB patient with control samples (Clinical study) were compared to human leukocytes transcripts (*in vitro* experiment) and transcripts from Mtb infected lungs of resistant wild type and susceptible congenic mice (*in vivo* experiments).

First, host response to Mtb infection was characterized in clinical samples. Excised lung tissue from 16 TB patients were compared to 6 non-TB samples with universal human reference RNA (UHR) as control.

Secondly, differences in disease response were characterized *in vitro* with human and murine cells. Human PMN and PBMCs were cultured with or without Mtb and the transcriptome were analysed. Murine BMDM were cultured with or without co-stimulatory molecules and assayed to identify specific differences in MHC II expression, nitric oxide secretion and lactate dehydrogenase release.

Furthermore, established *in vivo* mouse models were profiled and sequenced for differences in disease burden and control of Mtb. B6.I-9.3.19.8 and B6.C3Hsst1 were studied in contrast to the wild type B6 mice.

I.

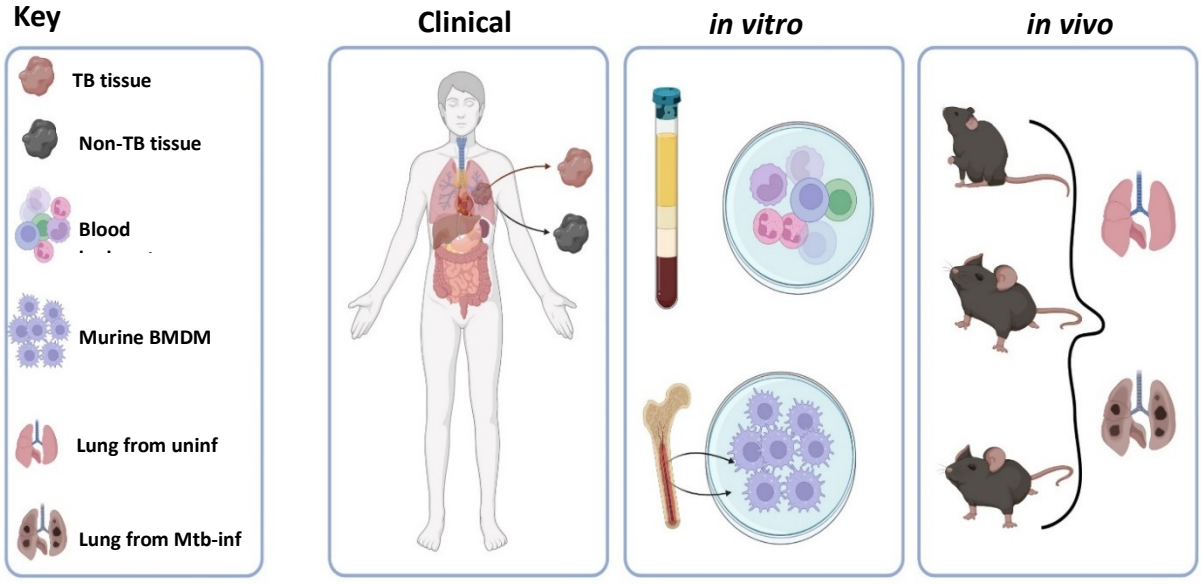

II.

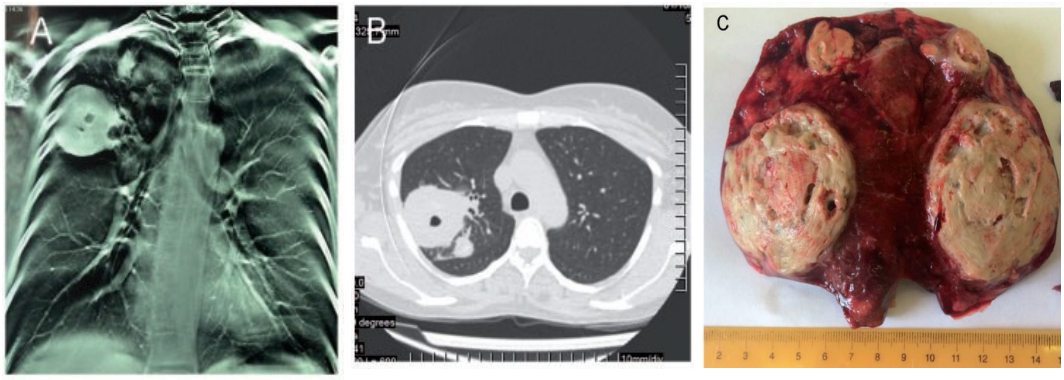

Fig. 4.1: Clinical and experimental TB studies. Host gene response to Mtb infection was analysed *in vitro* and *ex vivo*. (I) Study design, RNA from wall and parenchyma of TB and control non-TB human samples, human leukocytes from peripheral blood, murine bone marrow derived macrophages, and murine lung RNA were studied. (II) An example of excised lung specimen X-ray (A) CT-Scan (B) and photograph (C), Pictures II provided by Vladimir Yeremeev. *Figure 4.1 (I) designed using Biorender.

4.1.1 Human TB: Differentially expressed genes in human samples

In human TB, the pathogen is contained within the lung in a structure called granuloma. The granuloma is a niche that prevents the bacteria from causing damage to the host. In rare cases of TB, the area of the lung occupied by the granuloma may have to be surgically removed to improve patient health[50,57,58]. Most studies on the human TB granuloma provide detailed description of the granuloma architecture but not a comparative analysis of the host lesion specific transcriptomes. Transcriptional changes within the granuloma offers a complex detail of gene regulation potentially induced either as defence mechanisms against the bacteria or potentially pathogenic tissue reaction[41,59,60].

To study these transcriptional changes, RNA samples extracted from excised lung tissue of 22 patients were sequenced. From each patient's tissue material, two samples were prepared,

one from the granuloma “affected area” termed wall and the other one from the “relatively healthy” surrounding parenchyma tissue (PT). The 16 TB samples were grouped into two according to the granuloma morphology; 10 were categorized as fibro-cavernous tuberculoma (FCT), and the other 6 were non-FCT. At the start of TB treatment, all patients had drug susceptible TB except one patient who had isoniazid resistant TB. All patients were HIV negative. The control (non-TB) samples were associated healthy tissue samples from 6 cancer patients with varied forms of adenocarcinoma, alveolitis and Hodgkin’s lymphoma. There were also two samples each from the control non-TB patients, one sample from the wall and one sample from the parenchyma.

Out of the 44 human tissue RNA samples sequenced, 38 samples have >5000 genes covered with at least 5 reads mapped to the reference genome (Fig. 4.2). The cluster analysis shows that the sample do not clearly separate into distinct groups. TB and control samples nearly form a distinct cluster except for one control sample clustering within the TB samples (Fig. 4.2A). All the TB and non-TB samples from the wall (Fig 4.2A) and the parenchyma (Fig 4.2B) irregularly cluster around each other giving the impression that the gene expression in all samples are neither clearly different nor the same (Fig 4.2 C and D). However, the global comparison of all TB versus non-TB samples revealed a distinguished clustering (Fig. 4.2E).

A. **Gene Coverage (wall)**

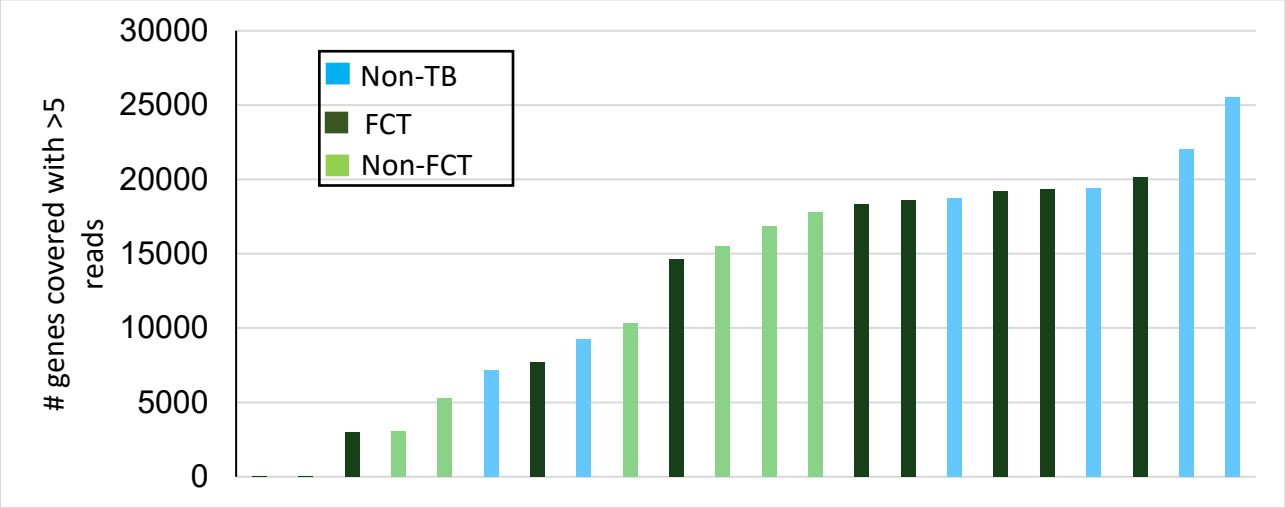

B. **Gene Coverage (pt)**

Samples n = 22

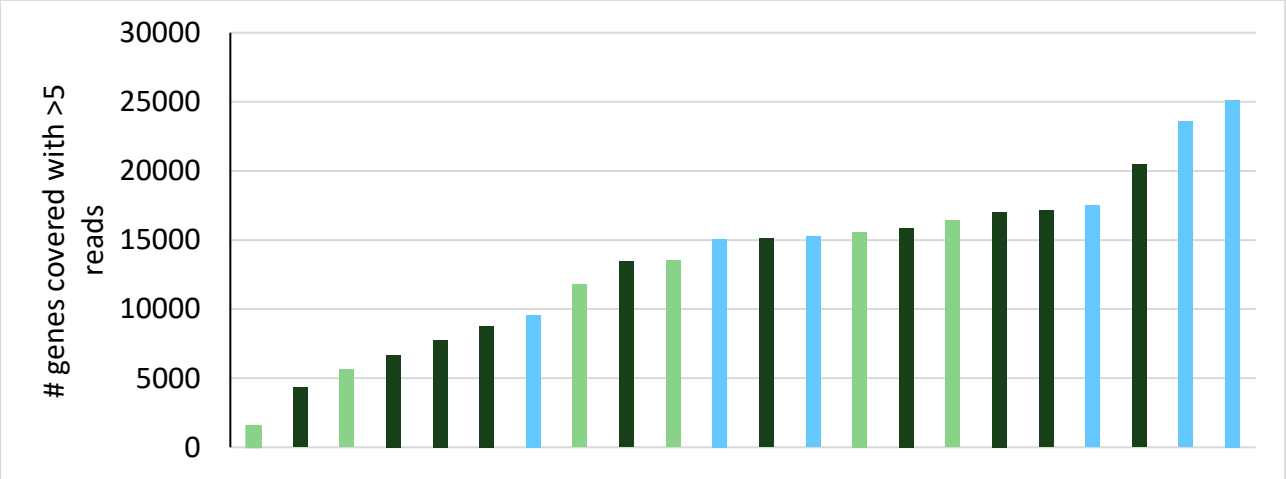

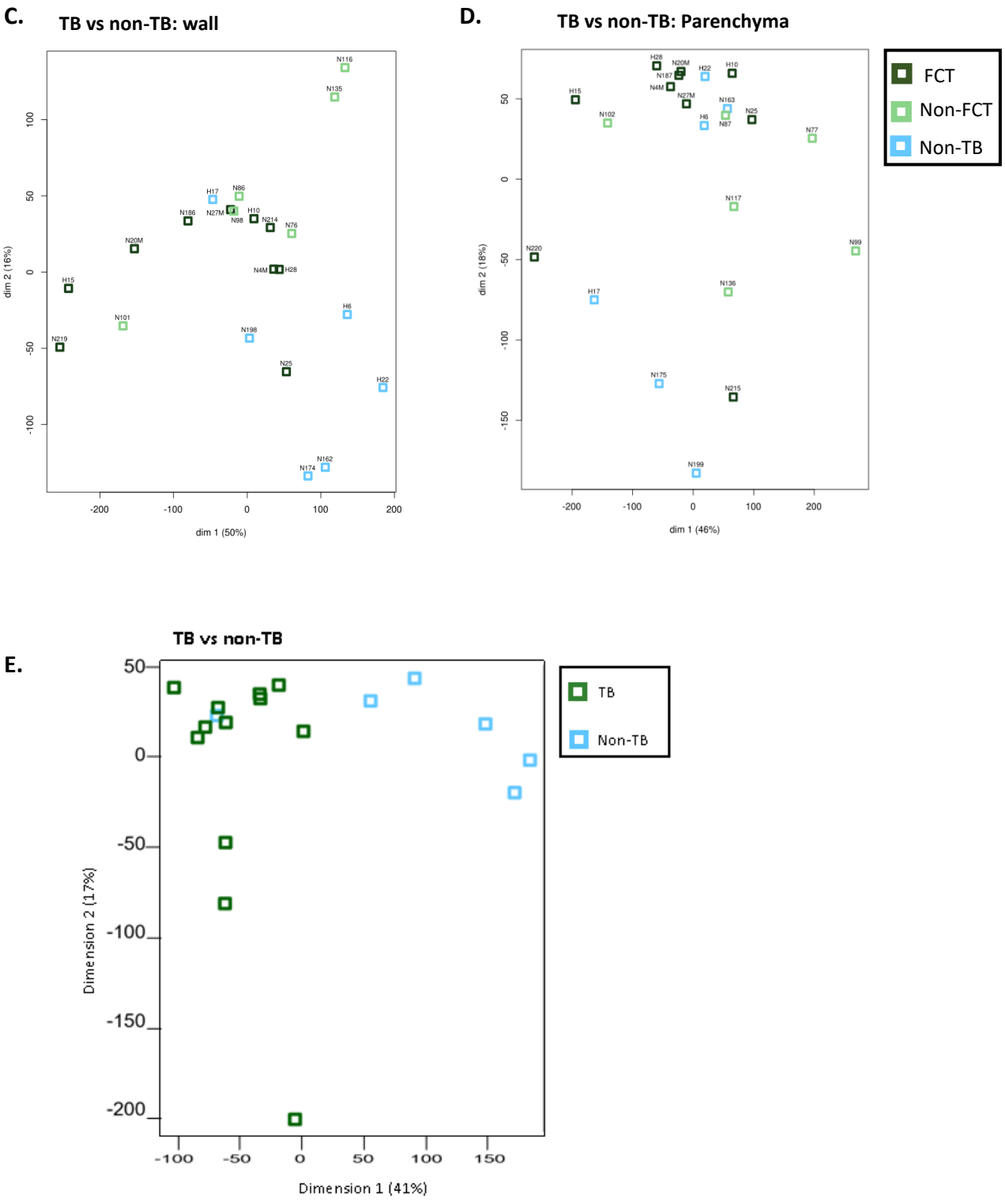

Fig. 4.2: Gene coverage and sample clustering analysis of the TB and control samples. Total RNA was extracted from 44 human TB and non-TB samples, depleted of rRNA and sequenced. Gene coverage

of **A.** samples from the wall and **B.** the samples from parenchyma tissue (pt). Multi-dimensional scale plots with dimension 1 (x-axis) and dimension 2 (y-axis) **C.** for samples from the wall and **D.** samples from the parenchyma tissue (FCT dark green, non-FCT light green and non-TB blue). **E.** Unique clusters of the TB (dark green) versus the control non-TB (blue) samples. Total number of samples n= 22.

Considering samples from the wall only, TB and non-TB sequences were probed for the top 50 differentially expressed genes. The differentially regulated genes are shown as heatmap in Fig. 4.3. Genes upregulated in the human TB samples (red) which are down regulated in non-TB samples (blue) are protein encoding genes that are important for cellular functions including transcription, assembly of actin cytoskeleton, cell adhesion, differentiation, and migration. In contrast, the genes downregulated in TB but upregulated in non-TB samples are genes connected to various transcriptional repressors, tumour suppressor, neurodegeneration, and cancer pathways (Fig. 4.3). However, two samples seem to slightly deviate (top arrows Fig. 4.3) and do not entirely show similar expression patterns within the TB and non-TB samples. This could be due to sample cross-contamination during the library preparation steps.

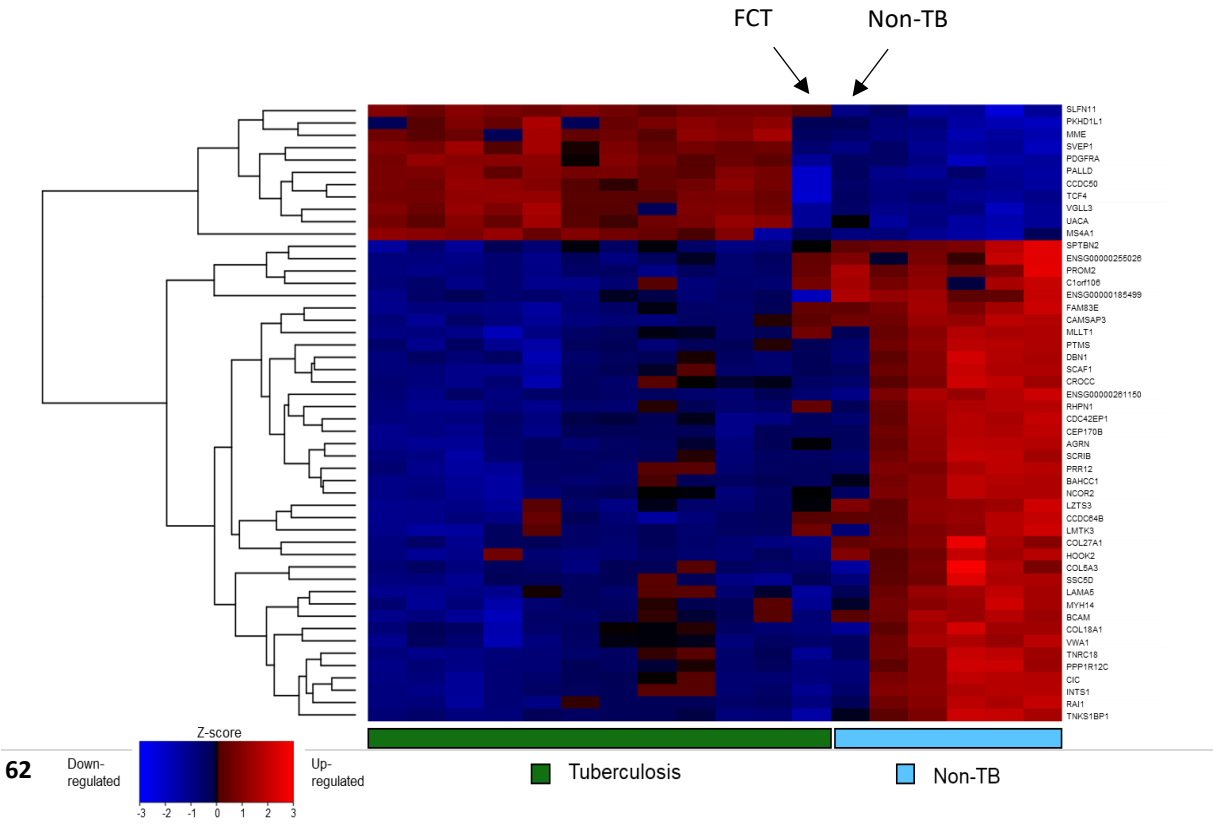

Fig. 4.3: The top 50 significantly differentially expressed genes. Total RNA was extracted from 18 clinical samples and sequenced after rRNA depletion. Good quality reads were mapped to the human genome and top 50 ($p < 0.05$) significantly differentially expressed genes were filtered, for visualization, upregulated genes are in red and downregulated are in blue (Z-score -3 to +3, to the left are Tuberculosis (TB) samples in green and right are the control non-TB samples (cyan). The gene names are indicated on the far right of the heatmap.

Genes that were upregulated in TB but downregulated in non-TB samples from wall as shown in the heatmap in Fig 4.3 are linked to “immune response”, “tissue remodelling” and “cellular signalling” to contain and resolve TB.

4.1.2 Differentially regulated pathways and network in human TB

Recognizing that most of the genes that were upregulated are in the control non-TB samples, a network analysis (Fig. 4.4A) was done for the significantly differentially regulated genes with the control samples only. Then the network was queried with the FCT and Non-FCT data sets to identify the genes that are differentially expressed in the FCT data set only (dark green), non-FCT data set only (light green) or in both FCT and non-FCT data sets (blue) in comparison to the control. The lines connecting the dots (genes) in the network means that the genes may be functionally linked to the same cellular processes.

A.

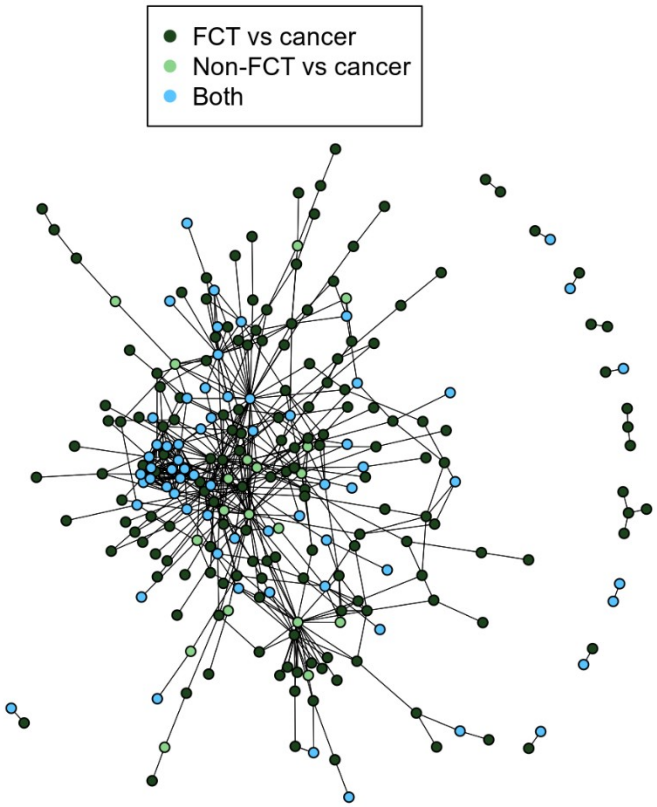
FCT vs cancer
Non-FCT vs cancer
Both

B.

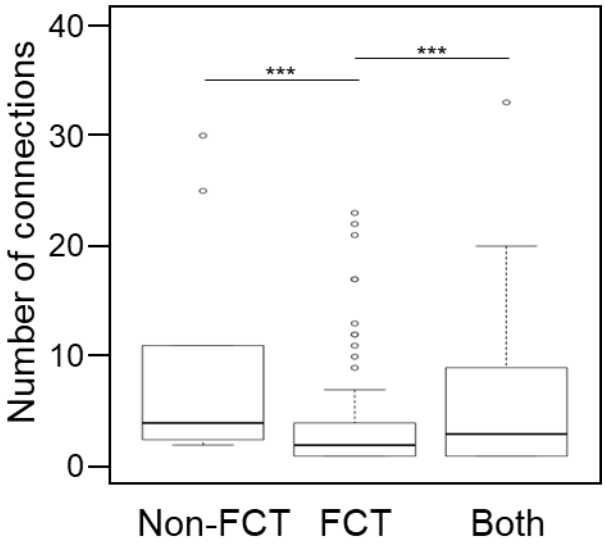
Number of connections
40
30
20
10
0
***
***
Non-FCT
FCT
Both

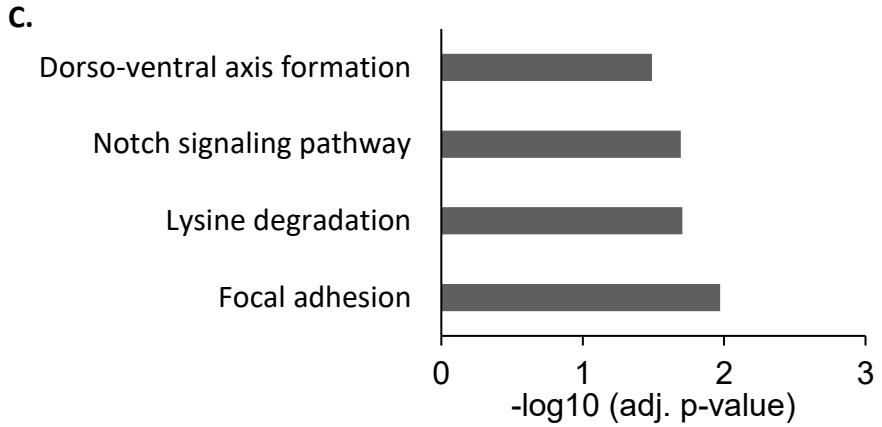

Fig. 4.4: Network interaction and KEGG pathways differentially regulated in human tissue samples. Gene-gene interaction analysis of non-TB data with genes differentially regulated in **A.** non-FCT (light green) and FCT (dark gene) and are also regulated in both data sets (blue) were computed, **B.** number of connections for FCT, Non-FCT and both data sets, and **C.** the pathways identified by KEGG analysis.

The central genes holding the network together are important for each pathway they regulate. The number of connections in the data sets were counted and are represented in Fig. 4.4B. The differentially expressed genes in both FCT and non-FCT data set in comparison to the control are genes connected to dorso-ventral axis formation, notch signalling pathway, lysine degradation and focal adhesion, and are significantly regulated KEGG pathways (Fig. 4.4C).

Furthermore, network interaction analysis was done for the TB data sets. Within the Non-FCT data sets, only 2 genes were significantly differentially regulated between the wall and the parenchyma and no KEGG pathway was identified. These two genes are not yet characterized nor annotated in gene ontology. However, there is an ID for both genes, they are ENSG00000275530 and ENSG00000260757. In contrast, within the FCT data set, network analysis was done for genes differentially regulated between the wall and parenchyma (pt) as shown in Fig. 4.5 A, with upregulated genes in the wall (red), which are downregulated in the

parenchyma, and downregulated genes in the wall (blue), which are upregulated in the parenchyma. Enriched pathways as analysed by KEGG for the network in Fig 4.5 A are represented in Fig. 4.5 B. The four differentially regulated pathways as identified by KEGG were focal adhesion, B cell receptor signalling pathway, Extracellular matrix (ECM) receptor interaction and primary immunodeficiency.

A.

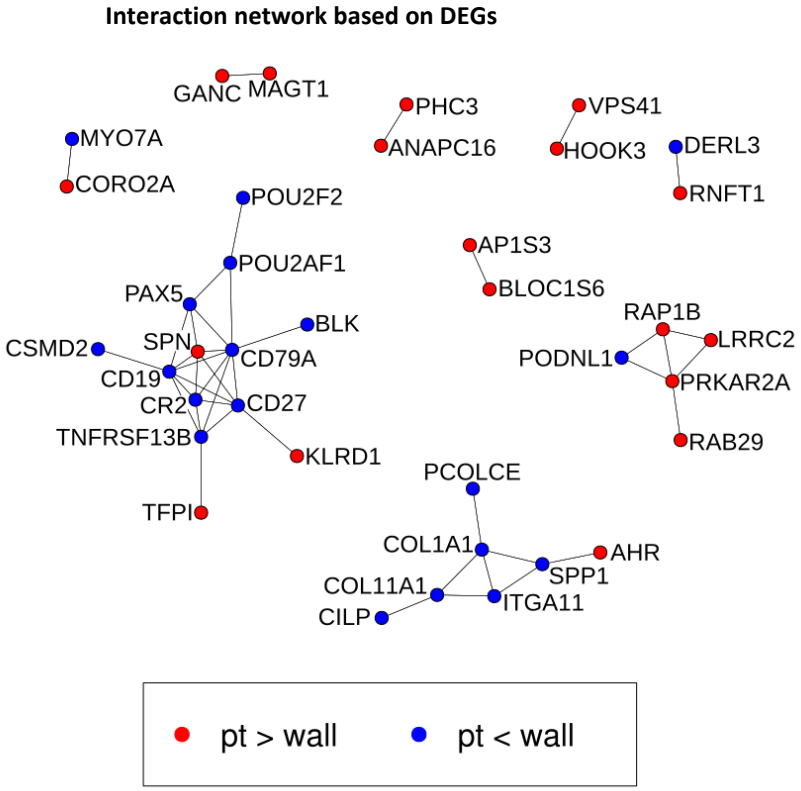

B.

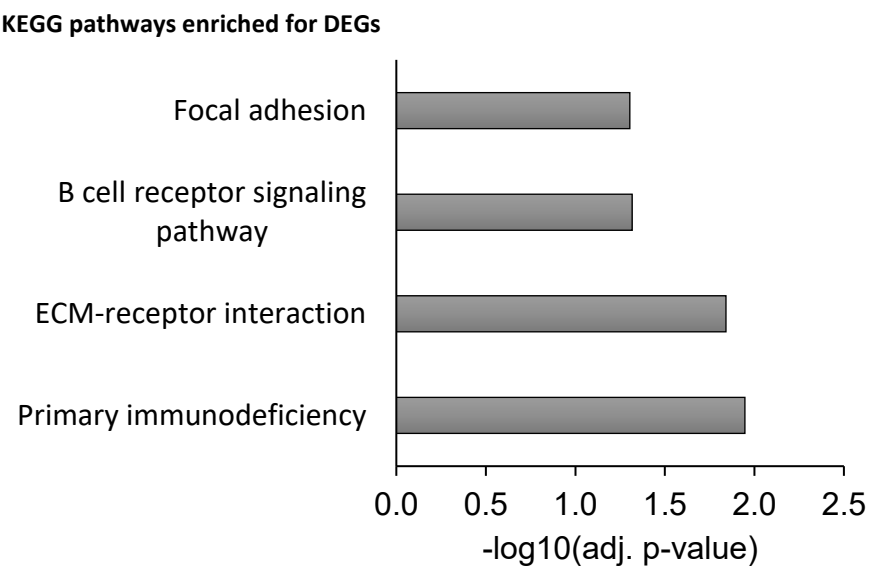

Fig. 4.5: Network interaction and KEGG pathway analysis of genes differentially regulated in wall and parenchyma tissue (PT) within the FCT. Total RNA was extracted from 44 clinical samples and sequenced after rRNA removal. **A**. Within the FCT data set, network interaction of differentially expressed genes (DEGs) was done, with upregulated genes in the wall in red and upregulated genes in the parenchyma (PT) in blue and **B.** the -log10 of adjusted p-value of enriched pathways for the DEGs in FCT in comparing wall and PT samples as analysed by KEGG.

Although sequencing technology has improved and is becoming gradually more affordable, to date the gold standard for confirming gene expression is still polymerase chain reaction (PCR). However, PCR has it's laborious and time-consuming disadvantage. In two independent experiments, we confirmed expression of selected genes in the human samples (Fig 4.6, & Appendix Fig. 7.1 A-D). The selected genes are important for cell signalling and tissue remodelling. Genes regulating cellular interactions such as cell motility, adhesion and expression of functional surface markers required for effector functions are indispensable for homeostasis[59,61–64].

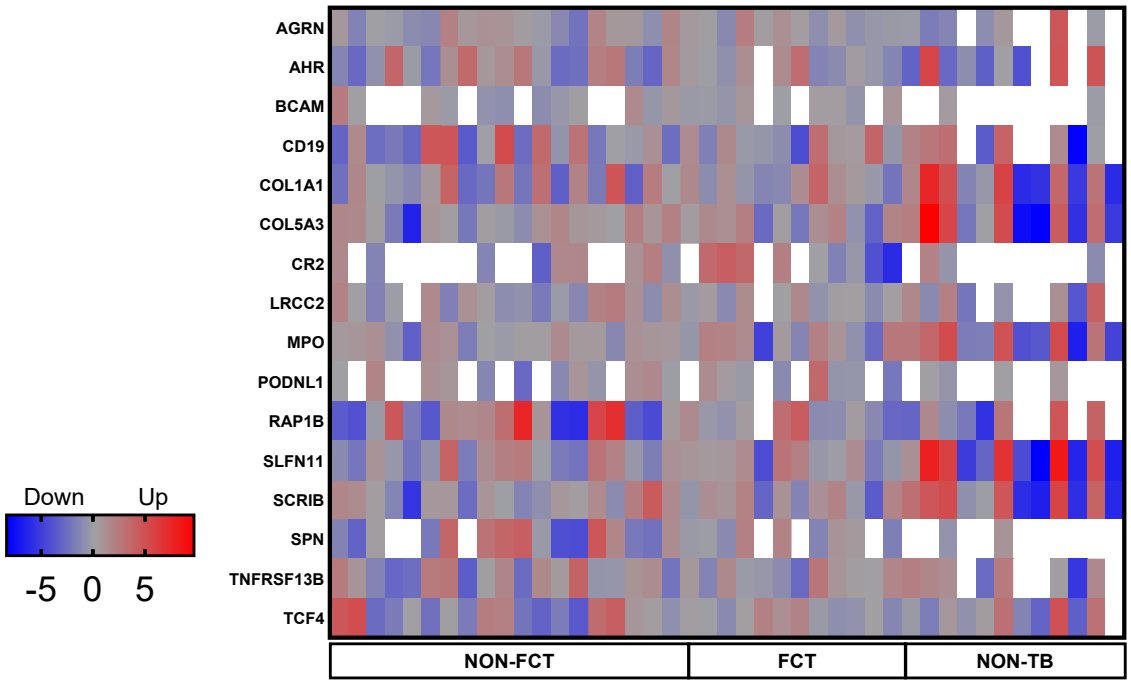

Fig. 4.6: Validation of expression of selected genes by qPCR. Total RNA extracted from tissue biopsies were transcribed to cDNA and gene expression of selected genes from the transcriptome data was quantified by qPCR with GAPDH as reference. Up regulated genes are represented in red, down regulated genes in blue and genes with failed ct threshold are coloured white for each sample or data sets (x-axis). The total number of cycle was 45 and the threshold was set to 40. Gene expression with ct higher than 40 were not included in the analysis.

By PCR, we confirmed the expression of AHR, AGRN, BCAM, CR2, LRCC2, MPO, PODNL1, COL1A1, COL1A5, CD19, RAP1B, SLFN11, SCRIB, SPN, TNFRSF1B and TCF4 (Fig 4.6). The expression pattern of the aforementioned genes did not clearly distinguish between TB and NON-TB control samples but were confirmed to be up (red) or down (blue) regulated in the TB compared to the non-TB controls.

Human pro-inflammatory and anti-inflammatory cytokine genes, which were characterized by qPCR by our collaborators in Moscow (See appendix Fig 7.1 A – D) show differential expression of IL-6, IL-11, IL-17, mmp9, CSF3, CXCL3, IL-12, IFN-γ, TNF-α, CXCL3, CXCL-1, CXCL-10, IL-8, PF-4, CEBP8 and APOD depending on the granuloma type and site of samples. For

example, expression of IL-8 which is an attractant chemokine for PMN was significantly higher in the parenchyma tissue than carvena wall (Fig 7.1 A) but caution is required in the interpretation of the data as the fold increase is very low (≤ 1), across the comparison.

To sum up, the transcriptome signatures in the human TB samples compared to the non-TB samples showed differential expression of genes important for tissue remodelling and anti-tumour response, as well as primary immune deficiency. Selected genes from the RNAseq data could be confirmed by low resolution qPCR but not all.

4.2 Experimental TB *in vitro*

4.2.1 Human PMN contribute significantly to transcriptional changes in PBMCs

The human peripheral blood cells have been studied and harnessed to solve various infectious diseases including TB. Tissue resident cells get refreshed and replenished through the white blood cells. The human blood represents a key sample source for transcriptomics studies. How the human PMN and PBMCs respond transcriptionally to Mtb infection has not been clearly defined. We were interested in the role of human PMN in Mtb infection as this is a widely debated topic[6,12,42,65].

The transcriptional changes in myeloid cells upon interaction with Mtb might account for the differences between protective and pathologic host response. Hence understanding the human PMN within a physiologic environment with other innate and adaptive immune cells is crucial to dissect the unique differences PMN contribute to human TB.

The human PMN is an active phagocytic cell and an innate strong responder to almost any "foreign-body" not recognized as self[66–68]. In contrast, maintenance of immune defence is the

function of innate monocytic cells comprised by the PBMCs, consequently, they are more long-lived about 2 – 3 weeks in vitro than the PMN that live for about 24 hours in culture[69,70].

A. PBMC-uninf Acidfast-

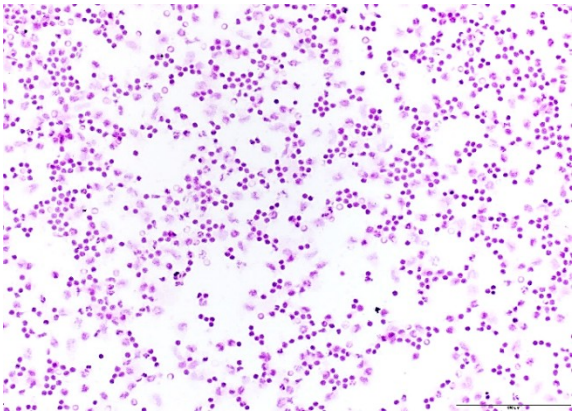

B. PBMC-Mtb Acidfast-

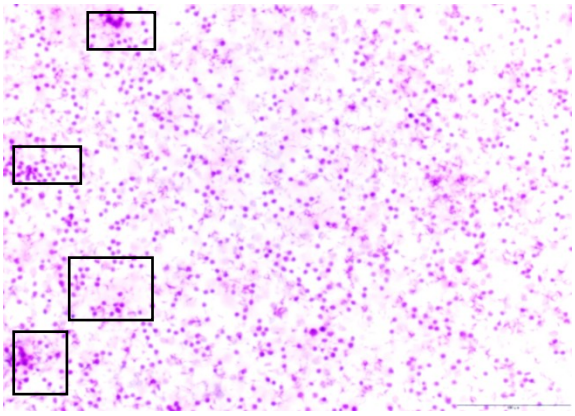

C. PBMC-PMN-uninf Acid-fast-

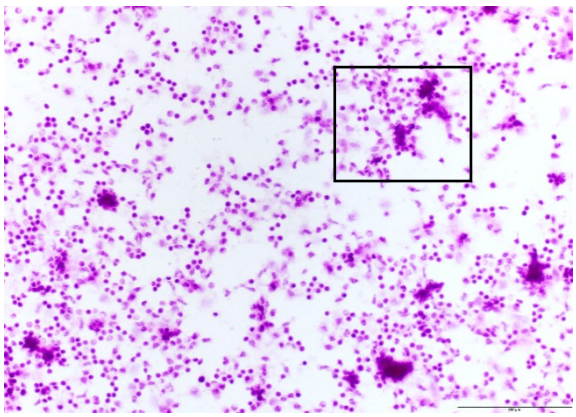

D. PBMC-PMN-Mtb Acidfast-

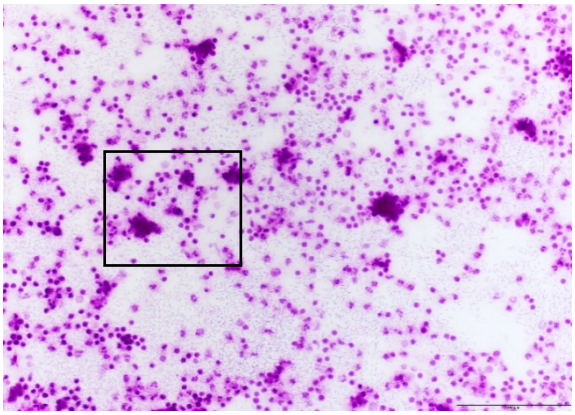

E.

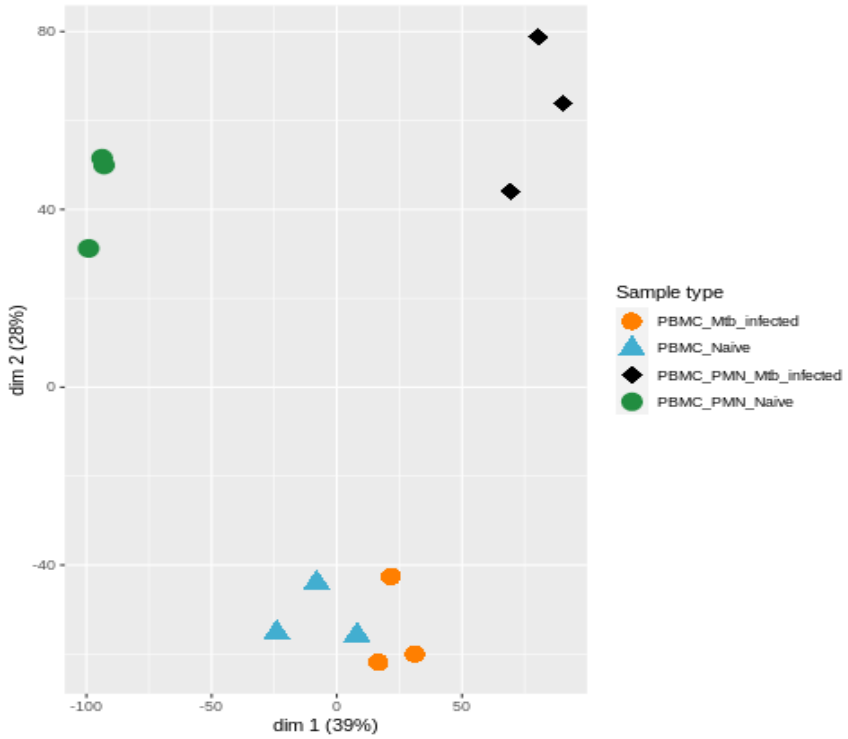

Fig. 4.7: PMN are transcriptional regulators of innate immunity. Human PBMCs were cultured with or without equal numbers of PMN (8 – 10^6 cells/mL) and were infected with or without Mtb (MOI=3). Cells were incubated overnight (~20hrs). Cells were either fixed with 4% PFA for microscopy or lysed with Trizol for RNA isolation. Microscopy acid-fast and haematoxylin staining of **A.** PBMCs naïve or uninf, **B.** PBMC-Mtb infected, **C.** PBMCs+PMN uninf and **D.** PBMCs+PMN-Mtb infected. **E.** MDS plot of PBMCs+Mtb infected or PBMC-naïve or uninfected PBMC+PMN-Mtb-infected and PBMC+PMN naïve.

Therefore, we analysed gene expression in PBMC with or without Mtb infection and compared these patterns with PBMCs co-cultured with PMN with or without Mtb infection of the co-cultures. We observed that PMN induce formation of cellular aggregates when co-cultured overnight with PBMCs (Fig 4.7 C and D), PBMCs alone form few aggregates in the presence of Mtb infection (Fig 4.7 and B). This observation was reflected in the transcriptome (Fig 4.7 E) as PBMC naïve (blue triangle) and PBMC-Mtb cultured overnight (orange circles) expressed less transcripts, 1008 differentially expressed genes, compared to PBMC+PMN naïve (green circles) and PBMC+PMN-Mtb (dark rhombus) with 7627 differentially expressed genes. The DESEgs in PBMCs+PMN-Mtb compared to PBMCs+PMN uninfected cultures were

genes regulating 24 key pathways in “infection and inflammation” including “toll-like receptor signalling”, “NOD-like receptor signalling”, “RNA transport”, “leishmaniasis”, “apoptosis”, “DNA replication” and “nucleotide excision repair” among others. Whereas in the comparison of PBMC and PBMC+Mtb only two KEGG pathways were differentially regulated, namely, “cytokine-cytokine receptor interaction” and “epithelial cell signalling in *Helicobacter* infection”. This suggest that Mtb infection elicits immune response to pathogen that were previously encountered by the host. The differences, however, are striking in the presence of PMN comprising pathways and genes associated with inflammatory responses upon pathogen encounter, indicating PMN as amplifiers of innate responses to infection. These genes include *PLD1*, *PTAFR*, *MCTP1*, *PID1*, *MT1/MMP14*, *CLEC4E*, *CASP5*, *RBM47*, *TLR8* and *CCRL2. Phospholipase D1* (*PLD1)*, regulates macrophage polarization[71]. *Platelet activating factor receptor* (*PTAFR)* is involved in tumor growth and proinflammatory process[72]. *Multiple C2 domains transmembrane protein 1* (*MCTP1)* regulates biogenesis of lipid droplets and cellular vessicles[73]. *Phosphotyrosine interaction domain containing* 1 (*PID1)* controls glucose balance and protein phosphorylation[74]*.* Differential regulation of the four genes indicate alteration in macrophage metabolism upon interaction with Mtb-infected neutrophils. The following differentially regulated genes have important functions in innnate immune reactions of macrophages to Mtb. *C-type lectin receptor 4 E or macrophage inducible c-type lectin (CLEC4E/MINCLE)* is a receptor for Mtb lipid trehalose dimycolate (TDM), also a necrotic cell sensor that restricts survival of Mtb through autophagy[75,76]. *Membrane type 1 matrix metalloproteinase* (*MT1* or *MMP14)* is important for leukocyte evasion into tissue and destruction of collagen[77]. *Caspase 5 (CASP5)* is required for inflammasome signalling[78]. *RNA binding motif 47 (RBM47)* is important for RNA editing, inflammation, cell proliferation and autophagy[79]. *Toll-like receptor 8* (*TLR8)* is a receptor for bacterial RNA and it is involved in T

regulatory cell metabolism and function[80,81] while *C-C Chemokine receptor like 2* (*CCRL2)* regulates leukocyte migration[82,83].

4.2.2 Murine TB: BMDM response to inflammatory stimuli

Prior to Mtb infection, it was important to know whether single cells from the wild type and congenic mice differ in their response to inflammatory stimuli. This will give a clue to how the murine cells control Mtb replication *in vitro* and perhaps *in vivo* too[31,32,84].

BMDM from resistant B6, susceptible C3H and the intermediate B6.C3Hsst1 were stimulated with IFN-ɤ, TNF-α, LPS and a combination of TNF-α and LPS, or LPS and IFN-ɤ as surrogate inflammatory stimuli. The cultures were incubated overnight, and the expression of MHC-II, important for antigen presentation and T Cell activation, and secreted nitric oxide (NO), as antimicrobial effector, were measured (Fig 4.8 A and B).

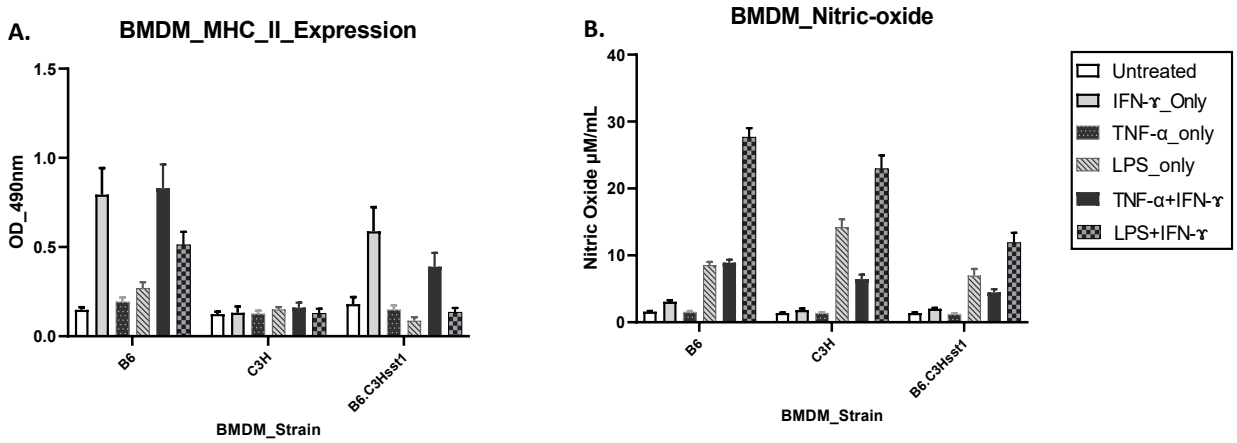

Fig. 4.8: Differential response of BMDM to inflammatory stimuli prior to infection. 1 x 10^5 Bone marrow derived macrophages from C57BL/6J mice (B6), C3HeB/FeJ and congenic B6.C3Hsst1 mice were untreated, treated overnight with 500 IFN-ɤ only, 20ng/ml TNF-α only, 1µg/ml LPS only, 500 IFN-ɤ and 20ng/ml TNF, or 500 IFN- ɤ and 1µg/ml. **A**. MHC-II expression and **B.** Nitric oxide secretion.

We observed that the bone marrow derived macrophages from the resistant B6 express MHC molecule in higher amount than the congenic B6.C3Hsst1 upon stimulation with IFN-ɣ only, TNF-α only, TNF-α (+) IFN-ɣ, LPS (+) IFN-ɣ but not LPS only (Fig 4.8A). However, MHC II expression was not detected in the C3H because the antibody used was specific for the B6 MHC haplotype. Indeed, MHC II haplotype differ (MHC-IIA^{K} in C3H versus MHC-IIA^{b} in B6) across species and can only be detected with haplotype specific antibodies.

In contrast, NO which is a reactive oxygen species required for pathogen control including Mtb was detected in substantial amount in BMDM from B6, C3H and the congenic B6.C3Hsst1 mice (Fig 4.8 B). When the BMDM cultures were treated with LPS only, TNF-α only, IFN-ɣ only, TNF-α (+) IFN-ɣ and LPS (+) IFN-ɣ, NO secreted into cell culture supernatants differ in concentration depending on the mouse strain the BMDM derived from. Macrophages from the resistant B6 strain expressed higher amount MHC II and secreted more NO when stimulated or treated with LPS (+) IFN-ɣ in comparison to the macrophages from susceptible C3H and B6-C3Hsst1. However, BMDM from the susceptible C3H secreted slightly higher amounts of NO than BMDM from resistant B6 and the congenic B6.C3Hsst1 mice when treated with LPS only. These data suggest that the capacity to secrete NO might be genetically controlled and account for differences in Mtb control as previously reported[45,85–87].

To sum up, BMDM from the resistant B6, susceptible C3H and the congenic B6C3Hsst1 respond but to different degrees to inflammatory stimuli in the absence of Mtb infection.

4.2.3 Host cell specific increase in bacterial burden and cell death

Interferons, particularly gamma interferon are immune modulatory and have been used in treatment and as biomarker in diagnosis of tuberculosis to monitor protective immunity[40,88–

[90]. The differences in response to infection, leading to either cell survival or cell death is genome, and cell type specific.

To observe this hypothesis *in vitro*, we generated macrophages from bone marrow of B6, C3H and the congenic B6.C3Hsst1. The cells were either pre-treated (+/-; +/+) or not with IFN-ɣ (-/-; -/+) and cultured overnight prior to infection with Mtb (MOI=1). After Mtb infection, the cell culture supernatant were collected for LDH Assay (Fig. 4.10 A-D) and the medium was exchanged with fresh medium with (+/-; +/+) or without fresh IFN-ɣ (-/-; -/+) and further cultured for 1d, 2d or 3d. The bacterial burden was estimated by CFU (Fig. 4.9 A-D).

We observed that BMDM from all three murine strains were permissive for Mtb growth after ~24hrs without IFN-ɣ treatment (Fig 4.9 A). Upon IFN-ɣ stimulation, macrophages from all the mouse strains controlled Mtb growth in similar manner. However, the B6.C3Hsst1 performed better than the wild type B6 without IFN-ɣ treatment though not statistically significant. In contrast, the C3H succumbed quickly to cell death, thereby providing less host cells for Mtb growth (Fig. 4.10 A – D, Fig 4.9 A - C). Pre-treating and maintain the BMDM in IFN- ɣ after Mtb infection kept the bacterial replication low (Fig 4.9 D).

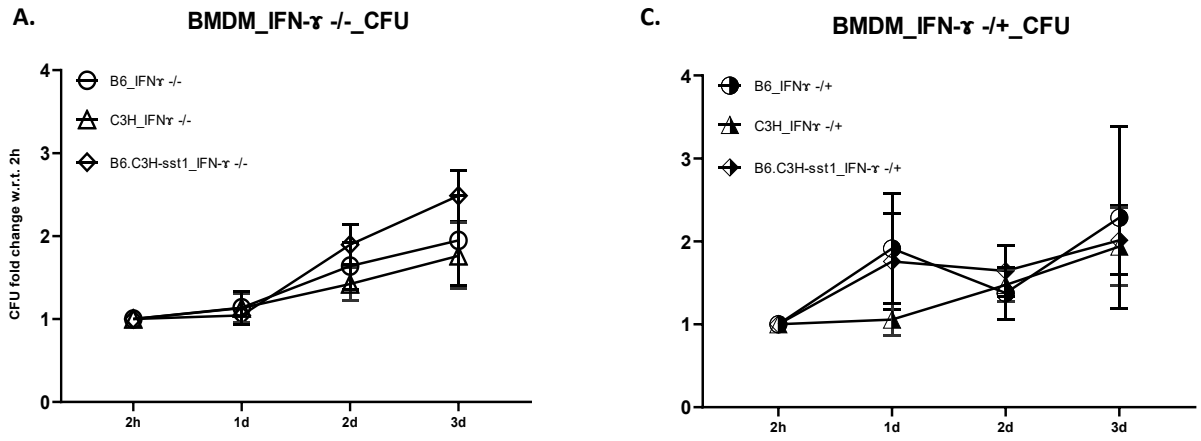

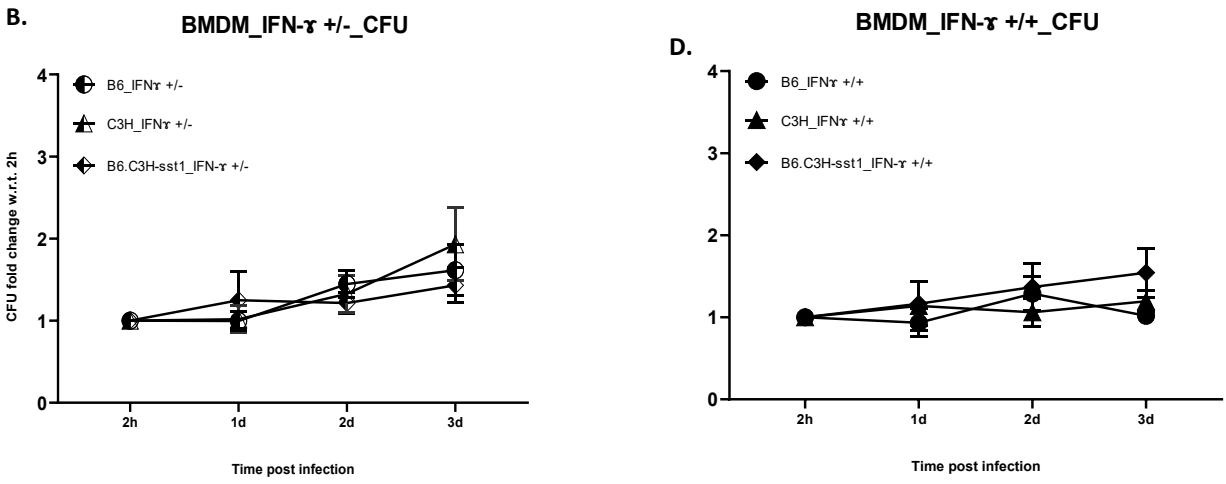

Fig. 4.9: Pre-treating and maintaining BMDM in IFN-ɤ controls bacterial burden. 1 x 10^5 Bone marrow derived macrophages from C57BL/6J mice (B6), C3HeB/FeJ and congenic B6.C3Hsst1 mice were untreated (IFN-$ɤ^{-/-}$ **A**); pre-treated but not maintained (IFN-$ɤ^{+/-}$ **B**); not pre-treated but maintained (IFN-$ɤ^{-/+}$ **C**); pre-treated and maintained (IFN-$ɤ^{+/+}$ **D**) in 500 units/mL IFN-ɤ and infected with 1 x 10^5Mtb (MOI=1). Culture mediums in cells for 1d, 2d and 3d time points culture medium was exchanged with fresh medium with or without IFN-ɤ post as appropriate at 2h post infection. At each time point, cells were lysed, plated on agar, incubated for 3 weeks and bacteria colonies were counted. Each graph represent average of at least three independent experiments. No statistically significant differences were observed between the mouse strains as tested by Turkey multiple comparison test.

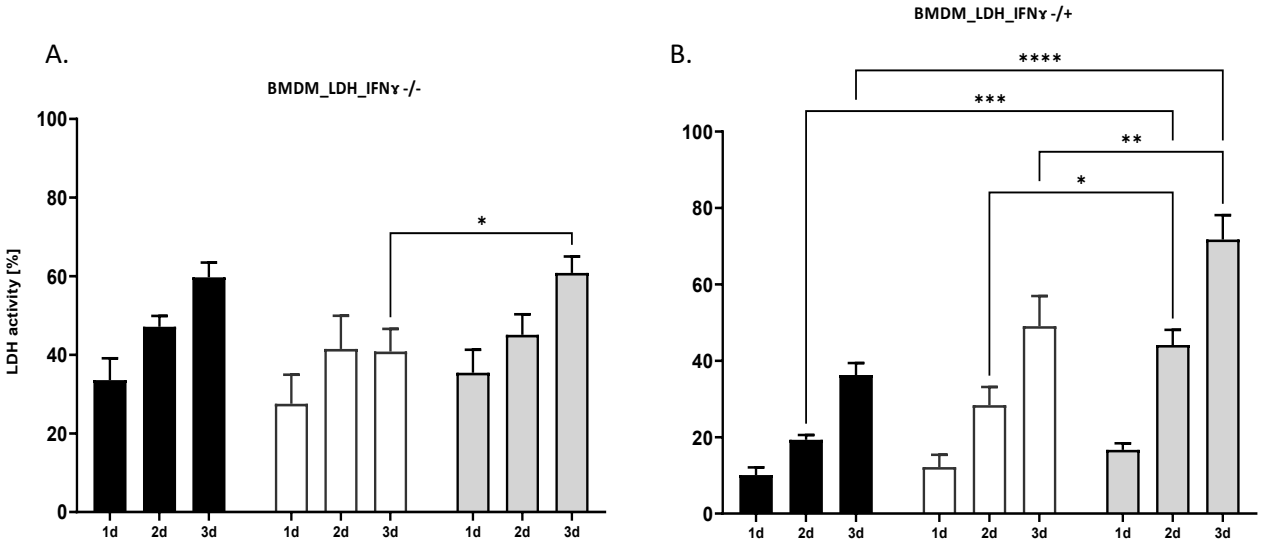

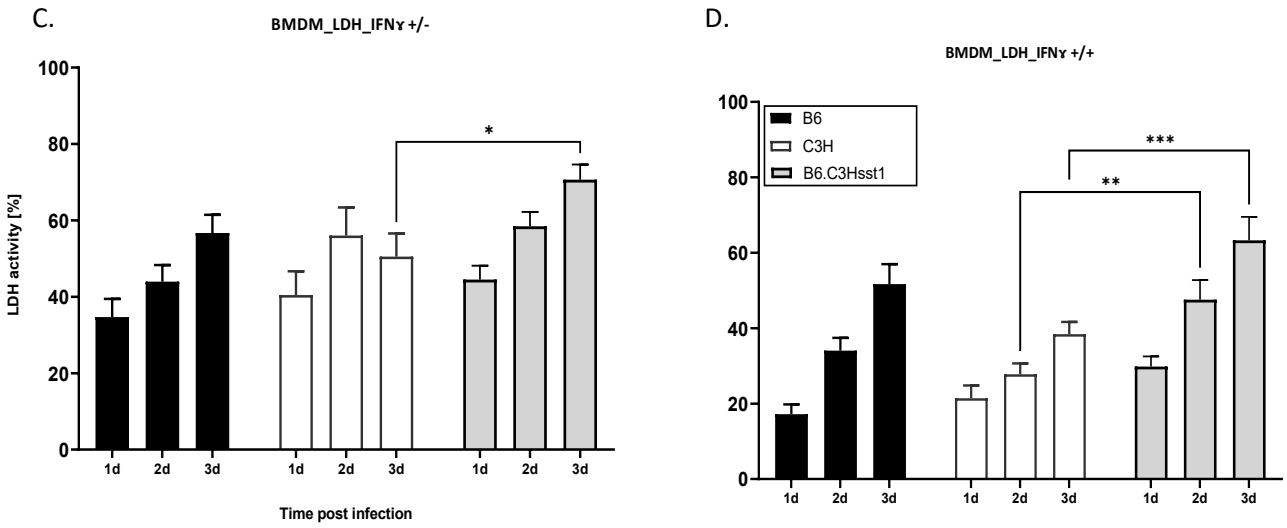

Fig. 4.10: Significant differences in LDH activity are seen in BMDM from B6.C3Hsst1 maintained in medium with IFN-ɣ 1 x 10^5 Bone marrow derived macrophages (BMDM) from C57BL/6J mice (B6), C3HeB/Fej and congenic B6.C3Hsst1 mice were untreated (IFN-$ɣ^{-/-}$ **A**); pre-treated but not maintained (IFN-$ɣ^{+/-}$ **B**); not pre-treated but maintained (IFN-$ɣ^{-/+}$ **C**); pre-treated and maintained (IFN-$ɣ^{+/+}$ **D**) in 500 units/mL IFN-ɣ and infected with 1 x 10^5Mtb (MOI=1). Culture mediums in cells for 1d, 2d and 3d time points culture medium was exchanged with fresh medium with or without IFN-ɣ post as appropriate at 2h post infection. At each time point, cell culture supernatants were collected for LDH assay. Each graph represent average of at least three independent experiments. Error bars depict +/- SEM 2-Way Tukey's multiple comparison test where **** is $p < 0.0001$, *** is $p < 0.001$, $p < 0.005$ and * is $p < 0.05$

To sum up, an inflammatory micro-environment as shown by pre-treatment with IFN-ɣ (Fig 4.9 C) might modulate the host cells towards better antimycobacterial response than exogenous addition of IFN-ɣ upon infection without prior stimulation (Fig 4.9 B).

The type of host cell death induced upon IFN-ɣ treatment depends also on the host genetics. Several host cell death mechanisms have been proposed for *in vitro* cell death of Mtb infected cells[31,91–93]. For the above experimental setup (Fig 4.9) the relative lactate dehydrogenase (LDH) enzyme release into the cell culture supernatant was quantified (Fig 4.10 A-D). The LDH does not explicitly differentiate between necrosis and secondary necrosis upon apoptosis[56].

We found that BMDM neither pre-treated nor maintained with IFN-ɣ released similar amount of LDH upon Mtb infection (Fig 4.10 A), and that the relative LDH release on 3dpi was slightly significantly higher in BMDM from the B6.C3Hsst1 mice compared to the BMDM from the C3H mice. In contrast, Mtb infected BMDM from the B6.C3Hsst1 mice not pre-treated but maintained in IFN-ɣ (Fig 4.10 B), showed significantly higher release of LDH on 2d and 3dpi compared to the BMDM from the B6 and C3H mice. Mtb infected BMDM IFN-ɣ pre-treated but without IFN-ɣ post-treatment led to relatively higher LDH release in BMDM from the B6.C3Hsst1 mice compared to BMDM from the C3H mice on 3dpi (Fig 4.10 C). Whereas BMDM cultures from the B6.C3Hsst1 pre-treated and maintained in IFN-ɣ upon Mtb infection released relatively higher amount of LDH on 2d and 3dpi which was statistically significant in comparison to the relative LDH activity in the BMDM from the C3H mice.

Moreover, IFN-ɣ treatment upon Mtb infection was beneficial to the BMDM from wild type B6 and C3H when compared to the congenic B6.C3Hsst1 mice (Fig 4.10 B). The role of IFN-ɣ treatment in controlling necrosis in Mtb infected BMDM from B6.C3Hsst1 mice as measured by the LDH assay does not seem to be under the control of the sst1/Ipr1 locus (Fig 4.10 B and D). The data suggests that activation of the BMDM from B6.C3Hsst1 mice with IFN-ɣ is rather controlled by the B6 background.

Taken together, maintaining BMDM cultures in IFN-ɣ after Mtb infection (Fig 4.10 B and D), slowed down the rate of LDH release, that is necrotic cell death, especially in cells from B6 and C3H mice compared to BMDM cultures that were not maintained in IFN-ɣ (Fig 4.10 A and C).

4.3 Experimental TB *in vivo*

Focusing specifically on the lungs, we employed two genetically defined experimental TB models, both on a resistant B6 background. Many of the available experimental tools are designed mainly for the B6 mice, hence our choice of the B6 congenic. The B6.C3Hsst1 mice was compared to wild type B6 mice in Borstel while the B6.I-9.3.19.8 mice was compared to wild type B6 mice by our collaborators in Moscow.

4.3.1 Higher bacterial loads in lungs of B6.C3Hsst1 vs parental B6 mice

Previous body of knowledge have shown how imperative the B6.C3Hsst1 mice are to study wide range of intracellular pathogens and the results have varied in terms of murine survival time, based on the infection route and dose[88].

The resistant B6 and susceptible B6.C3Hsst1 mice were infected per aerosol with ~100 Mtb per mouse and the bacterial loads in the lung, spleen and liver were estimated by colony forming unit (CFU) after 14, 28 and 76dpi (Fig 4.11 A-C). The rate of Mtb growth in the lung, liver and spleen compared to 14dpi was calculated (Fig 4.11 D-F).

Mtb load and the rate of Mtb replication in lungs of susceptible B6.C3Hsst1 was significantly higher than resistant B6 lungs on 28d and 76dpi (Fig 4.11 A & D). Although Mtb load in the spleen steadily increased over the period of infection, there was no statistically significant difference between the bacterial load in the resistant wild-type B6 in comparison to the susceptible B6.C3Hsst1 mice (Fig. 4.11 B). However, the differences in the rate of bacterial burden in the spleen was statistically significantly higher in the B6.C3Hsst1 on d28 post infection in contrast to the resistant B6 mice (Fig 4.11 E). In the liver, the log (Fig. 4.11 C) and the rate (Fig. 4.11 F) of Mtb load was statistically significantly higher in the susceptible B6.C3Hsst1 than the resistant B6 mice at d28 and d76 post infection. The lesion count and

sizes (Fig 4.11 E, F) were also higher in the congenic B6.C3Hsst1 than the resistant wild type B6 mice.

The bacterial load and infection route suggests that the Ipr1/sst1 is involved in restricting Mtb growth to the lungs and liver. Differences in Mtb loads in the spleen were less pronounced (Fig. 4.12 B-F) and became equal at day 76pi.

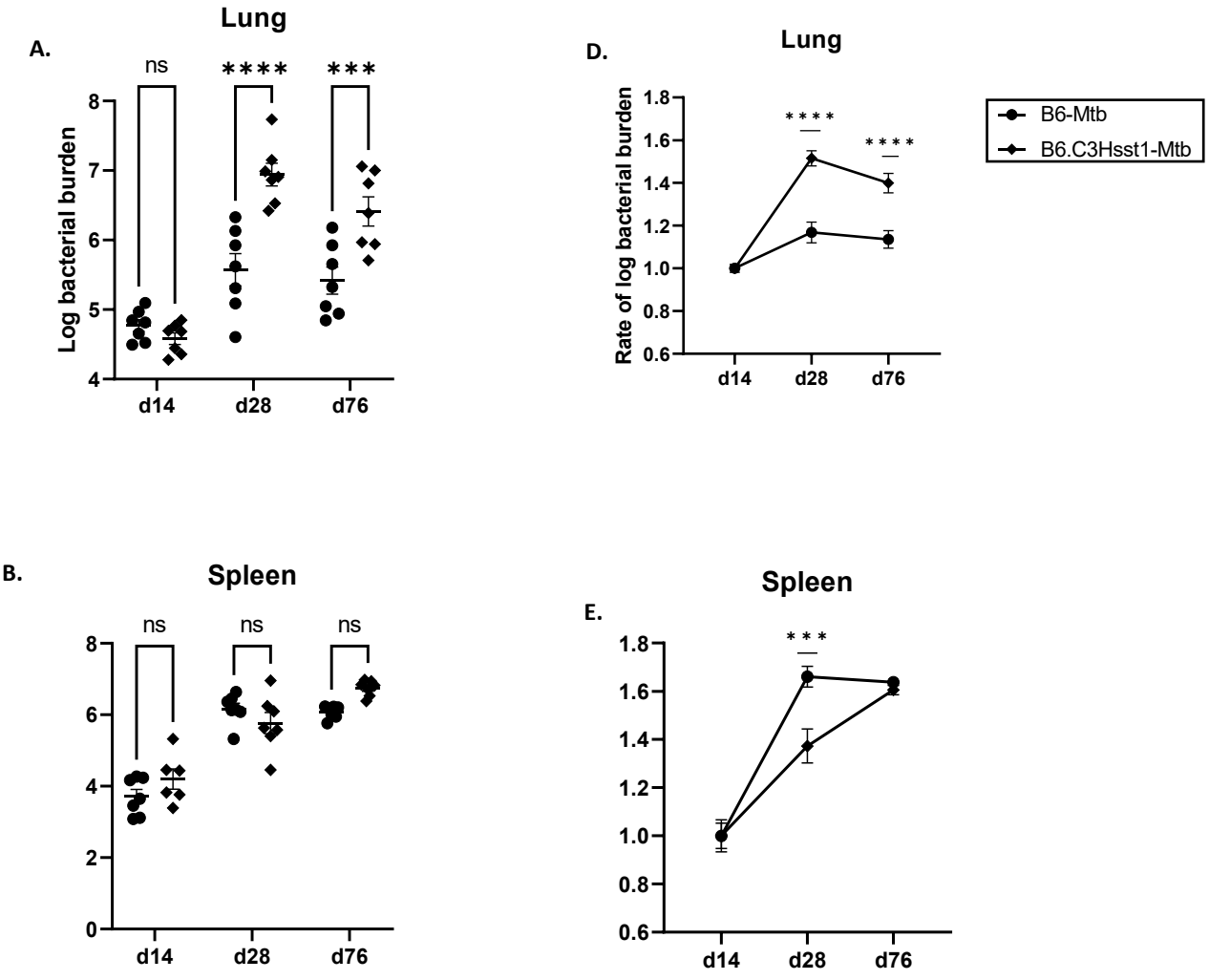

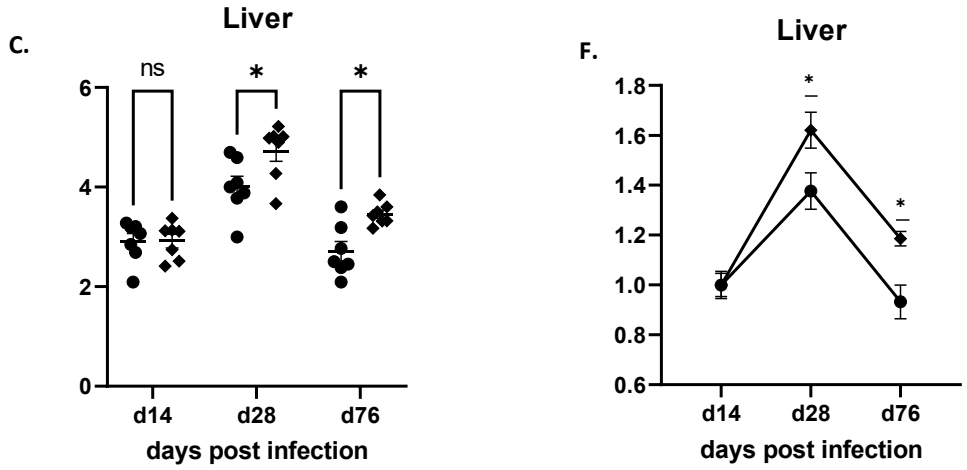

Fig. 4.11: Increase bacterial burden in organs of susceptible B6.C3Hsst1 mice. C57BL/6 mice (B6) and congenic B6.C3Hsst1 mice were infected per aerosol sacrificed at days 14, 28 and 76 post infection, n = 7 mice in each group, per time point. Organs were harvested and homogenized. Tissue homogenates were plated, and bacteria colonies were counted after ~ 4 weeks of incubation. Mtb colony forming units in; lungs **A**, spleen **B**, and liver **C**. The rate of Mtb growth with respect to CFU load 14dpi in lungs **D**, spleen **E** and liver **F**. Error bars depict +/- SEM 2-Way Anova Sidak's multiple comparison test where **** is p<0.0001, *** is p = 0.0007 , p = 0.0005 and* is p = 0.0182, p=0.0136

As expected, the lungs of uninfected B6 and B6.C3Hsst1 showed no cellular aggregates and the airway epithelium had no signs of inflammation on d0, d14, d28 and d76 (Fig 4.12 A and B). In contrast, infected B6 and B6.C3Hsst1 mice on d14, d28 and 76dpi showed cellular aggregates and granulomatous lesions (Fig. 4.12 B and D). The lesions were counted, and the size of the lesions were estimated from the Mason-Goldner (MG) stained lung sections (Fig. 4.12 E and F). In B6.C3Hsst1 mice infected through aerosol ~ 100 CFU per lung were more susceptible than the wild type B6 mice and higher bacillary load led to a well-formed and larger granulomatous lesion (Fig. 4.12 D HE, MG d28 and d76). The average lesion sizes were significantly higher in the infected B6.C3Hsst1 mice compared to the B6 mice on d28 (Fig.

4.12F). Ziehl-Neelsen staining also confirmed the CFU counts in Fig 4.11 revealing more acid-fast mycobacteria in B6.C3Hsst1 mouse lungs (Fig 4.12, ZN 40X).

A. B6-uninfected

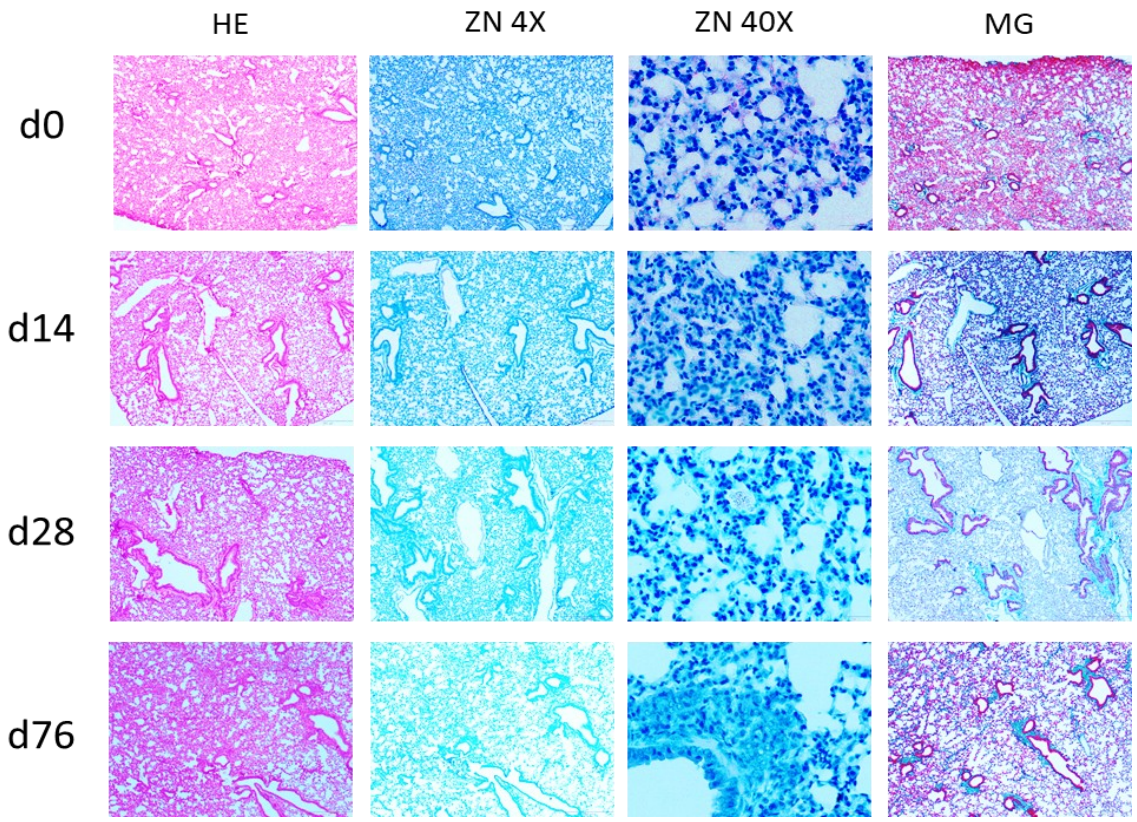

B. B6.C3Hsst1-uninfected

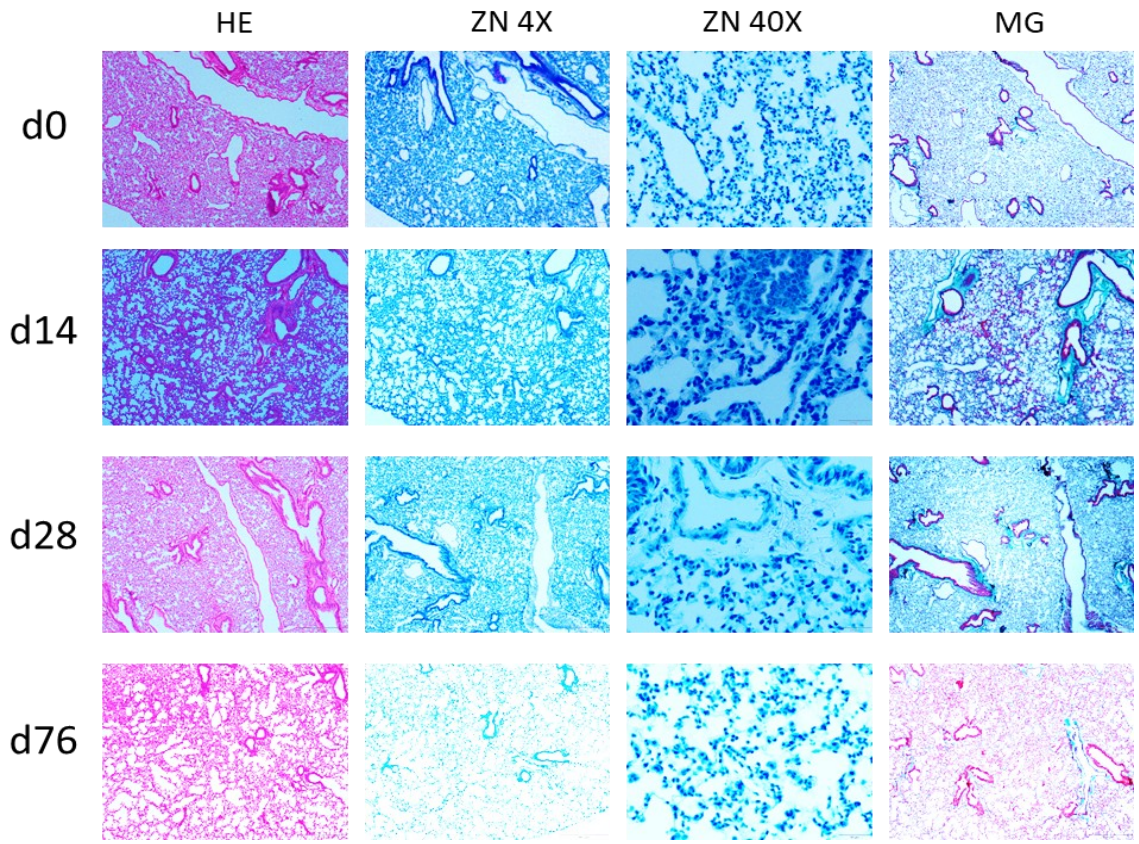

C. B6-Mtb-infected

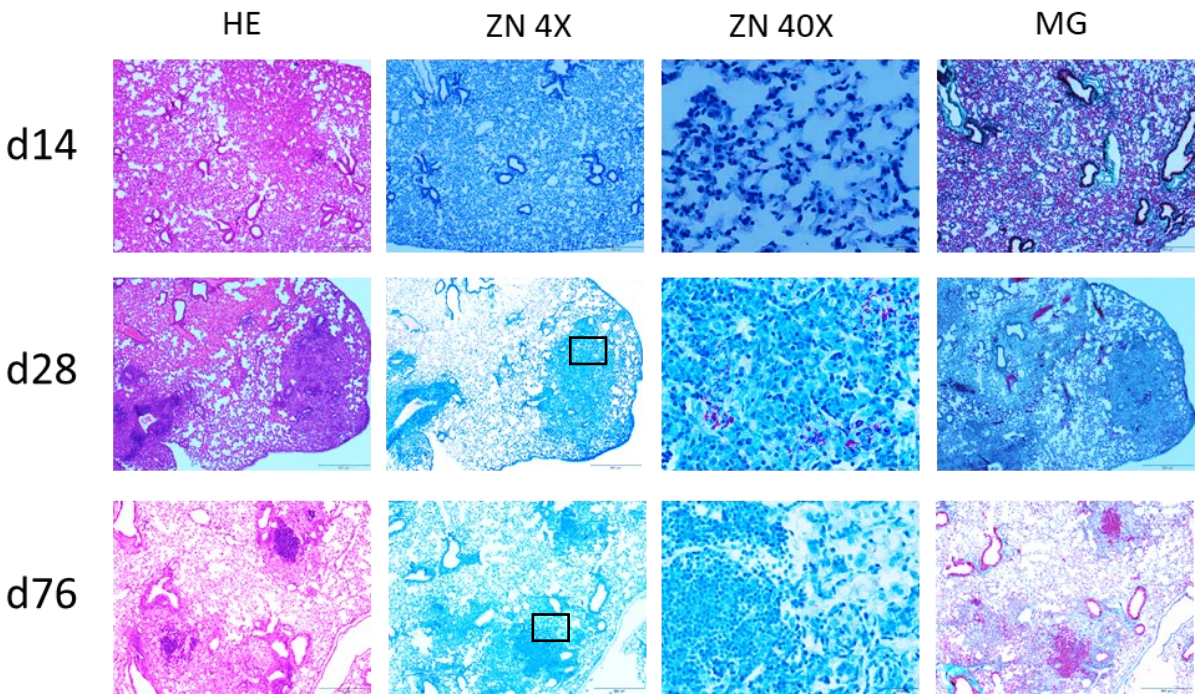

D. B6.C3Hsst1-Mtb-infected

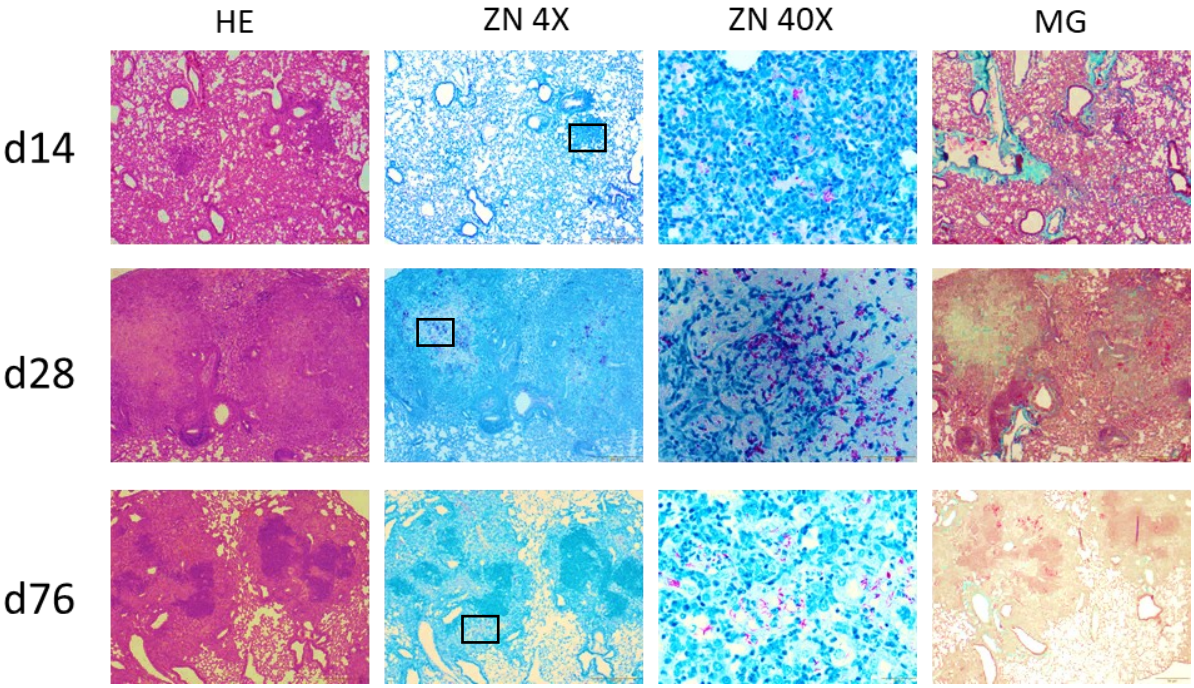

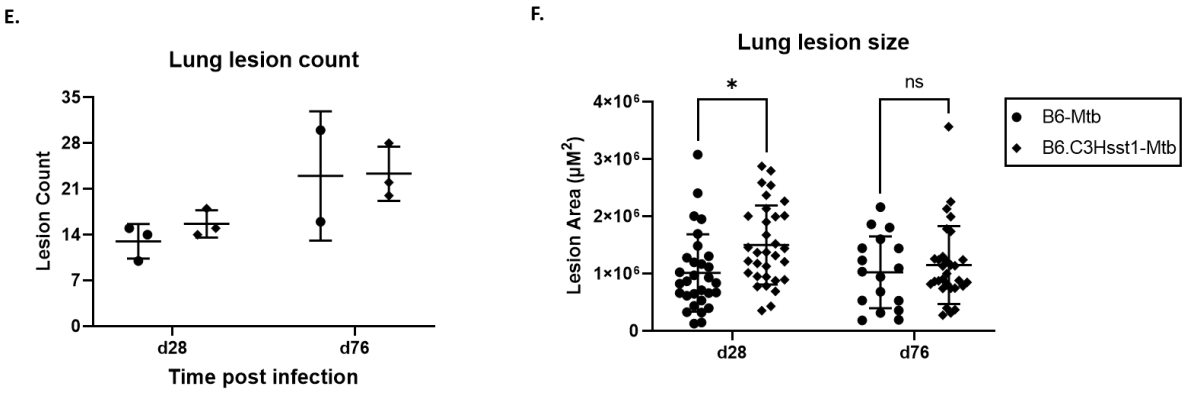

Fig. 4.12: Higher bacterial load and bigger lesions in susceptible B6.C3Hsst1 congenic mice. Female B6 and B6.C3Hsst1 aged 8-12 weeks were infected with ~100 CFU Mtb per aerosol, mice were sacrificed at 0-, 14-, 28-, and 76-day(s) post infection. Paraffin sections were processed and stained with haematoxylin (HE), Ziel-Nielson (ZN) and Masson-Goldner (MG) to determine the lung pathology and Mtb lesions **A-D**. The lesions were counted **E**, and the sizes were estimated **F**. Images and graph represent 1 mouse (d0), 3 mice (d14, d28) and 2 or 3 mice (d76). *p<0.05 2way ANOVA Šídák's multiple comparisons test.

4.3.2 Phenotypes of cell infiltrating the lungs of infected B6 and B6.C3Hsst1 mice

Following phagocytosis of Mtb by resident alveolar macrophages in the lungs, signalling processes to control infection are immediately initiated. Immuno-competent and resistant wild type B6 do not readily show signs of disease. They develop immune response to keep the pathogen under control. The susceptible but immune competent B6.C3Hsst1 are similar to B6 on day 14 post infection (pi) in appearance and cell recruitment. On later days namely d28 and d76 pi cellular infiltrates and immune cell aggregates form well-structured granulomatous lesions in the lungs of B6.C3Hsst1 mice.

To characterize the cells recruited to the lungs and compare immune cells in resistant B6 to susceptible B6.C3Hsst1, the lung tissues were digested to separate single cell suspensions

(Fig. 4.13 A). Cells were stained for surface markers: $Ly6G^+$ for PMN, $CD68^+$ for Macrophages, $CD3^+$ $CD4^+$ for $CD4^+$ T cells, $CD3^+$ $CD8^+$ for $CD8^+$ T cells, and $CD19^+$ for B cells (see appendix 7.3 for the cytochromes). In comparison to uninfected mice, the cellular infiltrations were higher in infected mice on day 36 and 75 post infection (Fig. 4.13 A). On d14, d36 and d77 post infection, the number of $Ly6G^+$ cells in the lungs of the Mtb infected mice were higher than in uninfected mice (Fig. 4.13 B). However, the difference between $Ly6G^+$ cells in the Mtb infected resistant B6 and the susceptible B6.C3Hsst1 were not statistically significant. The amount of $CD68^+$ macrophages decreased overtime (Fig. 4.13 C) while the amount of $CD19^+$ B cells increased on 77dpi in infected mice (Fig 4.13 D).

An interesting observation is the steady increase in $CD4^+$ and $CD8^+$ T cells counts on 36dpi (Fig 4.13 E & F) in the infected mice compared to uninfected. While $CD4^+$ T cells counts in the infected mice though higher than in uninfected mice on 77dpi, the amount compared to 36dpi was reduced (Fig 4.13 E). In contrast, the numbers of $CD8^+$ T cells on 36dpi and 77dpi in infected mice were comparable (Fig 4.13 F). Again, within the B6 and the B6.C3Hsst1 infected mice, no statistically significant difference in cell counts was observed.

In summary, the cells infiltrating the lungs of infected mice were predominantly $Ly6G^+$ PMN on 14dpi, and $CD4^+$, $CD8^+$ T cells on 36dpi, and slightly less $CD4^+$ T cells, moderate amount of $CD19^+$ B cells and $CD8^+$ T cells on 77dpi.

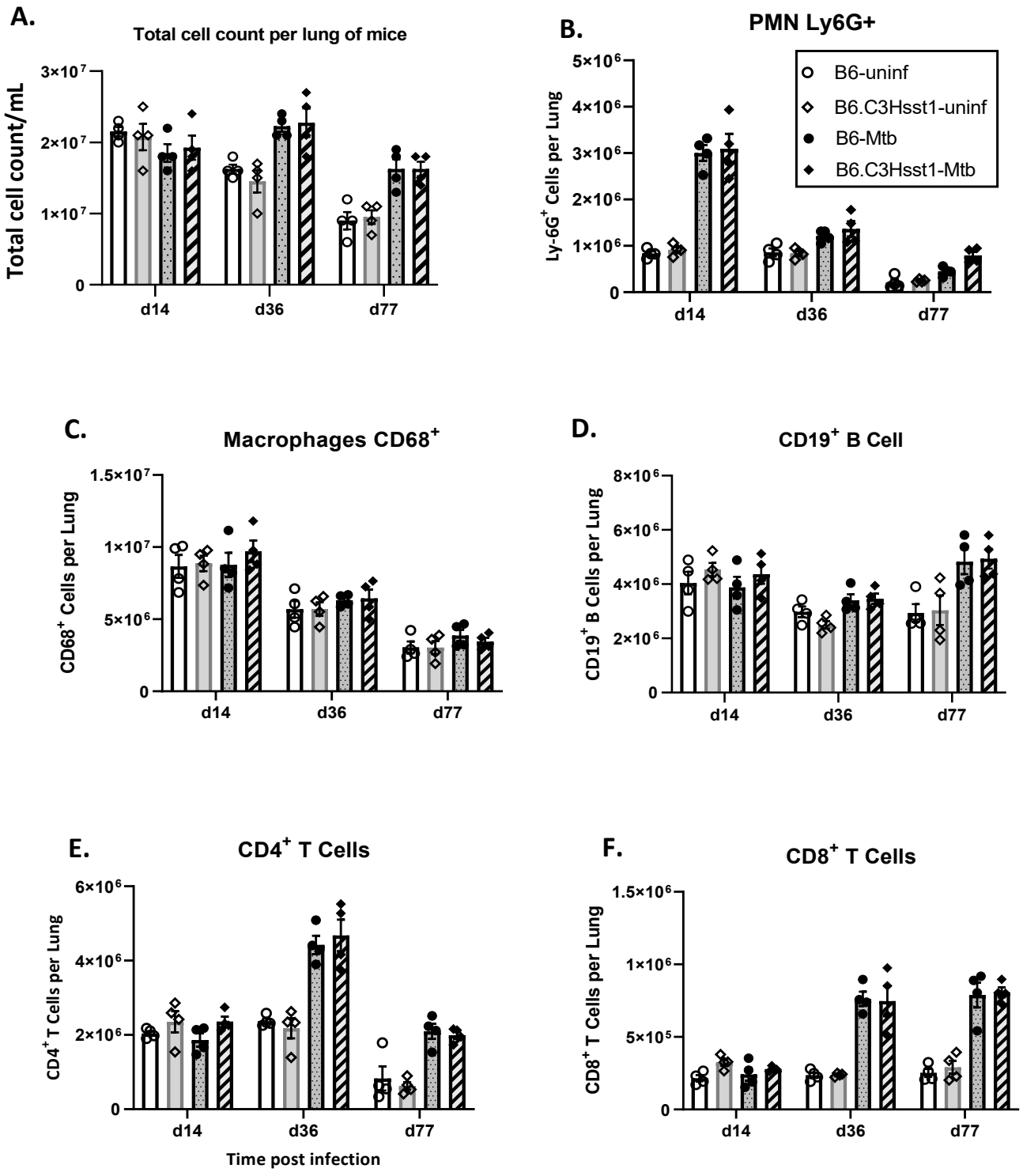

Fig. 4.13: Increase cell infiltration into the lungs of Mtb infected mice. Female B6 and B6.C3Hsst1 aged 12-14 weeks were infected with ~100 CFU Mtb per aerosol, mice were sacrificed at 14-, 36-, and 77-days post infection. Lungs were digested and the cells were counted **A**. Cells were stained and analysed for expression of surface

markers of neutrophils (PMN) **B**, Macrophages **C**, B cells **D**, $CD4^+$ T cells **E** and $CD8^+$ T cells **F**. Error bars depict +/- SEM, n = 4 mice.

4.3.3 Increase cellular infiltrates in lungs of susceptible B6.I-9.3.19.8

The B6.I-9.3.19.8 is a murine model derived from back crossing of the resistant B6 and susceptible I/St (I-strong) mice. The MHC-II haplotype (H2) varies in each genetic population. On the B6 background, genetic differences in the MHC II have been studied and mapped to different regions of the chromosome 17, yet variation in experimental results exist. The genes are linked and inherited together but the effect of the penetrance varies in male and female mice. Moreover, the amount of bacterial load and route of infection strongly determine the strength of the innate and adaptive immune response. Protective T and B Cells that are long-lived are required to keep Mtb under the control of the host immunity in all tissues[94].

As analysed by our collaborators in Moscow, clearly, at earlier time points post infection, namely 14dpi, we observed no significant difference in the bacterial loads in the lung and spleen and cell types except T cells in the resistant B6 mice (Fig. 4.14A - E).

Worthy of note, the bacterial load in the lung and spleen are significantly higher in the susceptible congenic B6.I-9.3.19.8 than the resistant B6 (Fig 4.14A and B) on days 28 and 75pi. Mtb-specific CD4 T Cells were slightly higher in the susceptible B6.I-9.3.19.8 at 28dpi as shown by the $CD44^{hi}CD62L^{lo}$ lymphocyte populations (Fig. 4.14F). This is further confirmed by larger cellular lesions especially on day 75pi (Fig 4.14 G).

In both independent experiments in Moscow and Borstel, the bacterial load in the resistant B6 mice were lower than in the susceptible B6.I-C3Hsst1 and the B6.I-9.3.19.8 (Fig. 4.11 A and 4.14 A). The cell surface markers expressed by the immune cells infiltrating the lungs as characterized by flow cytometry, were predominantly macrophages (CD68+ cells) and PMN

(Ly6G+ cells) on day 14pi. In the B6.I-9.3.19.8, the percentage of PMN infiltrating the lungs as observed by our collaborators in Moscow became statistically significant only on 77dpi. In contrast, in our hands, there was no statistically significant difference in PMN numbers between the Mtb infected resistant B6 and susceptible B6.C3Hsst1 mice.

Also, while our collaborators observed more of CD4 T cells in resistant B6 mouse lungs than those from susceptible B6.I-9.3.19.8 at 14d, 28d and 75dpi, no statistically significant differences in CD4 and CD8 T cell counts was observed at 14d, 36d and 77dpi between Mtb infected B6 and B6.C3Hsst1 mice.

Furthermore, our collaborators characterized the expression of CD44 and CD62 on T Cells and found the expression of $CD44^{hi}CD62L^{\%}$ was significant on $CD4^{+}$ T Cells in the susceptible B6.I-9.3.19.8 on 28dpi (Fig 4.14F).

The observed differences in pro-inflammatory and anti-inflammatory cytokines though not yet conclusive statistically, (the data have not been included in this thesis), suggests that the susceptible B6.I-9.3.19.8 and B6.C3Hsst1 secreted more IFN-ɤ, GMCSF, IL-8, IL-6, TNF-α, IL-1β and IL-10 than the resistant B6 mice.

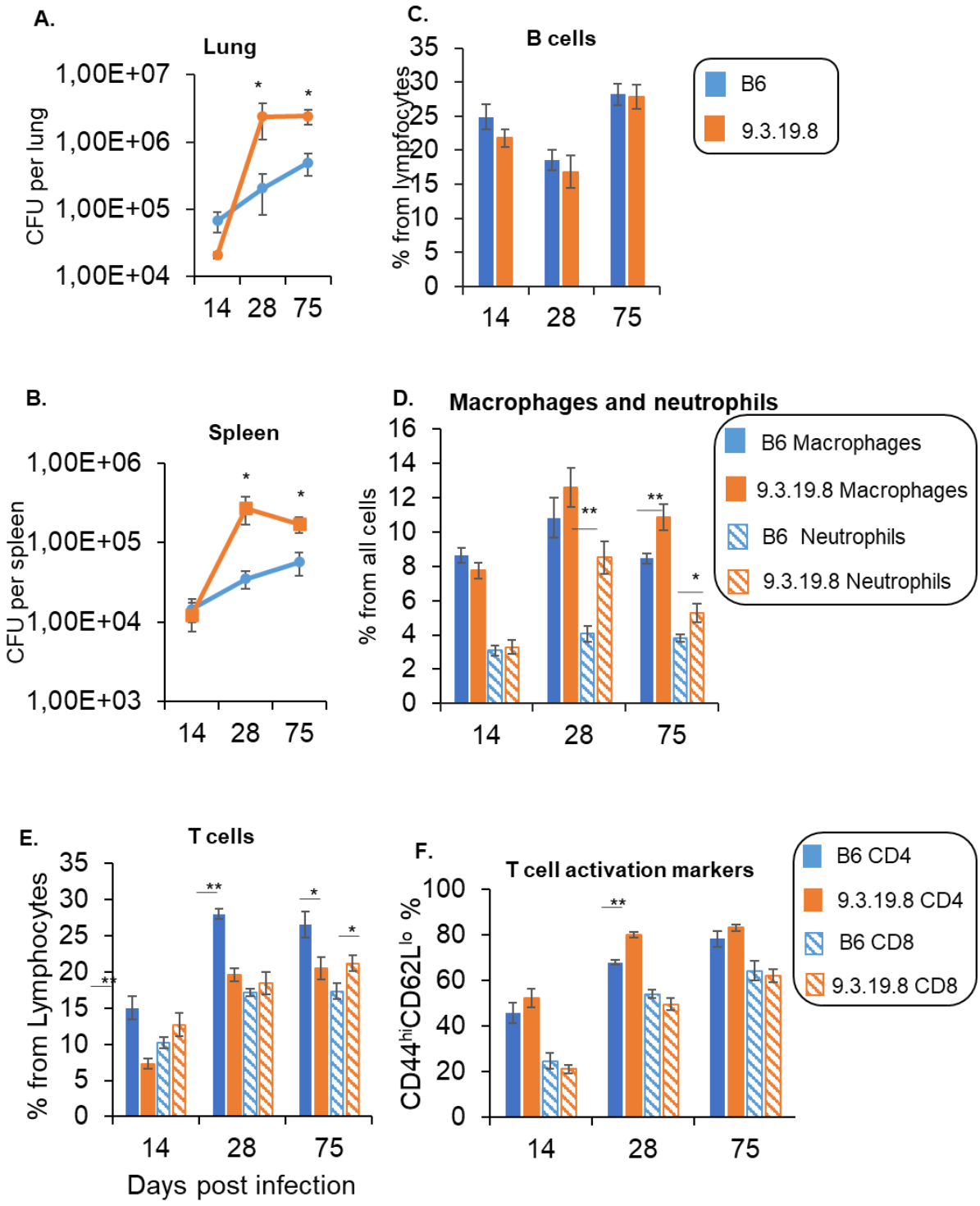
A.
Lung
CFU per lung
1,00E+07
1,00E+06
1,00E+05
1,00E+04
14 28 75
C.
B cells
% from lymfocytes
35 30 25 20 15 10 5 0
14 28 75
B6
9.3.19.8
B.
Spleen
CFU per spleen
1,00E+06
1,00E+05
1,00E+04
1,00E+03
14 28 75
D.
Macrophages and neutrophils
% from all cells
16 14 12 10 8 6 4 2 0
14 28 75
B6 Macrophages
9.3.19.8 Macrophages
B6 Neutrophils
9.3.19.8 Neutrophils
E.
T cells
% from Lymphocytes
35 30 25 20 15 10 5 0
14 28 75
Days post infection
F.
T cell activation markers
CD44hiCD62Llo %
100 80 60 40 20 0
14 28 75
B6 CD4
9.3.19.8 CD4
B6 CD8
9.3.19.8 CD8

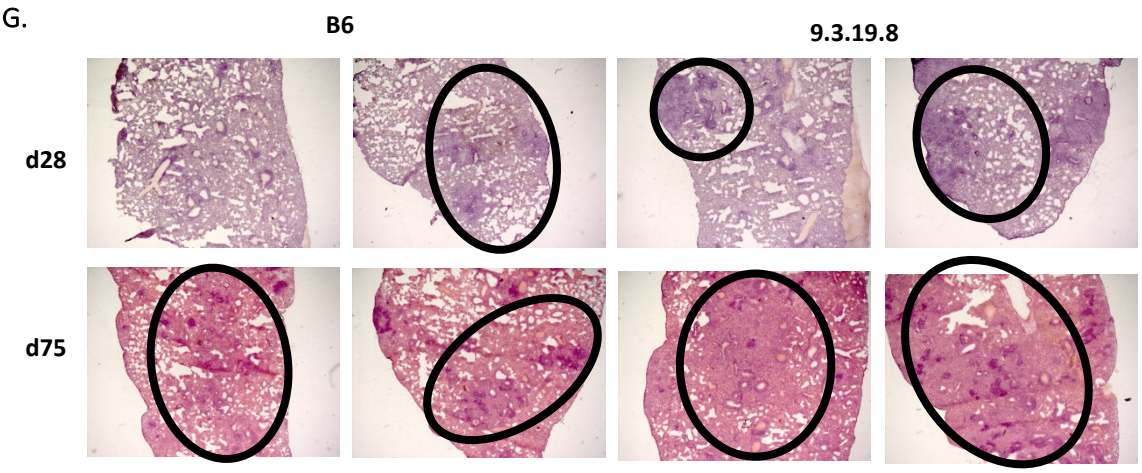

Fig. 4.14: Increase bacterial burden and cellular infiltrates in susceptible B6.I-9.3.19.8 mice. C57BL/6 mice (B6) and congenic B6.I-9.3.19.8 mice were infected per aerosol sacrificed at days 14, 28 and 75 post infection, n = 3 - 5 mice in each group, per time point. Organs were harvested and homogenized. Tissue homogenates were plated, and bacteria colonies were counted after ~ 4 weeks of incubation **A** and **B**. Lung were digested, cells were isolated and stained for surface markers **C** – **E.** Cells were treated with antigen P25 and expression of $CD44^{hi}$ and $CD26L^{lo}$ were measured by FACS, **F**. Histology H&E staining of lung tissue with circles around cellular lesions, **G.** MDS plot showing sample clustering, **H.** Error bars depict +/- SEM 2-Way Anova Tukey multiple comparison test where **** is p<0.0001, *** is p = 0.0007 , p = 0.0005 and* is p < 0.05

Based on these observations, we were interested in the transcriptional differences in the lungs of resistant B6 and susceptible B6.I-9.3.19.8. We received RNA samples of these mice from our collaborators in Moscow. And in Borstel, we studied the transcriptome of these mice prior to infection, d14, d28 and d75 post infection by RNA sequencing.

The transcriptional differences between the resistant B6 and susceptible B6.I-9.3.19.8 (represented as X9_3 in Fig 4.15) is mainly time point dependent. The samples prior to infection clustered together, same as the samples on 14dpi but on 28 and 75dpi, the

transcriptional differences were not as distinct as the naïve and 14dpi. However, the transcriptome of the resistant Mtb infected B6 was mostly “cancer-like”, as most of the DEGs were connected to key pathways involved in lung carcinoma. Whereas the susceptible B6.I-9.3.19.8 responded to Mtb infection with transcripts connected to “infection immunity” (data not shown see Table 8).

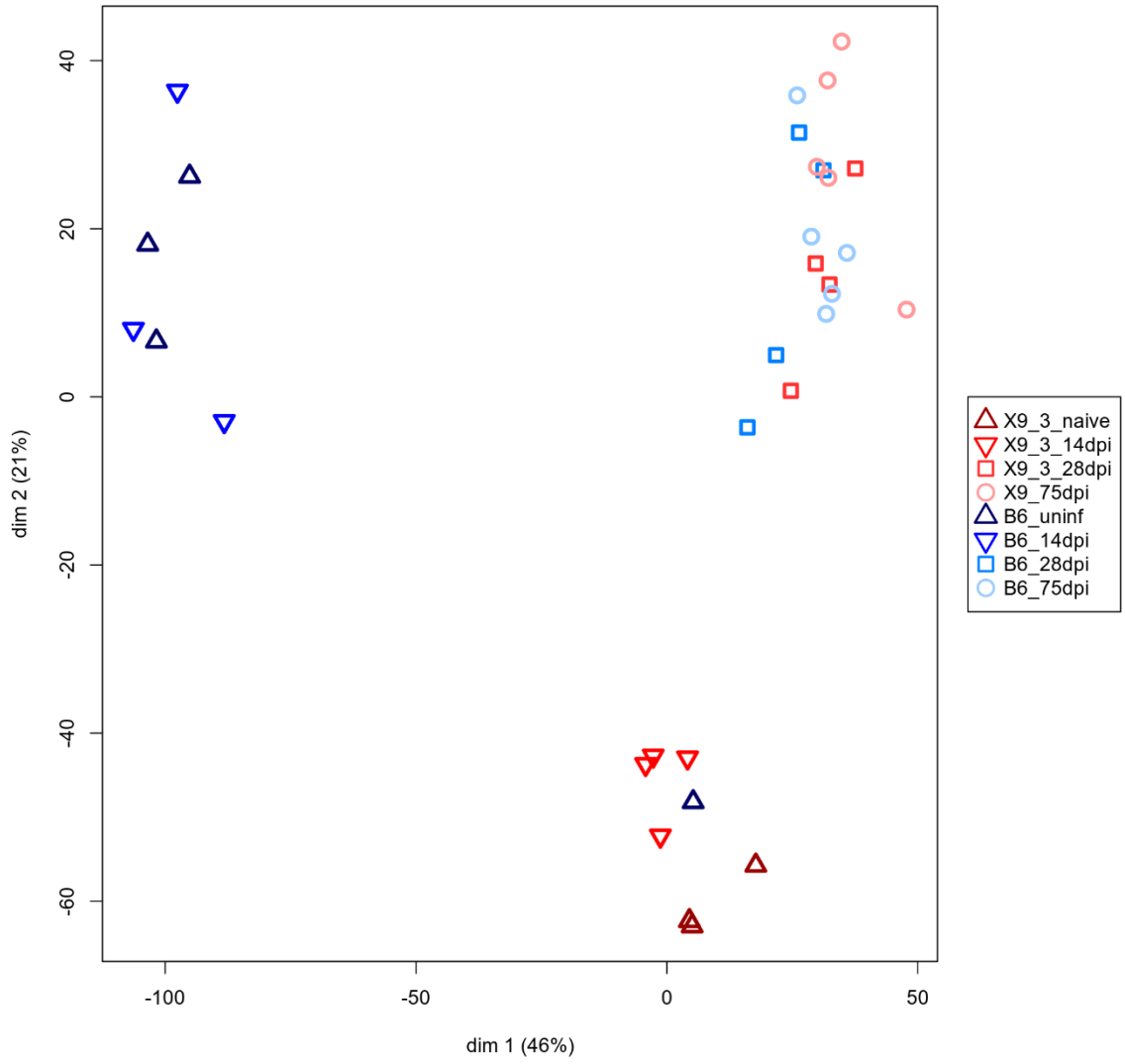

Fig. 4.15: MDS plot of B6 versus B6.I-9.3.19.8 mice. C57BL/6 mice (B6) and congenic B6.I-9.3.19.8 mice were infected per aerosol sacrificed at days 14, 28 and 75 post infection, n = 3 - 5 mice in each group, per time point. RNA were extracted from naïve and infected mice at the different time points. RNAseq samples were compared across the murine groups and time point.

4.3.4 Host genome specific lung inflammation

Inflammatory markers are key predictors of disease exacerbation. Inflammation regulates both disease resolution and exacerbation. On the part of the host, the earlier proinflammatory cytokines are induced, the faster the pathogen is cleared. However, on the other hand, pathogen exploits high inflammatory environment to escape intracellular cell death and enter a new activated host cell to replicate in. The specific turn of events of both pro- and anti-inflammatory cytokines must be tightly regulated within each host cell, but this is also specific to the host genetics.

Hypothetically, the differences in gene regulation leading to phenotypic variation in human and murine TB could be transcriptionally captured. These transcriptional changes might reveal common pattern explaining susceptibility and resistance in experimental and clinical TB.

The difference between the murine and human genome in response to Mtb infection was investigated by RNAseq. The human TB samples (green circles) were compared to the non-TB samples (blue circles Fig 4.16). The differences observed between the TB and non-TB samples and the murine and human TB samples resulted to about 11,885 differentially expressed genes. For visualization, the MDS plot as represented by two dimensions, show that the distance within the human samples is closer than comparing human and murine samples. At the core of the multiple comparison (Fig. 4.16 B) are 351 genes that are differentially expressed and along the intersect are shared genes while on the outermost part of the Venn diagram are unique number of genes for human and murine TB samples vs non-TB which is the cancer associated samples (418), human TB versus murine TB (394), human TB versus the susceptible B6.I-9.3.19.8 (9.3) (27), human TB versus resistant murine TB B6 (166), and human

TB versus non-TB cancer samples (14). The central 351 genes shared across the human and murine sample include but are not limited to *MARCKLS1, PABPC3, MS4A14, PATL2, ARFGAP1,* and *CCDC94*. *Myristoylated alanine-rich c-kinase substrate family* (*MARCKSL1)* is important for cytoskeletal regulation and formation of adherence junction[95]. *Polyadenylate-binding protein 3 (PABPC3)* is required for mRNA stability and translation[96]. *Membrane spanning 4 domains A14* (*MS4A14)* is an integral component of the membrane[97]. *DNA protein associated topoisomerase* (*PATL2)* also known as *PAT1* is an oocyte specific mRNA binding protein which regulates mRNA homeostasis[98]. *ADP ribosylation factor GTPase activating protein 1 (ARFGAP1)* is associated with dissociation of coat protein from Golgi-membrane and vessicles[99]. *Coiled coil domain containing 94 - CCDC94* protects cells from ionizing radiation[100].

To summarize, species specific and cross-species gene expression signatures were observed in both human and murine samples with shared and distinct genes in the multiple comparison. However, the functional roles of these genes in the TB pathogenesis has not yet been described. However *ARFGAP1* has been shown to prevent Mtb engulfment in epithelial cells[101].

A.

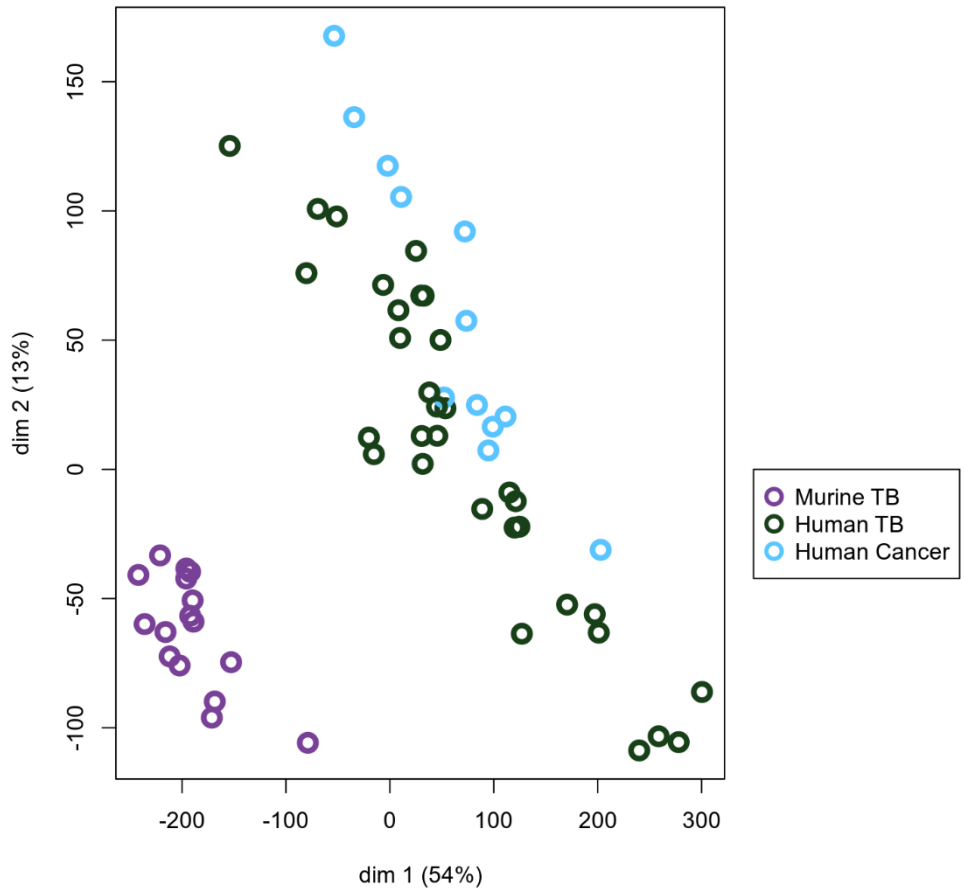
dim 2 (13%)
150
100
50
0
-50
-100
-200
-100
0
100
200
300
dim 1 (54%)
Murine TB
Human TB
Human Cancer

B.

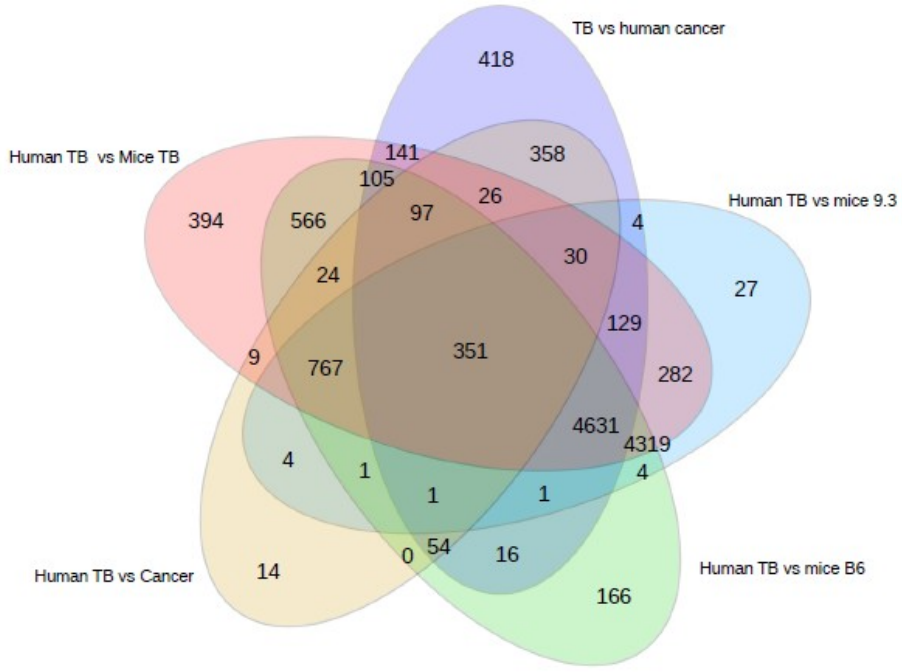
TB vs human cancer
418
Human TB vs Mice TB
141
358
105
26
394
566
97
4
Human TB vs mice 9.3
30
24
27
129
9
767
351
282
4631
4319
4
1
4
1
1
0
54
16
Human TB vs Cancer
14
Human TB vs mice B6
166

Fig. 4.16: Species specific and cross species differences in human and murine TB. Human TB lungs and non-TB samples were digested, and RNA was isolated and sequenced. Female B6 and B6.I.9.3.19.8 aged 12-14 weeks were infected with ~100 CFU Mtb per aerosol, mice were sacrificed at 14-, 25-, and 75-days post infection. Lungs were digested and RNA was isolated and sequenced. **A.** MDS plot showing clustering of human TB, control Non-TB (Cancer-associated) and murine experimental TB. **B.** Venn diagram showing multiple comparison of DEGs.

Table 8 sums up the host specific differences observed in human TB and murine TB. We do not have data for bacterial burden and immune cell types in the excised granuloma from TB patients, therefore this is designated as “not available data” (NA).

With RNAseq we found more than 10,000 differentially expressed genes when 16 human TB samples were compared to 6 non-TB samples. These genes were filtered for the top 50, and more than one-third of the top 50 genes were upregulated in the non-TB samples, and these genes were connected to cancer pathways. Whereas the genes upregulated in the TB samples were genes connected to “infection and immunity” pathways.

The transcriptional differences summarized in Table 8 is based on the number of differentially expressed genes that are connected to “cancer” or “infection and immunity” pathways. While the genes differentially regulated in the resistant B6 mice are mainly genes connected to cancer pathways, the genes differentially regulated in the susceptible B6.I-9.3.19.8 are connected to “infection and immunity” pathways. The transcriptome of the B6.C3Hsst1 have been sequenced but not yet analysed. Therefore, a complete comparison of human sample and both B6 versus B6.I-9.3.19.8 and B6 versus B6.C3Hsst1 will be the next step required to dissect the transcriptional differences in the susceptible murine models.

Table 8: Summary of observed differences between human and murine TB

Parameters	Human	B6	B6.I-9.3.19.8	B6.C3Hsst1
Bacterial Burden	**NA**	**+**	**++**	**++**
Lesion	**++**	**+**	**++**	**++**
Neutrophil	**NA**	**++**	**+++**	**++**
T cell count	**NA**	**+++**	**++**	**++**
B cell count	**NA**	**++**	**++**	**++**
Activation markers on T cells	**NA**	**-/+**	**++**	*****
Pro-inflammatory cytokines	**++**	**++**	**+++**	**+++**
Anti-inflammatory cytokines	**++**	**-/+**	**++**	**++**
Transcriptome	**Infection and cancer-like**	**Cancer-like**	**Infection immunity**	***In progress***

NA = not available *= not characterized

5.0 Discussion

Gene-gene interaction studies are beginning to help solve global health problems however, this has not yet contributed to eradication of infectious diseases. Immune responses to infectious diseases are genetically and environmentally determined.

Innate and adaptive immunity take precise turns to protect the host against invading pathogens. The exact sequence of events is genetically controlled but cannot be clearly defined without appropriate experimental models. Both innate and adaptive immune responses are made up of different cell types that have transcriptionally distinct programs depending on the site of action and can also be modulated by the tissue resident cells and the extracellular mileu.

However, pathogens can exploit the host response, and drive immune pathology, which in the case of TB enables transmission by coughing. The long-term consequence of host pathogen interactions in TB is defined by the sequence of immune responses which can cause post infection disease despite successful antibiotic therapy.

Active-TB patients are a risk to public health. Several policies formulated to control disease transmission are not fully sufficient to eradicate infectious diseases like TB due to host and pathogen genomics[1,102]. To better understand host responses at the transcriptome, cellular and whole tissue levels, we hypothesized that the genes mediating disease susceptibility or resistance to pathogens are the underlying reasons for differential phenotypes. And that these genes may serve as putative targets for therapeutic host-oriented treatment of TB in combination with effective antibiotics.

Due to the complex interactions of host and mycobacterial genomes as a result of long-term co-evolution processes, we focused on the comparison of M. *tuberculosis* infection between

humans and mice. Transcriptional differences within and across the host genomes could be the reasons for variations seen in tuberculosis (TB) pathology, transmission, and treatment outcomes. This comparative study was designed to understand some of the genes that could account for TB susceptibility or resistance in immune competent host. Thoroughly looking first in rare human lung samples from TB patients, probing human blood and then well-defined murine models with comparable wild-type controls revealed differences between susceptible and resistant mice, and to some extent parallel observations in TB patients.

This study focuses on the host response to tuberculosis (TB). It can explain the extent to which host cells can control mycobacterial replication and the transcriptional changes in host cells *in vitro* and in lungs of mice and humans.

5.1 Human TB and non-TB Lung Transcriptome

In our collaboration with scientists at the Central Institute for Tuberculosis Moscow, RNA from excised lung tissue of TB patients in comparison to non-TB patient specimen from tumor bearing lungs were studied by RNA sequencing to identify genes associated with TB disease putatively mediating TB susceptibility in humans (Fig 4.1 I).

To identify genes that could serve as putative target for host-directed therapy and the implication of these genes for TB pathogenesis, we focused first on the transcriptome from excised lung of patients with TB, by RNAseq and selected genes were validated by qPCR. Further studies on the human RNA could not be performed as we in Research Center Borstel did not have access to the excised tissue from the respective patients.

However, we gained some insights into a number differentially regulated genes which were important for cell cycle, cell proliferation, cell adhesion, and immune cell recruitment among other functions.

Most of the differentially expressed genes in the lung of the FCT TB patient were associated with four main pathways. These pathways are B cell receptor signalling, primary immunodeficiency, focal adhesion, and extracellular matrix receptor interaction (Fig 4.5 B). These are pathways that must interact together to restore lung homeostasis, tissue remodelling and wound healing. On the contrary, primary immunodeficiency is a major reason for loss of immune protection and tissue integrity. Disorder in one or more components of the immune system cannot be easily overcome by antibiotic therapy only. Notably, also the combination of most of the available anti-TB treatments are toxic and can damage the host tissue as a side effect of killing the mycobacteria.

The functions and anomalies associated with variants of the genes in the heatmap (Fig. 4.3) implies that differential gene expression could also be due to abnormal expression pattern of the control samples used for comparison (cancer), which may have been influenced by the neighbouring tumor tissue, the responses to the cancer cells or the effect of anti-cancer chemotherapy. In humans, *GBP2*, *FCGR1B* and *SERPING1* were shown to be significantly upregulated in blood of TB progressors[103]. These genes are connected to the IL-12-IFN-ɣ axis and could be associated with PMN involvement as shown in the human blood TB transcriptome nodules by Moreira-Teixeira et. al[41]. Without proper lung perfusion, which has not been done with the human samples, blood cell gene transcripts could bias transcriptomes for example through PMN signatures, the predominant myeloid cell type in peripheral blood.

Therefore, we cannot entirely rule out PMN associated blood derived transcripts in the human lung transcriptomes.

In this study, many unique genes have been identified in both murine and human samples these include genes with functions associated with the regulation of “extracellular adhesion molecules”, “primary immune deficiency” and “T and B cell receptor signalling”, amongst others.

5.2 *In Vitro* Human and Murine Data

To better understand the role of myeloid cells with focus on PMN in human TB, we studied human PMN and PBMCs *in vitro* (Fig. 4.1 I *in vitro* and 4.7 A – E). We especially focused on the role of PMN in TB in humans as these innate immune cells are the predominant cell in active TB patients’ lungs and have been recently associated with pathogenesis rather than clearance of the pathogen[6,43]. We also found that passage of Mtb through PMN. Which succumb to necrotic cell death paves the way for Mtb to survive and grow better in macrophages, which subsequently phagocytose infected PMN[32].

Mtb infected PBMCs compared to uninfected PBMCs showed 1008 differentially expressed genes, in contrast, 7627 differentially expressed genes were seen when Mtb infected co-culture of PBMC and PMN were compared to uninfected PBMC and PMN co-culture. We observed that PMN induced transcriptional changes in PBMCs when co-cultured overnight with or without Mtb infection. And that the PBMCs with or without Mtb show less gene regulation compared to PBMCs and PMN (Fig 4.7 E). With the foreknowledge that peripheral blood PMN are the most abundant in the lungs of active TB patients, and that these PMN are irregular in morphology, PMN thus become a multifactorial cell in human TB[6,32]. PMN necrosis

and subsequent macrophage phagocytosis of necrotic PMN could be the mechanism required for the lung tissue remodelling. However, the host specific differences in human TB is a major factor overwriting cell death mechanisms during anti-TB therapy.

In the presence of PMN, uninfected PBMCs quickly form cellular aggregates *in vitro*. These cellular aggregates are "*in vitro* like granuloma" (Fig 4.7 A – D) that readily increased in numbers upon Mtb infection and PMN necrosis. These differences observed microscopically reflected in the transcriptional profile. Equal PMN numbers co-cultured with PBMCs drastically increased the numbers of differentially expressed genes (DEGs) and KEGG pathways in comparison to PBMCs without PMN (Fig. 4.7 E). The differentially regulated genes in the uninfected PBMC-PMN co-cultures compared to those with Mtb infected were 7,627 while PBMC alone compared to PBMC-Mtb infected cultures were 1,008. The genes differentially regulated in uninfected PBMC-PMN cultures compared to Mtb infected PBMC-PMN cultures include *CASP5*, *CCRL2*, *CLEC4E*, *MCTP1*, *PLD1*, *TLR8,* which are important in inflammation, leukocyte migration, autophagy, macrophage polarization and metabolism, and T regulatory cell function.

Importantly, some of the genes observed in the *in vitro* PBMC-PMN cultures were also differentially regulated in the human TB tissue transcriptomes. Examples amongst others are CLEC4E/MINCLE, PLD1, CCRL2, and TLR8. CLEC4E/MINCLE in combination with TLR4 and TLR2 pathways have been shown to be a putative HDT target in Mtb infection, through restriction of bacterial growth[75] or limiting production of the immunocompromising IL-10 cytokine[104]. PLD1 together with ARF1 and ARFGAP1 signalling is required for Mtb entry into epithelial cells. CCRL2 biases macrophage towards M2 phenotype through Mtb heat shock protein 163[101]. M2 macrophages are anti-inflammatory and are unable to eliminate Mtb in contrast to pro-

inflammatory M1 macrophages which can kill Mtb. CCRL2 were observed to be upregulated in active TB patients[105,106]. Single nucleotide polymorphisms in some toll like receptor genes have been described in association with TB susceptibility[107]. We observed upregulation of TLR8 in both *in vitro* and *in vivo* transcriptome data. TLR7 and TLR8, TLR4 and TLR8 and TLR8 and TLR9 SNPs were associated with development of active pulmonary TB in Indian and Chinese Han population[108–110].

Notably, the *in vitro* samples represent a relatively short time period of Mtb infection, which is in contrast to the long-term duration of TB in the human lung tissue samples and therefore the transcriptomes between the *in vitro* and *in vivo* analyses differ considerably.

Furthermore, we tried to dissect the role of the Ipr1/sst1 gene in mediating susceptibility to Mtb *in vitro* as previously established[88]. In parallel, the bone marrow derived macrophages (BMDM) from B6.C3Hsst1 were compared to the wild-type B6 and C3H (Fig 4.1I BMDM *in vitro*) to understand the strain specific differences in resistance and susceptibility at the macrophage level. The B6 and C3H have been widely studied *in vitro* and *in vivo* but not in a comparative experimental setting[94,111–113]. The B6, C3H and B6.C3Hsst1 macrophages were stimulated with IFN-ɤ only, TNF-α only, LPS only and a combination of TNF-α and LPS, or LPS and IFN-ɤ. The expression of MHCII by the BMDM and nitric oxide (NO) secretion, Mtb replication and cell death was assessed (Fig 4.8 – 4.10).

As expected, the resistant B6 were able to control Mtb growth better than the susceptible C3H and intermediate susceptible B6.C3Hsst1 (Fig 4.9 A -D). The BMDM from C3H quickly became necrotic as shown by the relative LDH activity (Fig 4.10 A -D). Although the data for Mtb burden in the BMDM were not statistically significant, Mtb was better controlled in BMDM pre-treated and maintained in IFN-ɤ (Fig 4.9D). Likely because IFN-ɤ activates genes

encoding antimicrobial effectors such as NOS2 and creates an inflammatory and pro apoptotic environment in BMDM[87].

On the contrary, without pre-treatment of BMDM with IFN-ɣ, exogenous addition of IFN-ɣ after Mtb infection was still sufficient to control Mtb replication and necrotic cell death in the resistant B6 but not in susceptible C3H and B6.C3Hsst1 mice.

5.3 *In vivo* Murine Experiments

Subsequently, two independent *in vivo* experiments were designed in Moscow and Borstel to understand the role of host genetics in immune protection and lung pathology (Fig 4.1I *in vivo*). Our collaborators in Moscow focused on the role of a defined MHC-II locus from the susceptible I/St mice conferring susceptibility in resistant B6. The congenic susceptible mice of B6.I-9.3.19.8 strain were compared to the wild type resistant B6 in terms of bacterial load, immune cell recruitment to the lungs by flow cytometry, lung lesion characterization by H&E staining, and at the Research Center Borstel, we analyzed the lung transcriptome by RNA sequencing (Fig 4.14). Prior to infection, transcriptomes of B6.I-9.3.19.8 versus B6 mice showed distinct clusters of the samples as well as on day 14 post infection before adaptive immunity set-in. However, at later time points, 28 days and 75 days post infection, the transcripts of both mice became similar without clear clustering of the samples suggesting immune response dependent transcriptomes in both mouse strains, which were similar and therefore not distinct anymore as soon as specific immunity kicked in.

The second comparative *in vivo* TB experiment was done at the Research Center Borstel. The focus was on the Ipr1/sst1 locus from susceptible C3H mice crossed into resistant B6 mice. The resulting B6.C3Hsst1 mice which have been tested in different experimental studies in

the past[88,111,114], have not been transcriptionally characterized in comparison to parental resistant B6 mice.

The focus on congenic murine models has been successful in narrowing the window of differences across immune-competent hosts. However, the reasons for these differences remain less defined in many generations[14,49,87,115,116].

The B6.I-9.3.19.8 and B6.C3Hsst1 have been designed based on the role of host genetics and inheritance pattern in mediating resistance to intracellular pathogens. In line with previous findings on TB susceptibility and resistance in murine models based on the B6 background[88,94,117,118], we observed differences in granulomatous lesions and the $CD4^+$, $CD8^+$ T cell count in the lungs. Notably, Mtb count in the lungs of the susceptible B6.I-9.3.19.8 and B6.C3Hsst1 were significantly higher than in the resistant B6 strain on day 28 and 75/76 post infection. However, Mtb load in the spleen of the susceptible B6.C3Hsst1 was not significantly higher than in resistant B6 mice except on d28, with statistically significant differences in bacterial replication.

5.4 Complexity of host and mycobacterial genome interaction

Hypothetically, the human and mycobacterial genome co-evolution account for geographical differences in the disease response. On the part of the host, the long-term co-evolution may have succeeded in adaptive genetic modifications including advantageous and detrimental effects. Therefore, the interaction of resistant and susceptibility genes at different genetic loci could mediate disease pathology, tissue remodelling and ultimately whether the host overcomes and survives the infection or succumbs to and transmit the pathogen.

The outcome of human TB is governed largely by host factors. These factors include immune regulation, immuno competency, age, sex and comorbidities[35,119]. Genetic susceptibility to TB is polygenic and does not entirely follow the classical Mendelian genetics of one gene one trait. The complexity of human TB makes it difficult to understand the extent to which a genetic locus can be a risk factor for the development of pulmonary TB, or mediate disease susceptibility and severity.

The effect of a genetic locus is better studied in tractable murine models of experimental TB, precisely, congenic mice. B6.I-9.3.19.8 and B6.C3Hsst1 are distinct and attractive congenic models of the TB granuloma. While B6.I-9.3.19.8 and B6.C3Hsst1 both follow the Mendelian law of inheritance, the later controls innate immune response while the former regulates adaptive immunity. Importantly, we observed host specific differences in the human and murine transcriptome (Fig 4.16 and table 8)

In line with previous findings that inflammatory responses in human and mice are genotype specific[50,120], we observed a clear distinction between the human and murine TB samples (Fig 4.16B). These differences in sample cluster were rather based on genome architecture than the disease. In contrast, comparison within the human TB and NON-TB samples were influenced by read counts, hence samples with higher reads tend to cluster better together than samples with low read count (Fig 4.2 E and 4.16A).

The species-specific differences as shown in Fig 4.16B is wider when comparing human TB to murine TB, which means the data from experimental studies focusing on murine genes may not be directly linked to clinical TB. For example, TB severity in C3HeB/FeJ mice was shown to be mediated by defect in the interferon signalling pathway, which allows Mtb to drive the host cells into early necrosis providing an inflammatory environment that contributes to lung

tissue destruction[41,112,113,121,122]. The granulomatous lesions observed in the Mtb infected B6.C3Hsst1 is similar to those of observed in C3HeB/FeJ mice, with fibrous caseation, necrotic core and liquefactions as shown by the HE and MG staining (Fig 4.12 D), indicating that the *sst1* locus is involved these pathogenesis exacerbating processes.

Taken together, human, and murine transcriptome signatures in response to Mtb infection were compared to better understand TB susceptibility and pathology. The differentially regulated genes in experimental murine and clinical human TB might identify putative targets for host directed therapies as adjunct to antibiotic treatment. These genes could be involved in controlling disease exacerbation or amelioration. Targeting these genes may help to reduce immunopathology, overshooting inflammation, bacterial burden and to improve lung tissue remodelling. Therefore, functional studies analysing each of these genes and possible detrimental effects of modulating the activities of these gene are required. For example, in Mtb infected PBMC and PMN co-culture, we observed that TLR8 was upregulated compared to uninfected PBMC and PMN co-culture. Interestingly, single nucleotide polymorphisms (SNPs) in TLR4 and TLR8 in Indian population, TLR7 and TLR8 and TLR8 and TLR9 SNPs in Chinese Han population were shown to be associated with susceptibility to TB[107–110]. Worthy of note is also the putative host directed therapy possibility of targeting CLEC4 in reducing the growth of *Mycobacteria*[75].

5.5 Critical Appraisal

This research study was formulated to contribute to the question of TB susceptibility in immune competent host. The purpose of the study has been mostly achieved successfully, not without some challenges though. We have shown in our hands that both the B6.C3Hsst1 and B6.I-9.3.19.8 are suitable models to study neutrophil recruitment and granulomatous lesion formation in murine lungs as observed in humans with active TB. Both models do not completely recapitulate the polygenic nature of human TB. This challenge can however be met through modern methods like Liveseq, Dual-Seq of host and Mtb in different murine models like humanized mice and transgenic mouse models[123–125]. Microarray and RNAseq have been the methods of choice in probing the transcriptional signatures in human and murine TB studies[39,50,126–128]. While microarray chips have been designed to capture known genes, RNAseq offers discovery of unknown genes[59]. In contrast, RNAseq is more analytically intensive compared to microarray. To cover more genes than previously described, we have chosen RNAseq.

Our methods of choice in combining RNAseq, qPCR, bacterial colony forming unit assay, and flow cytometry to characterize cells in the lungs, helped to cover various aspects of the host response to Mtb infection. In contrast to the high resolution RNAseq data with 2x 75 cycles covering both strands of the DNA, the qPCR is low resolution with specific primer combination for forward and reverse reads of 45 cycles. Therefore, the qPCR data (Fig 4.6) based on selected genes from the RNAseq data are not entirely comparable due to differences in the resolution and analysis of the methods and result. However, it was impressive to confirm the expression of 16 selected genes by qPCR in the human TB and non-TB samples. These genes are AGRN, AHR, BCAM, CD19, COL1A1, COL5A3, CR2, LRCC2, MPO, PONL1, RAP1B, SLFN11, SCRIB, SPN, TNFRSF13B and TCF4.

Our study is still missing valuable functional experiment such as analysing IFN-ɣ and other cytokine production by $CD4^+$ and $CD8^+$ T cells recruited to the lungs during Mtb infection and whether the recruitment of IFN-ɣ producing T cells is dependent on the transferred locus 9.3.19.8 from I/St mice or the sst1/Ipr1 locus from the C3H mice. This will require adoptive T cell transfer of naïve or primed T-lymphocytes from the B6.I-9.3.19.8 and the B6.C3Hsst1 to the wildtype B6 mice[129]. The transcriptional changes in the lungs of the recipient mice might also provide information on gene regulation and protective role of the transferred lymphocytes.

5.6 Future Perspectives

Tuberculosis infection is not monogenic as previously described in immune-compromised individuals carrying mutations in Mendelian susceptibility loci. The polygenic trait in TB is further compounded by confounding factors across species. Species specific differences across labs and studies can be phenotypically explained with reference to study objectives and design[10,130–133].

There is not a one model fit all approach without bias. Each model is designed to meet the set purpose of the research work. Our animal models did not entirely unravel the genetic code on murine responds to TB, but it explains the specificity of strain and genetic background upon which the strain was generated. Optimistically, combining the result of different models to train and test data sets with the current possibilities of machine learning algorithms can bring research closer to reality of resolving the problem of TB disease.

Furthermore, combined analysis of both, host's and pathogen's genetic changes in parallel informs treatment options in timely manner to prevent the worsening of the lung

pathology[42,61,134,135]. Ultimately, better therapeutic options with less adverse effects needs to be developed to combat TB, hence breaking disease transmission.

6.0 References

1. Meyer, C. G. & Thye, T. Host genetic studies in adult pulmonary tuberculosis. *Semin. Immunol.* **26**, 445–53 (2014).
2. Fogel, N. Tuberculosis: A disease without boundaries. *Tuberculosis* **95**, (2015).
3. Ernst, J. D. The immunological life cycle of tuberculosis. *Nature Reviews Immunology* **12**, 581–591 (2012).
4. Kaufmann, S. H. E. & McMichael, A. J. Annulling a dangerous liaison: vaccination strategies against AIDS and tuberculosis. *Nat. Med.* **11**, S33–S44 (2005).
5. Kramnik, I., Beamer, G. & Beamer, G. Mouse models of human TB pathology : roles in the analysis of necrosis and the development of host-directed therapies. 221–237 (2016). doi:10.1007/s00281-015-0538-9
6. Dallenga, T. & Schaible, U. E. Neutrophils in tuberculosis--first line of defence or booster of disease and targets for host-directed therapy? *Pathog. Dis.* **74**, 1–8 (2016).
7. Reiling, N. *et al.* Clade-specific virulence patterns of Mycobacterium tuberculosis complex strains in human primary macrophages and aerogenically infected mice. *MBio* **4**, (2013).
8. Kramnik, I., Dietrich, W. F., Demant, P. & Bloom, B. R. Genetic control of resistance to experimental infection with virulent Mycobacterium tuberculosis. *Proc. Natl. Acad. Sci.* **97**, 8560–8565 (2000).
9. Dorhoi, A. *et al.* Type I IFN signaling triggers immunopathology in tuberculosis-susceptible mice by modulating lung phagocyte dynamics. *Eur. J. Immunol.* **44**, (2014).
10. Heitmann, L. *et al.* The <scp>IL</scp> -13/ <scp>IL-4R</scp> *α* axis is involved in tuberculosis-associated pathology. *J. Pathol.* **234**, 338–350 (2014).
11. Cadena, A. M., Fortune, S. M. & Flynn, J. L. Heterogeneity in tuberculosis. *Nat. Rev. Immunol.* **17**, 691–702 (2017).
12. Corleis, B. *et al.* Escape of Mycobacterium tuberculosis from oxidative killing by neutrophils. *Cell. Microbiol.* **14**, 1109–1121 (2012).
13. Hawn, T. R. *et al.* Tuberculosis Vaccines and Prevention of Infection. *Microbiol. Mol. Biol. Rev.* **78**, 650–671 (2014).
14. Grandjean, L. *et al.* Transmission of Multidrug-Resistant and Drug-Susceptible Tuberculosis within Households: A Prospective Cohort Study. *PLoS Med.* **12**, 1–22 (2015).
15. Dorhoi, A. & Kaufmann, S. H. E. Perspectives on host adaptation in response to Mycobacterium tuberculosis: Modulation of inflammation. *Seminars in Immunology* **26**, (2014).
16. World Health Organization. *Global tuberculosis report*. (2018).
17. Correa-Macedo, W., Cambri, G. & Schurr, E. The Interplay of Human and Mycobacterium Tuberculosis Genomic Variability. *Front. Genet.* **10**, 1–9 (2019).
18. Geluk, A., van Meijgaarden, K. E., Joosten, S. A., Commandeur, S. & Ottenhoff, T. H. M. Innovative strategies to identify M. tuberculosis antigens and epitopes using genome-wide analyses. *Frontiers in Immunology* **5**, (2014).
19. Brites, D. & Gagneux, S. Co-evolution of Mycobacterium tuberculosis and Homo sapiens. *Immunol. Rev.* **264**, (2015).
20. Lerm, M. & Netea, M. G. Trained immunity: A new avenue for tuberculosis vaccine development. *Journal of Internal Medicine* **279**, (2016).
21. Nemes, E. *et al.* The quest for vaccine-induced immune correlates of protection against tuberculosis. *Vaccine Insights* **1**, 165–181 (2022).
22. WHO. *WHO Global TB report*. (2023). ISBN: 978-92-4-008385-1

23. WHO. WHO treatment guidelines for drug-resistant tuberculosis : 2016 update. *WHO* 56 (2016). doi:WHO/HTM/TB/2016.04

24. Kleinnijenhuis, J., Oosting, M., Joosten, L. a B., Netea, M. G. & Van Crevel, R. Innate immune recognition of Mycobacterium tuberculosis. *Clin. Dev. Immunol.* **2011**, 405310 (2011).

25. van Laarhoven, A. *et al.* Low induction of proinflammatory cytokines parallels evolutionary success of modern strains within the mycobacterium tuberculosis beijing genotype. *Infect. Immun.* **81**, 3750–3756 (2013).

26. Wamala, D., Buteme, H. K., Kirimunda, S., Kallenius, G. & Joloba, M. Association between human leukocyte antigen class II and pulmonary tuberculosis due to mycobacterium tuberculosis in Uganda. *BMC Infect. Dis.* (2016). doi:10.1186/s12879-016-1346-0

27. Chapman, S. J. & Hill, A. V. S. Human genetic susceptibility to infectious disease. *Nat. Rev. Genet.* (2012). doi:10.1038/nrg3114

28. Gagneux, S. *et al.* Variable host-pathogen compatibility in Mycobacterium tuberculosis. *Proc. Natl. Acad. Sci.* **103**, 2869–2873 (2006).

29. Orme, I. M., Robinson, R. T. & Cooper, A. M. The balance between protective and pathogenic immune responses in the TB-infected lung. *Nat. Immunol.* **16**, 57–63 (2015).

30. Tamoutounour, S. *et al.* Origins and functional specialization of macrophages and of conventional and monocyte-derived dendritic cells in mouse skin. *Immunity* **39**, 925–938 (2013).

31. Martin, C. J., Peters, K. N. & Behar, S. M. Macrophages clean up: Efferocytosis and microbial control. *Current Opinion in Microbiology* **17**, 17–23 (2014).

32. Dallenga, T. *et al.* M. tuberculosis-Induced Necrosis of Infected Neutrophils Promotes Bacterial Growth Following Phagocytosis by Macrophages. *Cell Host Microbe* **22**, 519-530.e3 (2017).

33. Divangahi, M., Khan, N. & Kaufmann, E. Beyond Killing Mycobacterium tuberculosis: Disease Tolerance. *Front. Immunol.* **9**, 2976 (2018).

34. Loxton, A. G. Bcells and their regulatory functions during Tuberculosis: Latency and active disease. *Mol. Immunol.* **111**, 145–151 (2019).

35. Schurz, H. *et al.* The X chromosome and sex-specific effects in infectious disease susceptibility. *Hum. Genomics* **13**, 2 (2019).

36. de Welzen, L. *et al.* Whole-Transcriptome and -Genome Analysis of Extensively Drug-Resistant Mycobacterium tuberculosis Clinical Isolates Identifies Downregulation of ethA as a Mechanism of Ethionamide Resistance. *Antimicrob. Agents Chemother.* **61**, 1–12 (2017).

37. Chen, B. F. *et al.* Association between HLA-DRB1 alleles and tuberculosis: A meta-analysis. *Genet. Mol. Res.* (2015). doi:10.4238/2015.December.1.37

38. Singhania, A. *et al.* A modular transcriptional signature identifies phenotypic heterogeneity of human tuberculosis infection. *Nat. Commun.* **9**, 2308 (2018).

39. Singhania, A. *et al.* Transcriptional profiling unveils type I and II interferon networks in blood and tissues across diseases. *Nat. Commun.* **10**, 1–21 (2019).

40. Berry, M. P. R. *et al.* An interferon-inducible neutrophil-driven blood transcriptional signature in human tuberculosis. *Nature* (2010). doi:10.1038/nature09247

41. Moreira-Teixeira, L. *et al.* Type I IFN exacerbates disease in tuberculosis-susceptible mice by inducing neutrophil-mediated lung inflammation and NETosis. *Nat. Commun.* **11**, (2020).

42. Kimmey, J. M. *et al.* Unique role for ATG5 in neutrophil-mediated immunopathology during M. tuberculosis infection. *Nature* **528**, 565–569 (2015).

43. Eum, S. Y. *et al.* Neutrophils are the predominant infected phagocytic cells in the airways of patients with active pulmonary TB. *Chest* **137**, 122–128 (2010).

44. Cooper, A. M. & Khader, S. A. The role of cytokines in the initiation, expansion, and control of cellular

immunity to tuberculosis. *Immunological Reviews* **226**, 191–204 (2008).

45. Herbst, S., Schaible, U. E. & Schneider, B. E. Interferon gamma activated macrophages kill mycobacteria by nitric oxide induced apoptosis. *PLoS One* **6**, (2011).

46. Behar, S. M. *et al.* Apoptosis is an innate defense function of macrophages against Mycobacterium tuberculosis. *Mucosal Immunology* **4**, 279–287 (2011).

47. Amulic, B., Cazalet, C., Hayes, G. L., Metzler, K. D. & Zychlinsky, A. Neutrophil Function: From Mechanisms to Disease. *Annu. Rev. Immunol.* **30**, 459–489 (2012).

48. Leliefeld, P. H. C., Wessels, C. M., Leenen, L. P. H., Koenderman, L. & Pillay, J. The role of neutrophils in immune dysfunction during severe inflammation. *Crit. Care* **20**, 73 (2016).

49. Zak, D. E. *et al.* A blood RNA signature for tuberculosis disease risk: a prospective cohort study. *Lancet* **387**, (2016).

50. Subbian, S. *et al.* Lesion-specific immune response in granulomas of patients with pulmonary tuberculosis: A pilot study. *PLoS One* **10**, 1–21 (2015).

51. Kaufmann, E. *et al.* BCG Educates Hematopoietic Stem Cells to Generate Protective Innate Immunity against Tuberculosis. *Cell* **172**, 176-190.e19 (2018).

52. Fox, G. J., Orlova, M. & Schurr, E. Tuberculosis in Newborns: The Lessons of the "Lübeck Disaster" (1929–1933). *PLOS Pathog.* **12**, e1005271 (2016).

53. Mantovani, A., Cassatella, M. A., Costantini, C. & Jaillon, S. Neutrophils in the activation and regulation of innate and adaptive immunity. *Nat Rev Immunol* **11**, 519–531 (2011).

54. Lee, M.-R. *et al.* Diabetes mellitus and latent tuberculosis infection: a systemic review and meta-analysis. *Clin. Infect. Dis.* **64**, ciw836 (2016).

55. Mohanty, S. *et al.* A Mycobacterial Phosphoribosyltransferase Promotes Bacillary Survival by Inhibiting Oxidative Stress and Autophagy Pathways in Macrophages and Zebrafish. *J. Biol. Chem.* **290**, 13321–13343 (2015).

56. Chan, F. K.-M., Moriwaki, K. & De Rosa, M. J. Detection of Necrosis by Release of Lactate Dehydrogenase Activity. in (eds. Snow, A. L. & Lenardo, M. J.) 65–70 (Humana Press, 2013). doi:10.1007/978-1-62703-290-2_7

57. Keane, J. *et al.* Tuberculosis Associated with Infliximab, a Tumor Necrosis Factor α–Neutralizing Agent. *N. Engl. J. Med.* **345**, 1098–1104 (2001).

58. Sane Schepisi, M. *et al.* Burden and Characteristics of the Comorbidity Tuberculosis—Diabetes in Europe: TBnet Prevalence Survey and Case-Control Study. *Open Forum Infect. Dis.* **6**, (2019).

59. Singhania, A., Wilkinson, R. J., Rodrigue, M., Haldar, P. & O'Garra, A. The value of transcriptomics in advancing knowledge of the immune response and diagnosis in tuberculosis. *Nat. Immunol.* **19**, 1159–1168 (2018).

60. Briffotaux, J., Liu, S. & Gicquel, B. Genome-Wide Transcriptional Responses of Mycobacterium to Antibiotics. *Front. Microbiol.* **10**, 1–14 (2019).

61. Dheda, K., Schwander, S. K., Zhu, B., Van Zyl-Smit, R. N. & Zhang, Y. The immunology of tuberculosis: From bench to bedside. *Respirology* **15**, 433–450 (2010).

62. Sabat, R. IL-10 family of cytokines. *Cytokine Growth Factor Rev.* **21**, 315–324 (2010).

63. O'Garra, A. *et al. The Immune Response in Tuberculosis*. *Annual Review of Immunology* **31**, (2013).

64. Harishankar, M., Selvaraj, P. & Bethunaickan, R. Influence of genetic polymorphism towards pulmonary tuberculosis susceptibility. *Front. Med.* **5**, 1–1 (2018).

65. Kumar, V. & Sharma, A. Neutrophils: Cinderella of innate immune system. *Int. Immunopharmacol.* **10**, 1325–1334 (2010).

66. Scriba, T. J., Coussens, A. K. & Fletcher, H. A. Human Immunology of Tuberculosis. *Microbiol. Spectr.* **4**, 1–23 (2016).

67. Penn-Nicholson, A. *et al.* Discovery and validation of a prognostic proteomic signature for tuberculosis progression: A prospective cohort study. *PLOS Med.* **16**, e1002781 (2019).

68. Behar, S. M., Divangahi, M. & Remold, H. G. Evasion of innate immunity by Mycobacterium tuberculosis: is death an exit strategy? *Nat. Rev. Microbiol.* (2010). doi:10.1038/nrmicro2387

69. Crouser, E. D. *et al.* A novel in vitro human granuloma model of sarcoidosis and latent tuberculosis infection. *Am. J. Respir. Cell Mol. Biol.* **57**, 487–498 (2017).

70. Gierahn, T. M. *et al.* Seq-Well: portable, low-cost RNA sequencing of single cells at high throughput. *Nat. Methods* **14**, 395–398 (2017).

71. Hwang, W. C. *et al.* PLD1 and PLD2 differentially regulate the balance of macrophage polarization in inflammation and tissue injury. 5193–5211 (2021). doi:10.1002/jcp.30224

72. Bhosle, V. K., Rivera, J. C., Zhou, T. E., Omri, S. & Sanchez, M. Nuclear localization of platelet-activating factor receptor controls retinal neovascularization. **1**, 1–18 (2016).

73. Joshi, A. S., Ragusa, J. V, Prinz, W. A., Cohen, S. & Olzmann, J. Multiple C2 domain – containing transmembrane proteins promote lipid droplet biogenesis and growth at specialized endoplasmic reticulum subdomains. **32**, (2021).

74. Fischer, A. W. *et al.* intracellular sorting of GLUT4-storage vesicles. 1–25 (2020). doi:10.1016/j.bbadis.2019.03.010.PID1

75. Pahari, S. *et al.* Induction of autophagy through CLEC4E in combination with TLR4 : an innovative strategy to restrict the survival of Mycobacterium tuberculosis. *Autophagy* **16**, 1021–1043 (2020).

76. Patin, E. C., Orr, S. J. & Schaible, U. E. Macrophage inducible C-type lectin as a multifunctional player in immunity. *Frontiers in Immunology* **8**, (2017).

77. Sathyamoorthy, T. *et al.* Membrane Type 1 Matrix Metalloproteinase Regulates Monocyte Migration and Collagen Destruction in Tuberculosis. *J. Immunol.* **195**, 882–891 (2015).

78. Martinon, F., Burns, K., Boveresses, C. & Epalinges, C.-. The Inflammasome : A Molecular Platform Triggering Activation of Inflammatory Caspases and Processing of proIL- ᴺʟ. **10**, 417–426 (2002).

79. Soleymanjahi, S. *et al.* RBM47 regulates intestinal injury and tumorigenesis by modifying proliferation, oxidative response, and inflammatory pathways. *JCI Insight* **8**, (2023).

80. Eigenbrod, T., Pelka, K., Latz, E., Kreikemeyer, B. & Dalpke, A. H. TLR8 Senses Bacterial RNA in Human Monocytes and Plays a Nonredundant Role for Recognition of Streptococcus pyogenes . *J. Immunol.* **195**, 1092–1099 (2015).

81. Liu, X., Li, L. & Peng, G. TLR8 reprograms human Treg metabolism and function. **11**, 6614–6615 (2019).

82. Schioppa, T. *et al.* Molecular Basis for CCRL2 Regulation of Leukocyte Migration. *Front. Cell Dev. Biol.* **8**, 1–7 (2020).

83. Yin, W. *et al.* CCRL2 promotes antitumor T-cell immunity via amplifying TLR4-mediated immunostimulatory macrophage activation. *Proc. Natl. Acad. Sci. U. S. A.* **118**, 1–11 (2021).

84. Bhatt, K. & Salgame, P. Host innate immune response to Mycobacterium tuberculosis. *Journal of Clinical Immunology* **27**, 347–362 (2007).

85. Korbel, D. S., Schneider, B. E. & Schaible, U. E. Innate immunity in tuberculosis: myths and truth. *Microbes Infect.* **10**, 995–1004 (2008).

86. Weiss, G. & Schaible, U. E. Macrophage defense mechanisms against intracellular bacteria. *Immunol. Rev.* **264**, 182–203 (2015).

87. Cai, L. *et al.* The Research Progress of Host Genes and Tuberculosis Susceptibility. *Oxid. Med. Cell. Longev.* **2019**, 1–8 (2019).

88. Pan, H. *et al.* Ipr1 gene mediates innate immunity to tuberculosis. *Nature* **434**, 767–772 (2005).

89. Behar, S. M., Divangahi, M. & Remold, H. G. Evasion of innate immunity by mycobacterium tuberculosis: Is death an exit strategy? *Nature Reviews Microbiology* **8**, 668–674 (2010).

90. Dorman, S. E. & Holland, S. M. Interferon-γ and interleukin-12 pathway defects and human disease. *Cytokine Growth Factor Rev.* **11**, 321–333 (2000).

91. Lerner, T. R. *et al.* Mycobacterium tuberculosis replicates within necrotic human macrophages. *J. Cell Biol.* **216**, 583–594 (2017).

92. Martin, C. J. *et al.* Efferocytosis is an innate antibacterial mechanism. *Cell Host Microbe* **12**, 289–300 (2012).

93. Galluzzi, L. *et al.* Molecular mechanisms of cell death: recommendations of the Nomenclature Committee on Cell Death 2018. *Cell Death Differ.* **25**, 486–541 (2018).

94. Logunova, N., Korotetskaya, M., Polshakov, V. & Apt, A. The QTL within the H2 Complex Involved in the Control of Tuberculosis Infection in Mice Is the Classical Class II H2-Ab1 Gene. *PLoS Genet.* **11**, 1–22 (2015).

95. Liang, W. *et al.* MARCKSL1 promotes the proliferation, migration and invasion of lung adenocarcinoma cells. *Oncol. Lett.* **19**, 2272–2280 (2020).

96. Li, C. *et al.* MKRN3-mediated ubiquitination of Poly(A)-binding proteins modulates the stability and translation of GNRH1 mRNA in mammalian puberty. *Nucleic Acids Res.* **49**, 3796–3813 (2021).

97. Silva-Gomes, R. *et al.* Differential expression and regulation of MS4A family members in myeloid cells in physiological and pathological conditions. *J. Leukoc. Biol.* **111**, 817–836 (2022).

98. Christou-Kent, M. *et al.* PATL 2 is a key actor of oocyte maturation whose invalidation causes infertility in women and mice . *EMBO Mol. Med.* **10**, 1–24 (2018).

99. Boutet, A., Zeledon, C. & Emery, G. ArfGAP1 regulates the endosomal sorting of guidance receptors to promote directed collective cell migration in vivo. *iScience* **26**, 107467 (2023).

100. Sorrells, S. *et al.* Ccdc94 Protects Cells from Ionizing Radiation by Inhibiting the Expression of p53. *PLoS Genet.* **8**, (2012).

101. Song, O. *et al.* Arf GAP 1 restricts Mycobacterium tuberculosis entry by controlling the actin cytoskeleton . *EMBO Rep.* **19**, 29–42 (2018).

102. Barreiro, L. B. *et al.* Deciphering the genetic architecture of variation in the immune response to Mycobacterium tuberculosis infection. *Proc. Natl. Acad. Sci.* **109**, 1204–1209 (2012).

103. Penn-Nicholson, A. *et al.* R1. Penn-Nicholson A, Mbandi SK, Thompson E, Mendelsohn SC, Suliman S, Chegou NN, et al. RISK6, a 6-gene transcriptomic signature of TB disease risk, diagnosis and treatment response. Sci Rep. 2020; ISK6, a 6-gene transcriptomic signature of TB disease ri. *Sci. Rep.* (2020). doi:10.1038/s41598-020-65043-8

104. Patin, E. C. *et al.* Mincle-mediated anti-inflammatory IL-10 response counter-regulates IL-12 in vitro. *Innate Immun.* **22**, 181–185 (2016).

105. Zhang, Y. *et al.* Mycobacterium tuberculosis Heat-Shock Protein 16.3 Induces Macrophage M2 Polarization Through CCRL2/CX3CR1. *Inflammation* **43**, 487–506 (2020).

106. Petrilli, J. D. *et al.* Whole blood mRNA expression-based targets to discriminate active tuberculosis from latent infection and other pulmonary diseases. *Sci. Rep.* **10**, 1–9 (2020).

107. Varshney, D. *et al.* Systematic review and meta-analysis of human Toll-like receptors genetic polymorphisms for susceptibility to tuberculosis infection. *Cytokine* **152**, (2022).

108. Thada, S. *et al.* Interaction of TLR4 and TLR8 in the innate immune response against mycobacterium tuberculosis. *Int. J. Mol. Sci.* **22**, 1–23 (2021).

109. Wang, M. G. *et al.* Association of TLR8 and TLR9 polymorphisms with tuberculosis in a Chinese Han population: A case-control study. *BMC Infect. Dis.* **18**, 1–8 (2018).

110. Lai, Y. F. *et al.* Functional polymorphisms of the TLR7 and TLR8 genes contribute to Mycobacterium tuberculosis infection. *Tuberculosis* **98**, 125–131 (2016).

111. Li, N. *et al.* Effect of ipr1 on expression levels of immune genes related to macrophage anti-infection of

mycobacterium tuberculosis. *Int. J. Clin. Exp. Med.* (2015).

112. Harper, J. *et al.* Mouse Model of Necrotic Tuberculosis Granulomas Develops Hypoxic Lesions. *J. Infect. Dis.* **205**, 595–602 (2012).

113. Linnemann, L. C., Schaible, U. E. & Dallenga, T. K. Evaluation of Myeloperoxidase as Target for Host-Directed Therapy in Tuberculosis In Vivo. *Int. J. Mol. Sci.* **23**, (2022).

114. Pichugin, A. V, Yan, B., Sloutsky, A., Kobzik, L. & Kramnik, I. Dominant Role of the sst1 Locus in Pathogenesis of Necrotizing Lung Granulomas during Chronic Tuberculosis Infection and Reactivation in Genetically Resistant Hosts. *Am. J. Pathol.* **174**, 2190–2201 (2009).

115. Brosch, R. *et al.* A new evolutionary scenario for the Mycobacterium tuberculosis complex. *Proc. Natl. Acad. Sci.* **99**, 3684–3689 (2002).

116. Zak. A prospective blood RNA signature for tuberculosis disease risk. *Lancet* **14**, 1787–1799 (2017).

117. Png, E. *et al.* Polymorphisms in SP110 are not associated with pulmonary tuberculosis in Indonesians. *Infect. Genet. Evol.* **12**, 1319–1323 (2012).

118. Skvortsov, T. A., Ignatov, D. V., Majorov, K. B., Apt, A. S. & Azhikina, T. L. Mycobacterium tuberculosis transcriptome profiling in mice with genetically different susceptibility to tuberculosis. *Acta Naturae* **5**, 62–69 (2013).

119. Comas, I. *et al.* Mycobacterium tuberculosis with modern humans. *Nat. Genet.* **45**, 1176–1182 (2014).

120. Singhania, A. *et al.* A modular transcriptional signature identifies phenotypic heterogeneity of human tuberculosis infection. *Nat. Commun.* **9**, (2018).

121. Vilaplana, C. *et al.* Ibuprofen therapy resulted in significantly decreased tissue bacillary loads and increased survival in a new murine experimental model of active tuberculosis. *J. Infect. Dis.* **208**, 199–202 (2013).

122. Gautam, U. S., Mehra, S. & Kaushal, D. In-vivo gene signatures of Mycobacterium tuberculosis in C3HeB/FeJ mice. *PLoS One* **10**, (2015).

123. Kimmey, J. M. *et al.* Unique role for ATG5 in neutrophil-mediated immunopathology during M. tuberculosis infection. *Nature* **528**, 565–569 (2015).

124. Heitmann, L. *et al.* The IL-13/IL-4Rα axis is involved in tuberculosis-associated pathology. *J. Pathol.* **234**, 338–50 (2014).

125. Chen, W. *et al.* Live-seq enables temporal transcriptomic recording of single cells. *Nature* (2022). doi:10.1038/s41586-022-05046-9

126. Tailleux, L. *et al.* Probing host pathogen cross-talk by transcriptional profiling of both Mycobacterium tuberculosis and infected human dendritic cells and macrophages. *PLoS One* **3**, e1403 (2008).

127. Ottenhoff, T. H. M. *et al.* Genome-Wide Expression Profiling Identifies Type 1 Interferon Response Pathways in Active Tuberculosis. *PLoS One* **7**, (2012).

128. McLoughlin, K. E. *et al.* RNA-seq Transcriptional Profiling of Peripheral Blood Leukocytes from Cattle Infected with Mycobacterium bovis. *Front. Immunol.* **5**, 1–12 (2014).

129. Yan, B.-S. *et al.* Progression of Pulmonary Tuberculosis and Efficiency of Bacillus Calmette-Guérin Vaccination Are Genetically Controlled via a Common sst1 -Mediated Mechanism of Innate Immunity. *J. Immunol.* **179**, 6919–6932 (2007).

130. Skeiky, Y. a W. & Sadoff, J. C. Advances in tuberculosis vaccine strategies. *Nat. Rev. Microbiol.* **4**, 469–76 (2006).

131. Yu, Y. *et al.* Different Patterns of Cytokines and Chemokines Combined with IFN-y Production Reflect Mycobacterium tuberculosis Infection and Disease. *PLoS One* **7**, 1–11 (2012).

132. Kozakiewicz, L. *et al.* B Cells Regulate Neutrophilia during Mycobacterium tuberculosis Infection and BCG Vaccination by Modulating the Interleukin-17 Response. *PLoS Pathog.* **9**, e1003472 (2013).

133. Lin, W. *et al.* Transcriptional Profiling of Mycobacterium tuberculosis Exposed to In Vitro Lysosomal

Stress. *Infect. Immun.* **84**, 2505–2523 (2016).

134. Velayati, A. A. *et al.* Totally drug-resistant tuberculosis strains: Evidence of adaptation at the cellular level. *European Respiratory Journal* **34**, 1202–1203 (2009).

135. Boisson-Dupuis, S. The monogenic basis of human tuberculosis. *Hum. Genet.* **139**, 1001–1009 (2020).

7.0 Appendix

7.1 qPCR

A.

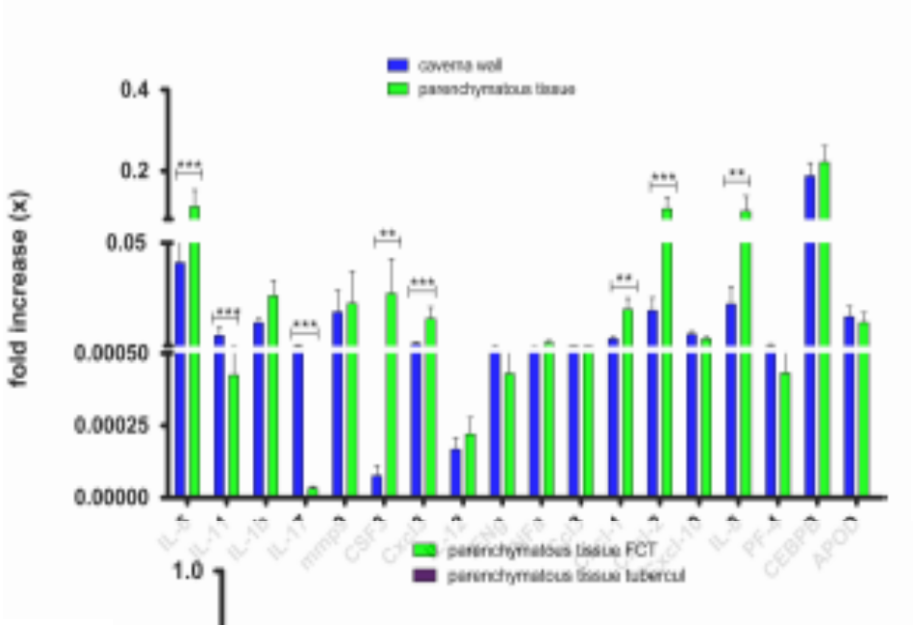

B.

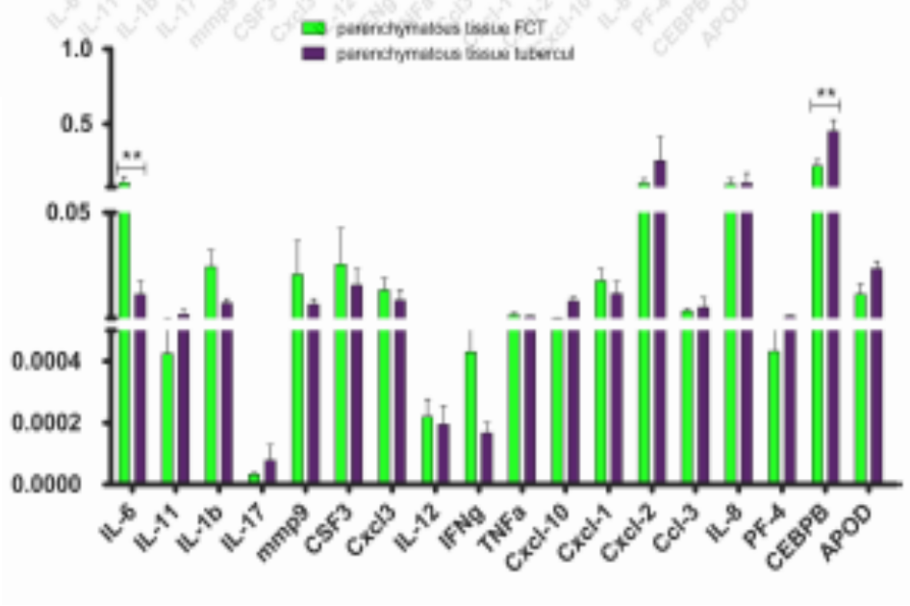

C.

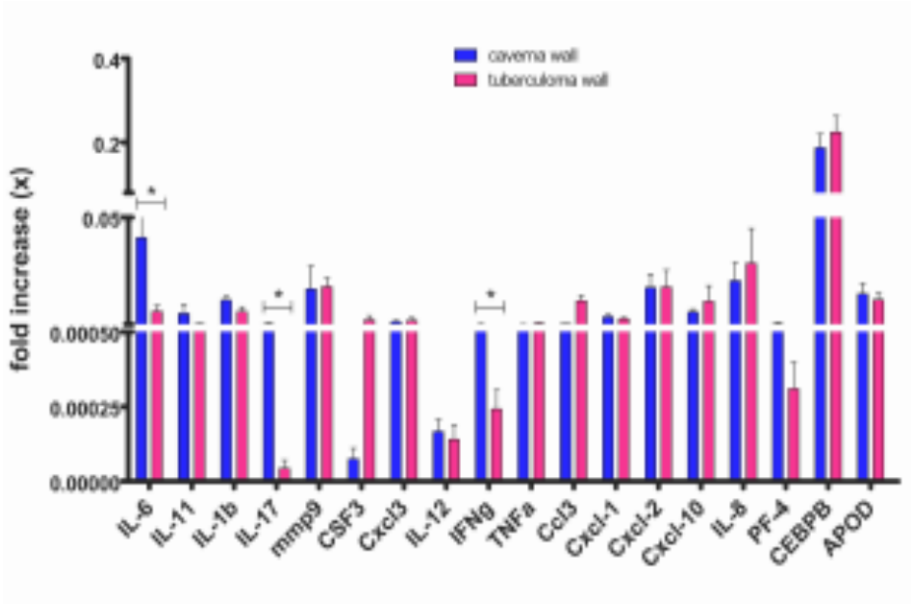

D.

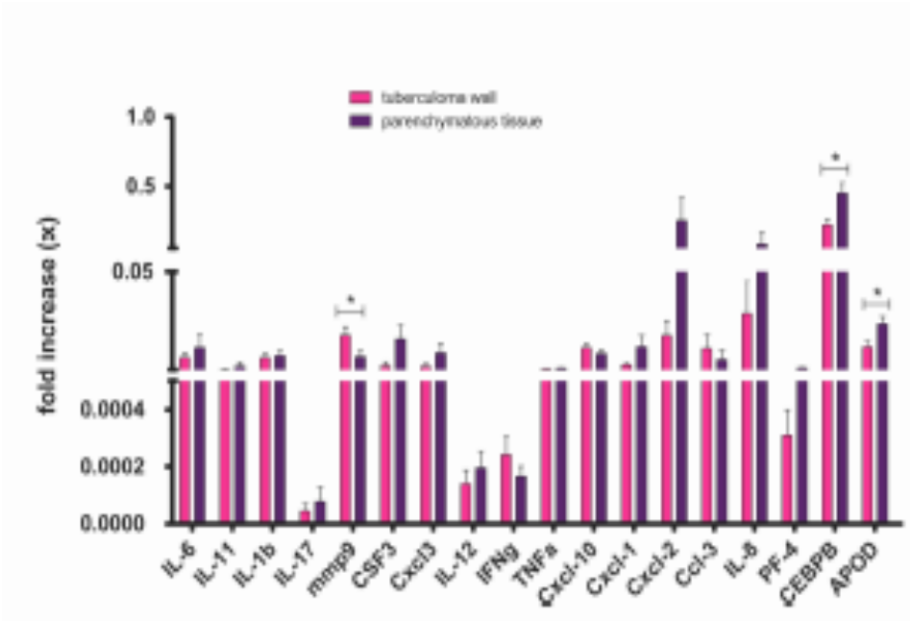

Fig. 7.1: Validation of expression of selected genes by qPCR. Most prominent differences in cytokine/chemokine gene expression were found when FCT caverna wall and parenchyma tissues were compared. Cxcl1 ($p \leq 0.03$) and Cxcl2 ($p \leq 0.01$), IL-6 ($p \leq 0.0001$), IL-8 ($p \leq 0.01$) were upregulated in parenchymatous tissue as compared to caverna wall. Up regulated genes are represented in red, down regulated genes in green and genes with failed Ct threshold are coloured white for each sample or data sets (x-axis). Graphs A-D were provided by Vladimir Yeremeev.

7.2 Murine body weight over time

A.

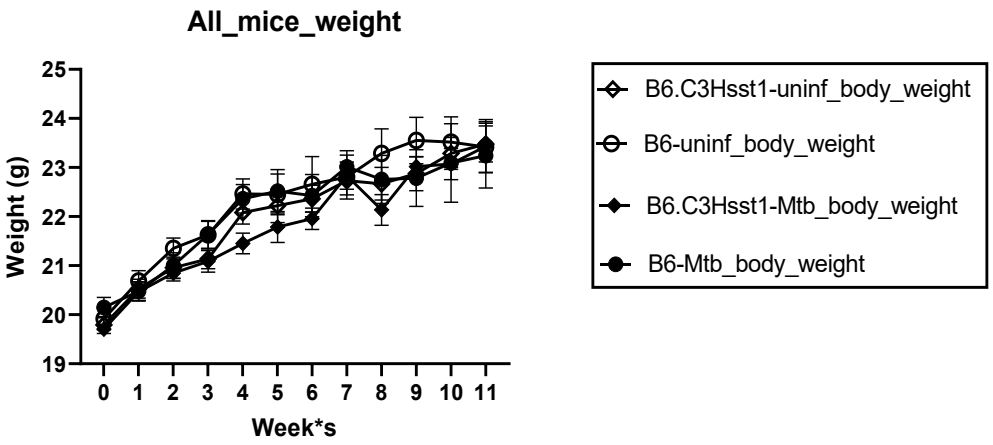

B.

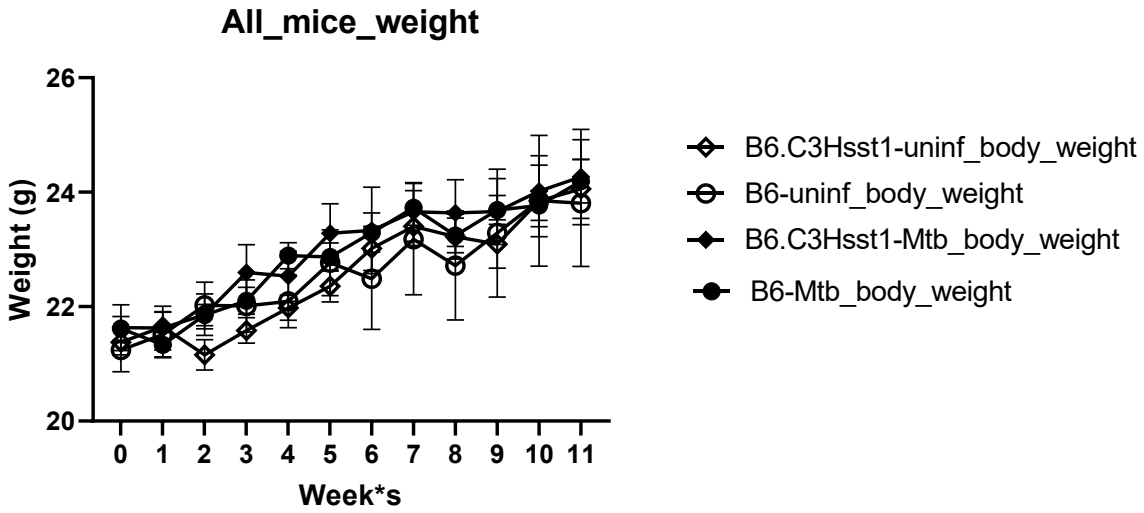

Fig. 7.2: Body weight dynamics of experimental mice. A. experiment I, 8 – 12 weeks old female mice B6 and B6.C3Hsst1 were infected with Mtb-H37Rv per aerosol, with uninfected controls and monitored weekly throughout the experiment n=10 mice per group with 3 end time points. **B.** 11 – 14 weeks old female mice B6 and B6.C3Hsst1 were infected with Mtb-H37Rv per aerosol, with uninfected controls, n=8 per group with 3 end time point. Error bars depict SE measurement.

7.3 Analysis of flow cytometry data

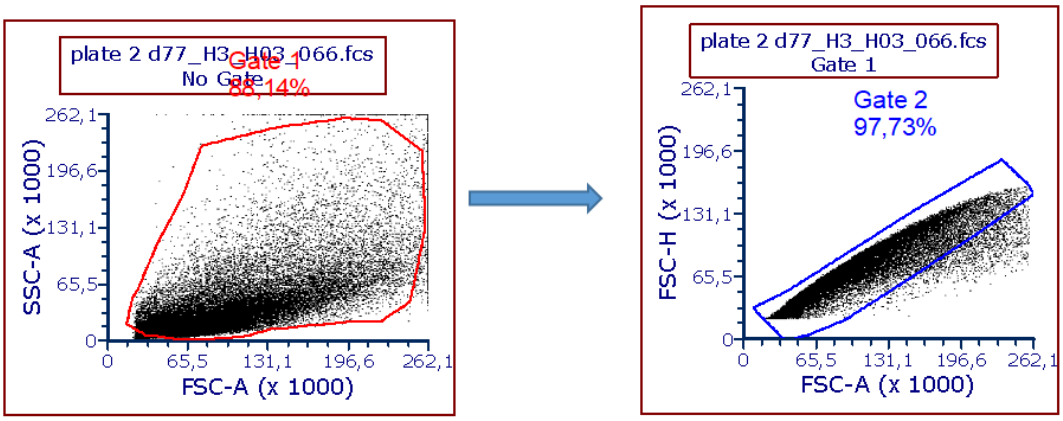

1. **T cell CD3-APC-Cy7**

2. **T cell CD4-PECy7**

3. **T cell CD8a-PerCp-Cy5-5A**
   Isotype- IgG2a-PerCp-Cy5-5A

4. **Activated T Cell -CD274(PD-1) -FITC**

5. **B Cell CD19-BV/AmCyan**

6. **Macrophage- CD68 PacBlue**

7. **PMN - Ly6G APC**

8. **Activated innate Macrophage - CD274 (PD-L1)-PE**
   isotype - IgG2b-PE

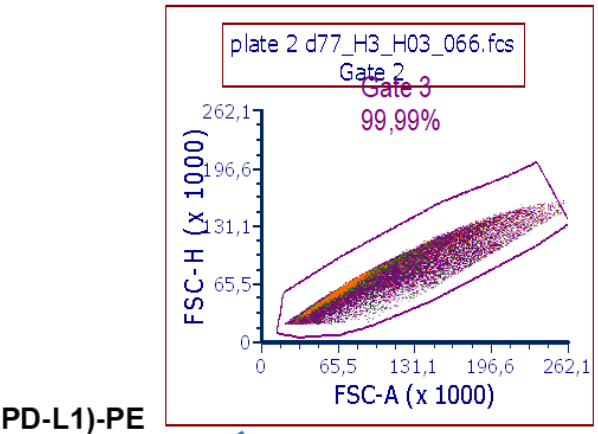

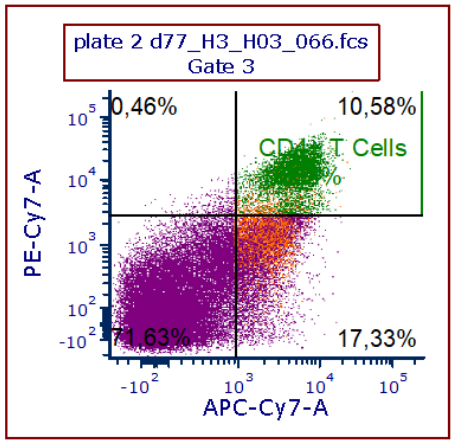

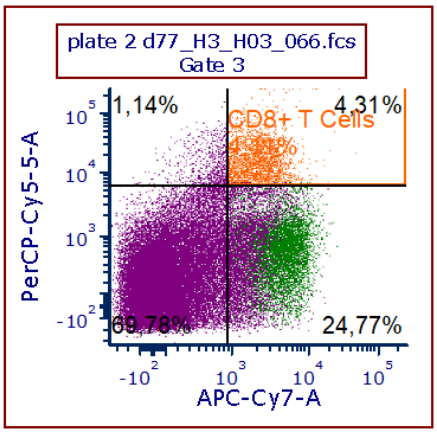

7.4 Analysis of cytokine data

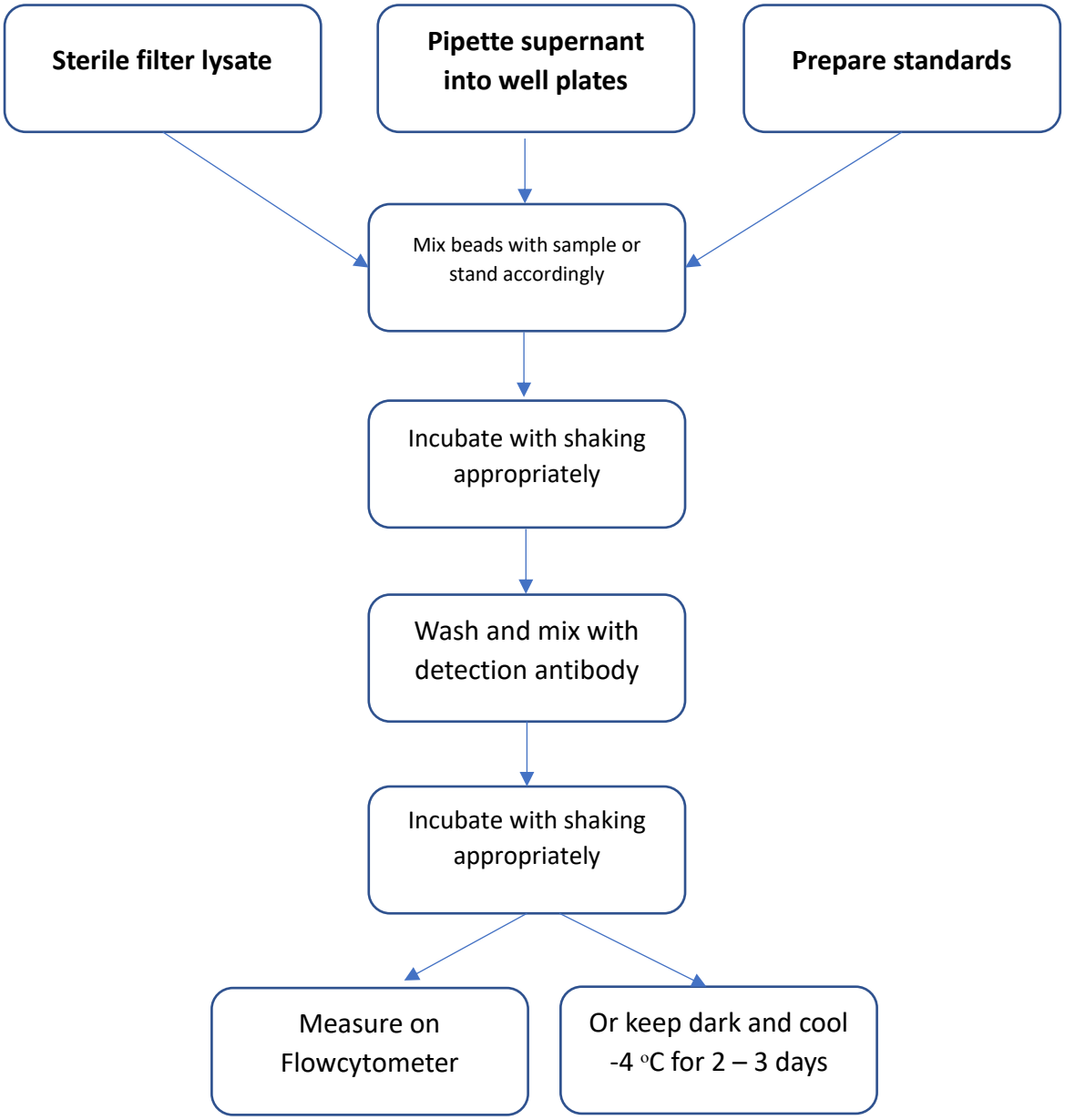

7.5 Scheme of RT-qPCR data generation

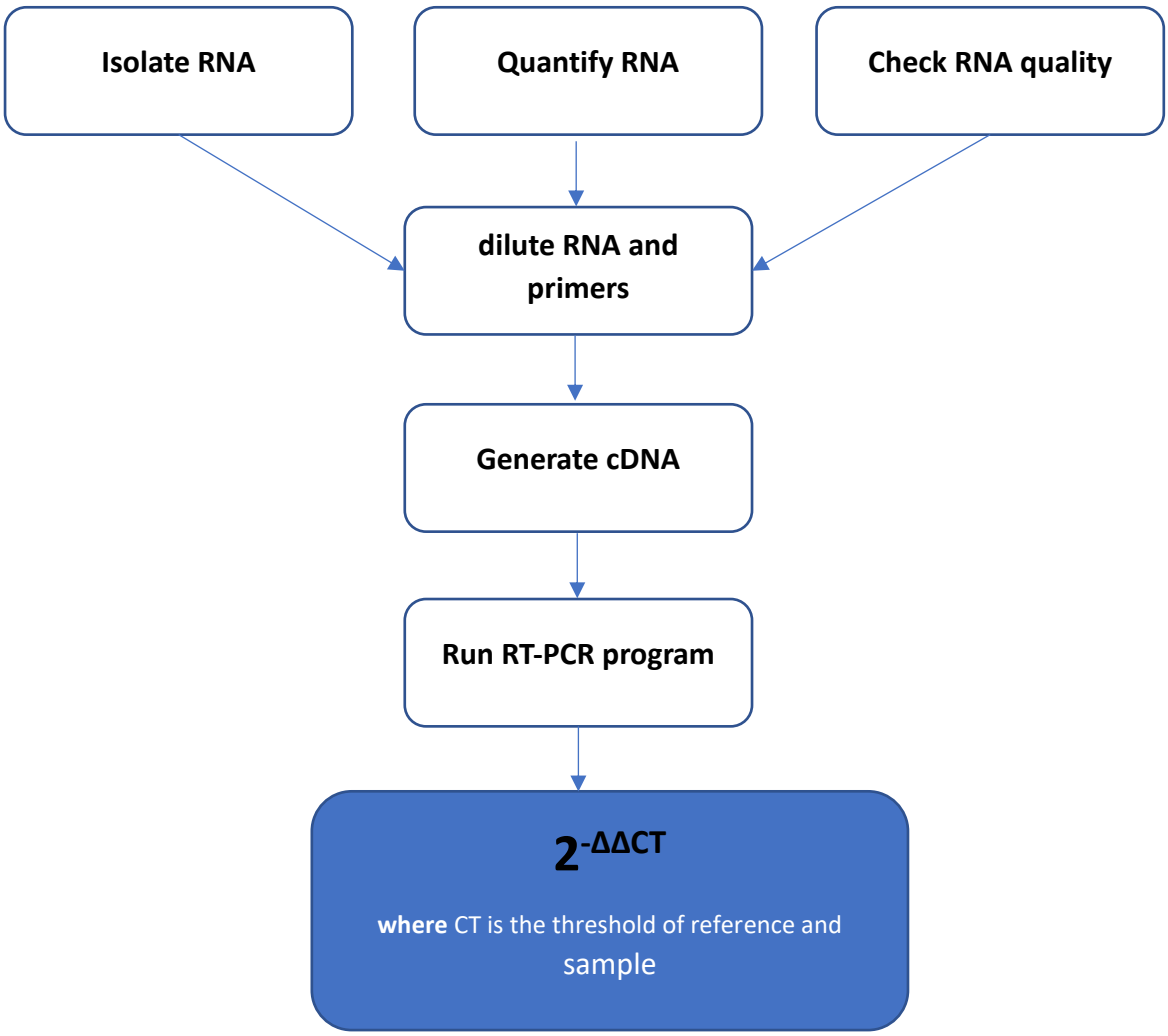

7.6 Sample preparation and analysis of mRNA sequencing data generation (A) and analysis (B)

A.

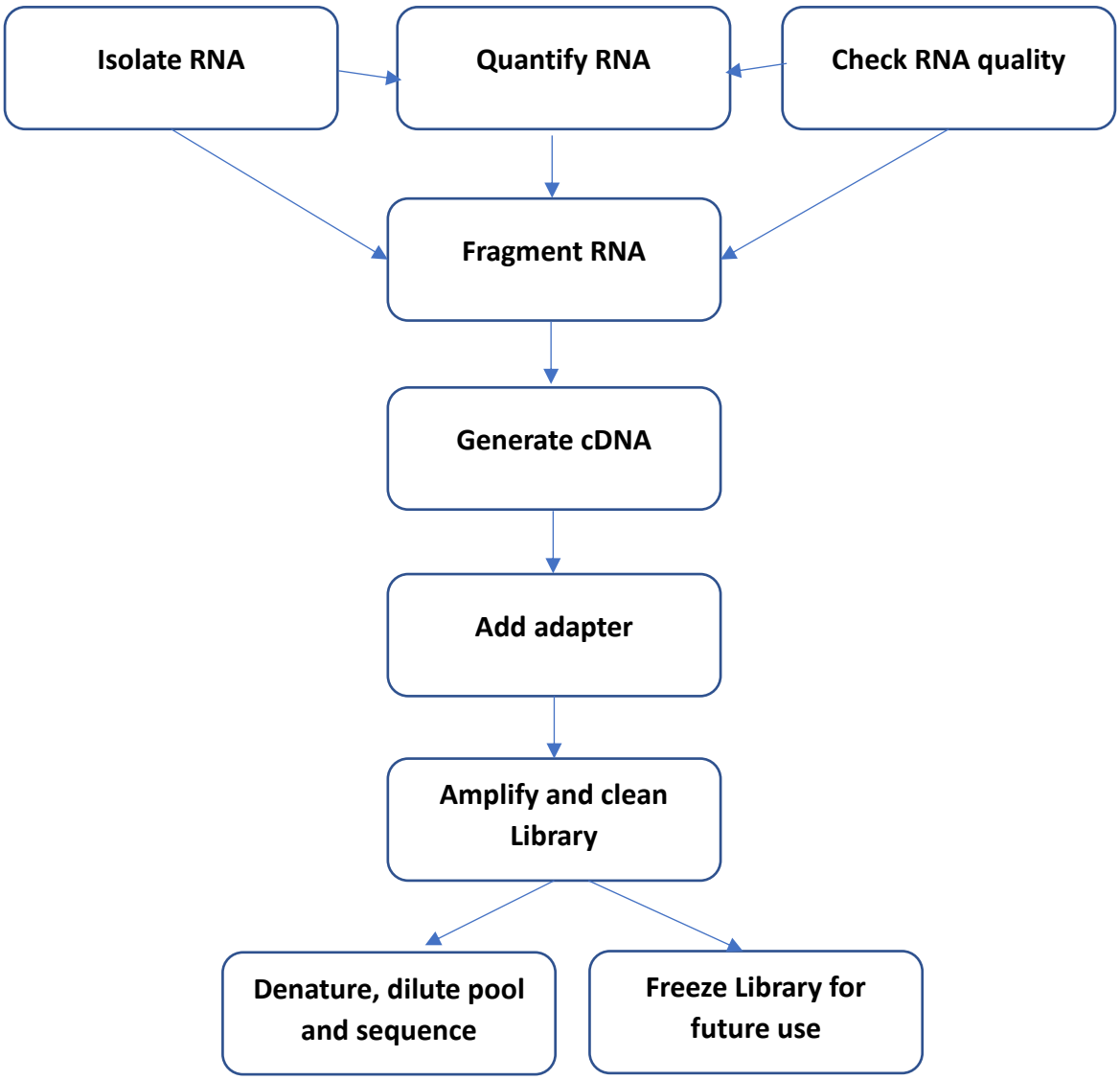

B.

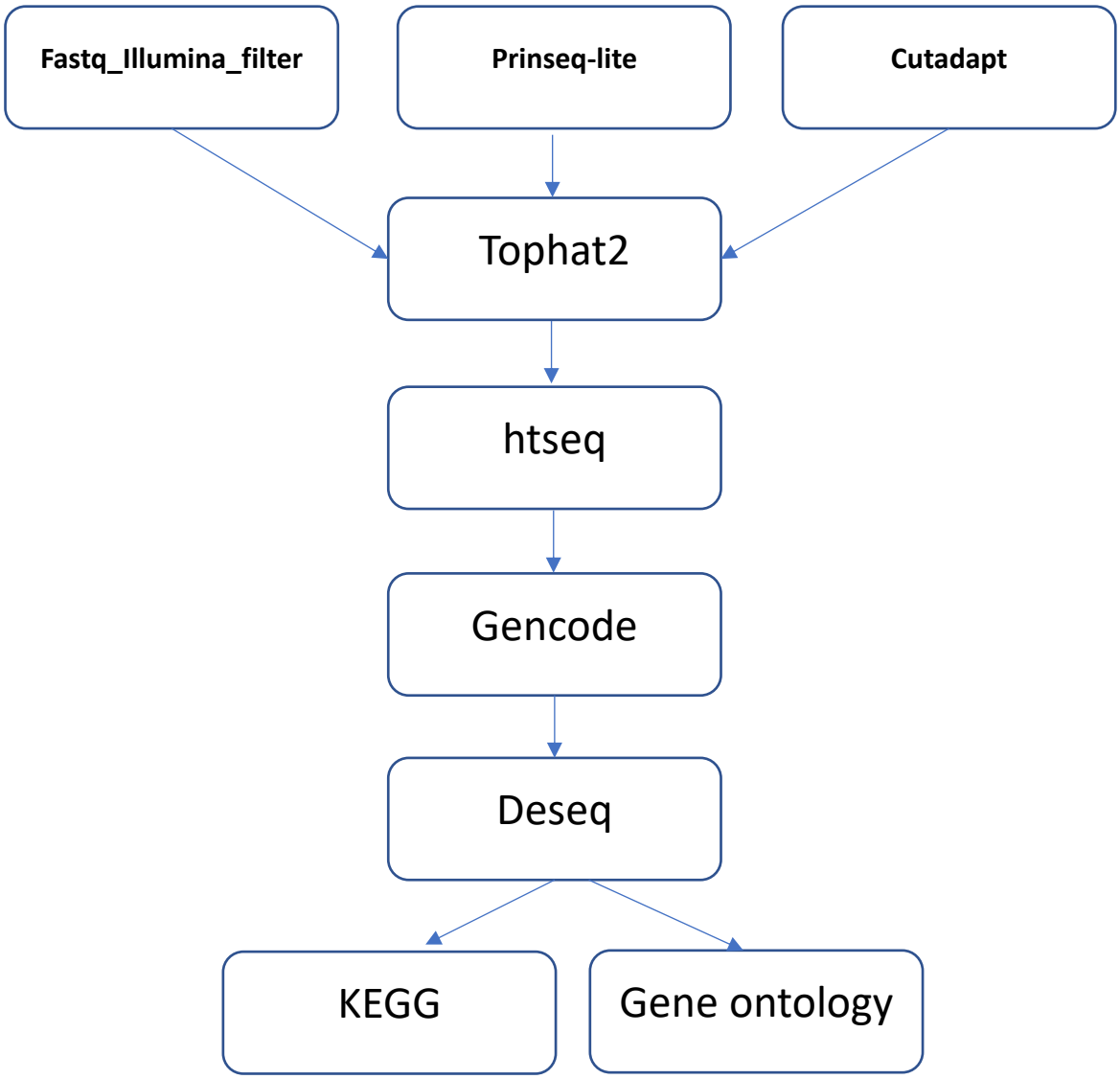
Fastq_Illumina_filter
Prinseq-lite
Cutadapt
Tophat2
htseq
Gencode
Deseq
KEGG
Gene ontology

7.7 Some putative targets for RNA-interference based HDT in human

1. AGRN

2. EPPK1

3. CLEC4E

4. COL5A3

5. MUC1

6. MPO

7. TCF4

8. SPN

9. UACA